Design and characterization of reactor concepts for microbial electrochemical technologies

Von der Fakultät für Lebenswissenschaften
der Technischen Universität Carolo-Wilhelmina zu Braunschweig
zur Erlangung des Grades eines
Doktors der Naturwissenschaften
(Dr. rer. nat.)
genehmigte
D i s s e r t a t i o n

von Thomas Stefan Krieg
aus Mutlangen

1. Referent: Prof. Dr. Uwe Schröder
2. Referent: Prof. Dr. Rainer Krull
eingereicht am: 28.11.2018
mündliche Prüfung (Disputation) am: 07.05.2019
Druckjahr 2019

Vorveröffentlichungen der Dissertation

Teilergebnisse aus dieser Arbeit wurden mit Genehmigung der Fakultät für Lebenswissenschaften, vertreten durch den Mentor der Arbeit, in folgenden Beiträgen vorab veröffentlicht:

Publikationen

Thomas Krieg, Jeffery A. Wood, Klaus-Michael Mangold, Dirk Holtmann (2018) Mass Transport Limitations in Microbial Fuel Cells: Impact of Flow Configurations. Biochemical Engineering Journal 138, 172-178

Thomas Krieg, Linh M. P. Phan, Jeffery A. Wood, Anne Sydow, Igor Vassilev, Jens O. Krömer, Klaus-Michael Mangold, Dirk Holtmann (2018) Characterization of a membrane-separated and a membrane-less electrobioreactor for bioelectrochemical syntheses. Biotechnology and Bioengineering 115 (7), 1705-1716

Thomas Krieg*, Anne Sydow*, Sonja Faust, Ina Huth, Dirk Holtmann (2018) CO_2 to Terpenes: Autotrophic and Electroautotrophic α-Humulene Production with *Cupriavidus necator*. Angewandte Chemie International Edition 57 (7), 1879-1882

Thomas Krieg*, Joana Madjarov*, Luis F.M. Rosa, Franziska Enzmann, Falk Harnisch, Dirk Holtmann, Korneel Rabaey (2017) Reactors for Microbial Electrobiotechnology. Advances in Biochemical Engineering/Biotechnology, https://doi.org/10.1007/10_2017_40

Thomas Krieg, Anne Sydow, Uwe Schröder, Jens Schrader, Dirk Holtmann (2014) Reactor concepts for bioelectrochemical syntheses and energy conversion. Trends in biotechnology 32 (12), 645-655

Anne Sydow*, Thomas Krieg*, Florian Mayer, Jens Schrader, Dirk Holtmann (2014) Electroactive bacteria—molecular mechanisms and genetic tools. Applied Microbiology and Biotechnology 98 (20), 8481-8495

** haben gleichermaßen zu dieser Arbeit beigetragen*

Tagungsbeiträge

Thomas Krieg: Characterization and operation of a separated electrobioreactor. DBU-Workshop "Mikrobielle Bioelektrotechnologie: Eine Plattforminitiative für Deutschland", Braunschweig (2016)

Thomas Krieg: Reaktorkonzepte für bioelektrochemische Systeme. DBU-Workshop "Mikrobielle Bioelektrotechnologie: Eine Plattforminitiative für Deutschland", Leipzig (2015)

Thomas Krieg: Reaktorkonzepte für bioelektrochemische Systeme. Stiftungstag des DECHEMA Forschungsinstituts, Frankfurt (2014)

Thomas Krieg: Reaktorkonzepte für mikrobielle Elektrosynthesen. DBU-Workshop "Mikrobielle Bioelektrotechnologie: Eine Plattforminitiative für Deutschland", Osnabrück (2013)

Posterbeiträge

Thomas Krieg, Anne Sydow, Linh M. P. Phan, Klaus-Michael Mangold, Jens Schrader, Dirk Holtmann: Integration of electrodes into a conventional bioreactor for microbial electrosynthesis. 3rd European International Society for Microbial Electrochemistry and Technology Meeting, Rome, Italy (2016)

Thomas Krieg, Tina Mai, Anne Sydow, Florian Mayer, Klaus-Michael Mangold, Jens Schrader, Dirk Holtmann: Reactor concepts for bioelectrochemical syntheses and energy conversion. Himmelfahrtstagung New Frontiers for Biotech-Processes, Koblenz (2016)

Thomas Krieg, Tina Mai, Anne Sydow, Florian Mayer, Jens Schrader, Dirk Holtmann: Reactor concepts for bioelectrochemical syntheses and energy conversion. Stiftungstag des DECHEMA Forschungsinstituts, Frankfurt (2015)

Thomas Krieg, Tom Zschernitz, Daniel Kleine, Anne Sydow, Klaus-Michael Mangold, Jens Schrader, Dirk Holtmann: Reactor concept for microbial electrosyntheses and fuel cells. 10th ESEE, European Symposium on Electrochemical Engineering, Chia, Domus de Maria, Sardinia, Italy (2014)

Die experimentiellen Arbeiten dieser Dissertation wurden am DECHEMA Forschungsinstitut in der Arbeitsgruppe "Industrielle Biotechnologie" in Frankfurt am Main angefertigt.

Danksagung

An vorderster Stelle möchte ich mich bei meinem Betreuer und Mentor Dr.-Ing. Dirk Holtmann bedanken. Danke, dass Du mich seit meinem Start als ”schmuddliger Praktikant” beim damals noch Karl-Winnacker-Institut, später dann als Bachelorand und schließlich im DECHEMA-Forschungsinstitut als Doktorand unterstützt und gefördert hast. Danke für all die Ratschläge, wissenschaftliche Diskussionen und ein immer offenes Ohr.

Ich danke Prof. Dr. Uwe Schröder für die freundliche Übernahme der Beutreuung meiner Doktorarbeit als Mentor. Danke für die wissenschaftlichen Diskussionen und Tipps, die mir sehr geholfen haben. Ich danke Prof. Dr. Rainer Krull für die freundliche Übernahme als Korreferent und für die akademische Begleitung meines Studiums an der TU Braunschweig. Ich danke Prof. Dr. Anett Schallmey für die freundliche Übernahme des Promotionsvorsitzes.

Ich danke Prof. Dr. Jens Schrader für die Möglichkeit der Durchführung meiner praktischen Arbeiten am DECHEMA-Forschungsinstitut. Danke für die wissenschaftlichen Diskussionen und die notwendige Ablenkung vom Tagesgeschäft beim Bier brauen.

Ich danke Dr. Klaus-Michael Mangold von der Arbeitsgruppe Elektrochemie des DECHEMA Forschungsinstituts. Danke für die Diskussionen und Erleuchtungen, vor allem in elektrochemischen Fragestellungen.

Ich danke dem Werkstatt Team des DECHEMA-Forschungsintituts für all die Ratschläge und den Enthusiasmus, mir auch den x-ten Entwurf eines Elektrobioreaktors zu bauen. Danke für alle Ratschläge, fürs Zuhören und die flotte Arbeitsweise.

Ich danke meinen Studenten Tom Zschernitz, Daniel Kleine, Linh Minh Phuc Phan und Tina Mai, die mich im Rahmen ihrer Abschlussarbeiten unterstützt haben. Vielen Dank für euren Einsatz, eure Ideen und für all die Diskussionen.

Many thanks to Dr. Jeffery Alan Wood for all the discussions, guidance and input regarding computational fluid dynamics and the English language.

Ich danke Igor Vassilev für die spannende Zeit am DECHEMA-Forschungsinstitut und die gemeinsame Forschung. Danke für die Diskussionen und den Input.

Ich danke allen Arbeitsgruppen des DECHEMA-Forschungsinstituts. Danke für eine su-

per tolle Arbeitsatmosphäre und all eure Hilfe. Danke für unzählige Abende auch neben der Arbeit, danke fürs Bier brauen, Zuhören und das Ertragen meiner Laborflüche. Es war mir eine Freude (auch wenn es sich nicht immer danach angehört hat).

Ich möchte mich herzlich bei meiner Familie und meinen Freunden bedanken. Danke für die bedingungslose Unterstützung, die ich seit Jahren von euch erfahren darf. Ohne euch hätte ich das alles niemals geschafft.

Der letzte Dank gebührt Dir Anne. Danke für alles, jedes Wort, die Geduld mit mir und dafür, dass Du immer für mich da bist. We've finally cracked it!

Table of Contents

List of Figures

List of Tables

Abbreviations

A: Ampere
BES: Bioelectrochemical system
C: Coulomb
CE: Coulombic efficiency or counter electrode
CoA: Coenzyme A
D: Diffusion coefficient
DAPI: 4',6-Diamidino-2-phenylindole
DMAPP: Dimethyl-allyl pyrophosphate
DET: Direct electron transfer
DF: Degree of freedom
DTT: Dithioerythrole
DNA: Deoxyribonucleic acid
DXP: 1-Deoxy-D-xylulose 5-phosphate
E: Energy in Joule (J)
EAM: Electroactive microorganism
EDTA: Ethylenediaminetetraacetic acid
EL: Electric load
F: Faraday constant (96485 C mol^{-1})
FPP: Farnesyl pyrophosphate
fw: Forward
g: Mass in grams
g: G-force
GGPP: Geranylgeranyl pyrophosphate
G3P: Glycealdehyde-3-phosphate
GP: Glycerate-3-phosphate
GPP: Geranyl pyrophosphate
HER: Hydrogen evolution reaction
I: Current in Ampere (A)
IPP: Isopentenyl pyrophosphate
IET: Indirect electron transfer
j: Oxygen transfer rate in mol h^{-1}
J: Joule
M: Molar concentration (mmol L^{-1})
MEC: Microbial electrolysis cell
MES: Microbial electrosynthesis
MET: Mediated electron transfer

MFC: Microbial fuel cell
MVA: Mevalonate
n: Amount of substance or number
OCP: Open circuit potential
OER: Oxygen evolution reaction
PCR: Polymerase chain reaction
PHA: Polyhydroxyalkanoate
PHB: Polyhydroxybutyrate
PPB: Potassium phosphate buffer
PS: Power source
P_{PW}: Octanol-water partition coefficient
ϕ: Potential in Volt (V)
Q: Charge in Coulomb (C)
q: Specific charge in Coulomb per electrode surface area (C m^{-2})
RE: Reference electrode
rev: Reverse
rpm: Rounds per minute
s: Standard deviation
SP: Specific productivity
STR: Stirred tank reactor
t: Time
T: Temperature
V: Volt or Volume in L
vs.: *versus*
WE: Working electrode
z: Number of transferred electrons
ZSSI: α-Humulene synthase

1 Introduction

Fossil fuels are finite and need to be replaced by renewable and sustainable energies. To date costs of oil production are steadily rising and climate change forces mankind to lower carbon emissions (Kircher, 2012; Scarlat et al., 2015). A new bioeconomy has to be formed not only on a national, but a global level (Kircher, 2012). The change will be hard and opens several challenges, which need to be overcome. For a successful change to an industry based on sustainable energy resources the entire economy needs to be changed to a circular bioeconomy based on renewable substrates in biorefinery models (Mohan et al., 2016). One of the biggest challenges is that renewable energy underlies natural variations (e.g. wind strength, sun intensity) and is supposed to substitute a very constant energy supply by fossil fuels (Ausfelder et al., 2015). This is a difficult task to achieve, because the storage of energy in this dimensions is complex and occupies researchers over the globe since decades (Ausfelder et al., 2015). The combination of biotechnology with electrochemistry opened the new research field electrobiotechnology and is a great opportunity to overcome several challenges of the necessary change.

The research field electrobiotechnology has gained a lot of interest among researchers over the world. Most publications were done in the past 30 years. The basic concept, however, was described in the early 20th century. Potter (1911) reported effects of electricity on the decomposition of organic compounds using microbes for the first time. In the recent years more and more of these electroactive microorganisms were reported and possible electron transfer pathways have been described (Marshall et al., 2012; Nevin et al., 2011, 2010; Torella et al., 2015). Later in the 20th century fermentations were influenced by the application of potentials and the caused electric current. The term electro-fermentation, however, was initially used in 2010 (Rabaey and Rozendal, 2010; Schievano et al., 2016). Besides microbes, also the interaction between enzymes and electrodes for redox equivalent supply has been described (Krieg et al., 2011; Lütz et al., 2004; Srikanth et al., 2014). Electrobiotechnology may be the key for a successful change to a new bioeconomy, because it may solve several problems: first, waste water can be cleaned at low energy demand using microbial fuel cells (MFCs) and microbial electrolysis cells (MEC), which use the organic loading energy from the waste water to produce electric current or chemical products such as hydrogen or methane (Verstraete et al., 2006; Zhang and Angelidaki, 2014). Second, electrons can be used in microbial electrosyntheses (MES) to reduce oxidized substrates, e.g. the greenhouse gas CO_2, to organic compounds such as acetate, butyrate or isopropanol (Ganigué et al., 2015; Nevin et al., 2010; Torella et al., 2015). It has been shown that MES can be used to store energy from renewable sources, because the technology is able to deal with the typical fluctuations described before (del Pilar Anzola Rojas et al., 2018). Third, new processes even enable unbalanced biocon-

versions (electro-fermentations), which would thermodynamically not possible without electrodes balancing the redox levels (Moscoviz et al., 2016). Electrobiotechnology has the potential to replace substrates such as sucrose, which compete with the food market, with renewable substrates such as CO_2 (Roy et al., 2016). Harnisch et al. (2015) compared the production costs of lysine from sucrose by a conventional process with an electrobiotechnological process and found possible cost savings between 8% and 18%. Therefore new bioreactors for this are needed.

Several reactor concepts have been described for bioelectrochemical systems (BES). For MFCs and MECs rather simple designs such as cubic, flat-plate or tubular reactors with limited mixing properties up to pilot-scale have been reported (Cusick et al., 2011; Janicek et al., 2014). These systems are mainly used to break down waste water to CO_2 and power at low levels. From an economic point of view, the components (electrodes, membranes, etc.) of the reactors need to be kept simple and cheap, because the levels of the produced power are quite low (Fan et al., 2012; Harnisch and Schröder, 2010; Leong et al., 2013). Several ideas have been postulated to improve power output and are discussed in Verstraete et al. (2006) and Fan et al. (2012). Furthermore, different reactor and electrode setups influencing the mass transport have a great influence on power production in MFCs (Cheng et al., 2006; Sleutels et al., 2011, 2009).

Recently, MES with monoseptic or mixed cultures and genetically engineered strains have been reported. More sophisticated reactor concepts were proposed in the recent years for these applications (Giddings et al., 2015; Hintermayer et al., 2016; Rosa et al., 2016). Monitoring of pH and other process parameters is crucial for high productivities. Many biotechnological laboratories started to do research on electrobiotechnological processes and designed reactors for their needs. Comparison of these studies used to be laborious or impossible, because critical parameters were missing or the reactor concepts are not comparable. An idea to overcome this issue is the modification of stirred tank reactors (STR), which are standardized and widely used in biotechnology since decades. This could ensure a better comparability of electrobiotechnological studies. Furthermore, it has been shown that productivities can be enhanced and variations of electrobiotechnological processes are reduced using these reactors (Hintermayer et al., 2016; Rosa et al., 2016). Further insights and characterization of these reactor concepts have to be gained to improve electrobiotechnology. Modeling and simulation by computational fluid dynamics using the finite element method can help interpreting experimental results (Kim et al., 2012; Luo et al., 2016; Zhao et al., 2016).

Besides the improvement of electrobioreactors also electroactive microorganisms (EAM) need to be engineered to elucidate the involved electron transfer mechanisms, increase production rates and enable the production of complex and more valuable products containing more than one or two carbon atoms (Rosenbaum and Henrich, 2014). However, less genetic tools are available for many EAM compared to typical microorganisms used

in biotechnology such as *Escherichia coli*. Influencing the product range and improving the electron uptake or release on a genetic level has a high potential for more effective electrobiotechnological processes (Flynn et al., 2010; Li et al., 2018). Therefore, (further) genetic tools for EAM need to be developed (Kita et al., 2013; Leang et al., 2013; Rosenbaum and Henrich, 2014; Sydow et al., 2014). An exception to this is the electroactive bacterium *Cupriavidus necator*, which has been extensively studied and genetically modified since decades (Gruber et al., 2015; Heinzle and Lafferty, 1980; Pohlmann et al., 2006; Steinbüchel and Schlegel, 1991). Furthermore, heterotrophic and autotrophic production of several products such as alcohols, fatty acids and other molecules by *C. necator* strains have been reported (Crépin et al., 2016; Grousseau et al., 2014; Li et al., 2012; Nybo et al., 2015).

2 Theoretical Background

In this chapter the status quo of the relevant electrobiotechnological research and literature is outlined. Furthermore, the theory of associated disciplines namely biotechnology, electrochemistry and process engineering is introduced. An introduction of fundamentals of so called electroactive microorganisms (EAM) is given, which can be found in ecological niches all over the planet (Koch and Harnisch, 2016). Especially *Geobacter sulfurreducens*, *Shewanella oneidensis*, *Corynebacterium glutamicum* and *Cupriavidus necator*, which are used in this study, are highlighted. EAM have developed several ways to interact with electrodes. These are extensively discussed in Section 2.1.1. Bioelectrochemical systems (BES) can in general be distinguished and are classified in anodic and cathodic processes, depending on at which electrode the biology interacts with (Figure 1). An exception to this is extensively discussed in Section 2.3.4, where substrates produced at the working and counter electrode are used for microbial electrosynthesis (MES).

2.1 Bioelectrochemical fundamentals

BES are characterized by a biological component (microorganism, enzyme) interacting with electrodes. Here only the interaction between EAM and electrodes is discussed, enzymatic bioelectrochemistry is out of the scope of this work. Electrons can either be produced by the biological component and taken up by the electrode (being defined as the anode in this case) or consumed by the biological component and released by a electrode (being defined as the cathode in that case) (Faraday, 1834). The energy a microorganism can generate from a given metabolic pathway is directly proportional to the energy difference ΔE^o between the electron donor and the electron acceptor (Schievano et al., 2016; Thauer et al., 1977). The ΔE^o can be calculated from the Gibbs free energy of the overall reaction with the Nernst equation (Equation 1),

$$\Delta E^o = -\frac{\Delta G}{nF} \tag{1}$$

where ΔG is the Gibbs free energy of the reaction in Joule per mol, n is the number of electrons involved in the reaction in mol and F is the Faradays constant, which is 96,485 coulombs per mol. The maximum amount of energy that a reaction can produce (exergonic) or needs (endergonic) is represented by the Gibbs free energy. The sign of ΔE^o determines whether electricity is produced or must be supplied to drive the reaction (Feiner and McEvoy, 1994; Gibbs W., 1873; Schievano et al., 2016).

For electrochemical processes at least an anode and a cathode are needed, forming a two electrode system. However, for laboratory scale experiments it is recommendable to

use reference electrodes to be able to control and/or measure the potential at the working and/or counter electrode. The potential determines the kind of process (oxidation or reduction) and the current the amount of oxidized or reduced reactants. In the following subsection typical BESs are introduced, where the working electrode is an anode or a cathode resulting in anodic or cathodic processes, respectively.

Anodic processes

One of the most investigated systems in bioelectrochemistry are microbial fuel cells (MFCs) and microbial electrolysis cells (MECs). In MFCs, organic waste is broken down by EAM at the anode to CO_2, and chemical energy is transduced to electrical energy, which can be used by an electric consumer (Verstraete et al., 2006). The electrode of an electrochemical cell where oxidation takes places is defined as the anode. Electrons are taken up from the electrolyte or, in the case of this study, from the EAM. Electrons produced by the anodic EAM are transferred *via* an external electrical circuit containing an electric load (EL, Figure 1, e.g. a resistor) to a cathode, where they are used to reduce oxygen with the help of catalysts such as platinum (Figure 1). If an external power source is used (PS, Figure 1), also energy rich compounds such as hydrogen can be produced at the cathode combining the anodic and the cathodic reaction and a MEC is created (Rozendal et al., 2006). Unbalanced fermentations have been reported, where the anode acts as an electron sink for the EAM. Respirative electrons are transferred from the EAM to the anode and the production of compounds with an unbalanced redox balance (e.g. the conversion of glycerol to ethanol or in general anodic respiration of a microorganism) is enabled (Bursac et al., 2017; Flynn et al., 2010; Förster et al., 2017; Hintermayer et al., 2016).

Cathodic processes

In recent years cathodic reactions became more interesting for researchers all over the world (Figure 1). The electrode of an electrochemical cell where reduction takes places is defined as the cathode. Electrons are released to the electrolyte or, in the case of this study, into EAM. Cathodes releasing electrons to microorganisms for biomass production or influencing the product spectrum have been reported starting in the end 1960s to the late 1980s and 1990s for several microorganisms (Emde and Schink, 1990; Kim and Kim, 1988; Schlegel and Lafferty, 1964). Metabolic shifts associated with a higher production of 1,3-propandiol from glycerol during heterotrophic cultivations of *Clostridium pasteurianum* have been reported recently (Choi et al., 2014). Even more interesting, particularly in the light of a new bioeconomy and the reduction of CO_2 release into the environment, is the MES to organic compounds from CO_2. Products such as acetate, butyrate and isopropanol have been reported to date in monoseptic and mixed cultures, respectively

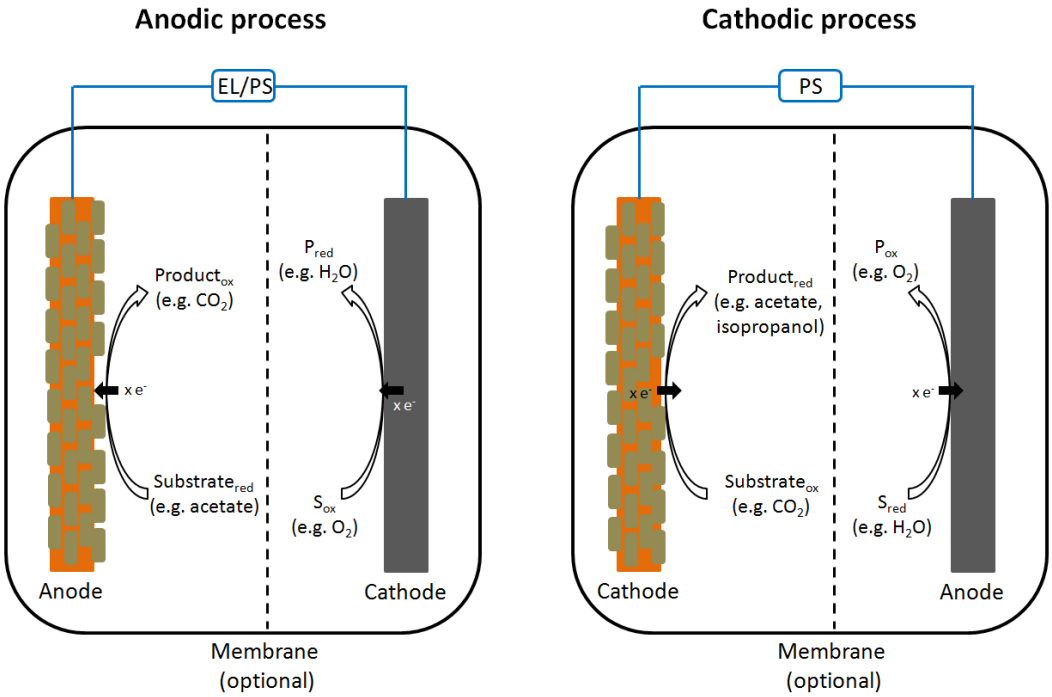

Figure 1: Scheme of anodic and cathodic processes bioelectrochemical systems.

(Batlle-Vilanova et al., 2016; Ganigué et al., 2015; Liu et al., 2016; Marshall et al., 2012; Nevin et al., 2010; Torella et al., 2015).

2.1.1 Electron transfer between electrodes and electroactive microorganisms

Extracellular electron transfer (EET) mechanisms are more or less well studied for EAM in anodic processes such as MFCs (Figure 2). One can distinguish between three electron transfer mechanisms: a direct electron transfer (DET, Lovley (2011); Nevin et al. (2010)), where the microbe is directly connected *via* pili or outer membrane cytochromes; a mediated electron transfer (MET, Marsili et al. (2008); Schmitz et al. (2015)), where a redox active compound (e.g. flavins or metal complexes) is shuttling the electrons between the microbes and the electrode; and the indirect electron transfer (IET, Li et al. (2012); Schlegel (1965); Udupa et al. (1971)), where an electrochemically active compound, such as hydrogen is produced by either the EAM or the electrode and interacts with the electrode or the EAM, respectively (Patil et al., 2012; Torella et al., 2015).

Apart from electron transfer pathways in anodic processes, the knowledge for cathodic ones is limited to date (Rosenbaum et al., 2011; Sydow et al., 2014). Most likely the electron transfer pathways of anodic and cathodic processes are using similar techniques but in-depth research on cathodic reactions needs to be performed in the future. IET is possible *via* electrochemically produced hydrogen or formate at fairly high cathodic potentials ($<$ -614 mV *vs.* Ag/AgCl at pH 7 depending on the electrode material, Lovley

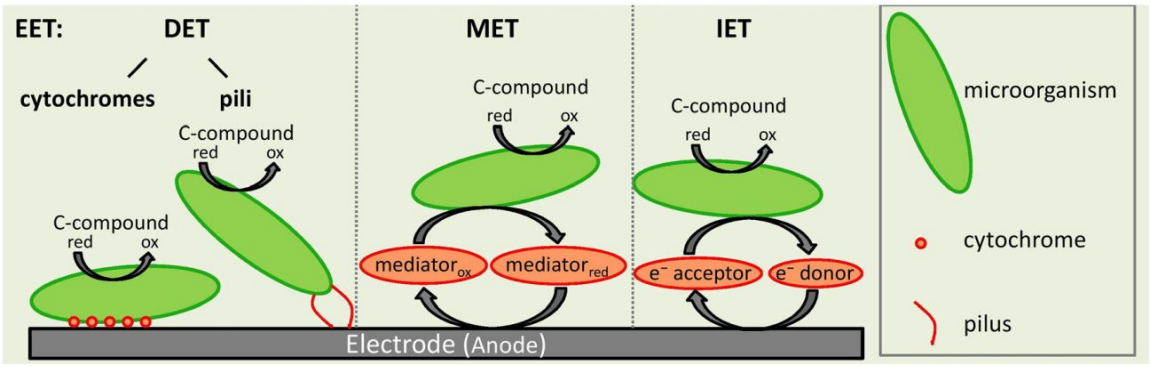

Figure 2: Electron transfer pathways of electroactive microorganisms exemplary for anodic processes Sydow et al. (2014).

and Nevin, 2013). However, MES from CO_2 also takes place at cathodic potentials as low as -600 mV (*vs.* Ag/AgCl), where no measurable hydrogen formation takes place and a DET is postulated (Nevin et al., 2010). Recently, Gildemyn et al. (2017) suggested that cathodic processes generally suffer from higher overpotentials than anodic processes. Abiotic hydrogen production cannot be thermodynamically excluded for any of the cathodic MES processes described thus far. Further data show that redox proteins such as hydrogenases adsorb to the cathode to catalyze hydrogen formation at a very low rate. Therefore it can be stated that there is most likely no DET reported so far for cathodic processes (Deutzmann et al., 2015).

2.1.2 Electroactive microorganisms

EAM do not belong to a specific ecological niche and can be found everywhere in the environment (Koch and Harnisch, 2016). Most probably all microorganisms can interact with an electrode in a certain way (Koch and Harnisch, 2016). The best studied EAM are without a doubt *S. oneidensis* and *G. sulfurreducens*, which are considered as model organisms for many BESs. One drawback is their very restricted product range. Therefore, *C. glutamicum* and *C. necator* are introduced to broaden the product spectrum of this study. Table 1 shows the differences of the described microorganisms and typical characteristics are discussed in more detail in this section.

Table 1: Comparison of the used electroactive microorganisms (EAM) in this study. Also their usual metabolism, biofilm building properties, typical application in bioelectrochemical system (BES) and extracellular electron transfer (EET) capabilities are summarized.

EAM	Metabolism	Biofilm	BES	EET
G. sulfurreducens	anaerobic	thick (> 50 µm)	MFCs, (MES)	DET
S. oneidensis	aerobic & anaerobic	monolayer	MFCs, MES	MET & DET
C. glutamicum	aerobic & anaerobic	-	MES	MET
C. necator	aerobic & anaerobic	-	MES	IET

Geobacter sulfurreducens

G. sulfurreducens, a dissimilatory metal- and sulfur-reducing microorganism was first isolated from surface sediments of a hydrocarbon-contaminated ditch in Norman (OK, USA) by the group of Caccavo et al. (1994). The microorganism can grow on a variety of organic substrates such as acetate under anaerobic conditions respiring with both, soluble electron acceptors (e.g. fumarate) and solid electron acceptors (e.g. iron(III) phosphate). *G. sulfurreducens* produces thick, multilayer biofilms (greater than 50 µm) and interacts directly with electrodes *via* membrane bound cytochromes (Schrott et al., 2011; Vargas et al., 2013). Aromatic amino acid containing pili are hypothesized to be responsible for this long-range electron transfer (Vargas et al., 2013). More cells per electrode area can thus contribute to the electron transfer. This is very interesting for MFCs, because besides the mentioned electron acceptors before, *G. sulfurreducens* can also respire with anodes producing power while breaking down the organic load of waste water (Nevin et al., 2008).

Cathodic processes and MES were also reported, but at rather low rates compared to MES with other EAM. However in comparison to anodic processes, other proteins are involved and only fumarate is reduced to succinate in the periplasmic space. Most likely no electrons are transferred into the cell (Dumas et al., 2008; Soussan et al., 2013). Furthermore, a CO_2 related reduction current was observed by Soussan et al. (2013) and a reaction with succinate to glycerol was postulated.

Shewanella oneidensis MR-1

S. oneidensis MR-1 was isolated in 1987 at the Oneida Lake (NY, USA) and characterized later by Venkateswaran et al. (1999). The strain can grow on organic substrates like lactate under aerobic and anaerobic conditions. Lactate is not oxidized fully to CO_2, but to acetate releasing four electrons under anaerobic conditions (Rosenbaum et al., 2010; Tang et al., 2007). These electrons can be transferred to soluble and solid electron acceptors similar to *G. sulfurreducens*. *S. oneidensis* is easier genetically accessible compared to *G. sulfurreducens* and several studies showed that the organism is capable to produce products with an unbalanced redox balance in unbalanced fermentations by releasing electrons to an anode (Bursac et al., 2017; Flynn et al., 2010). In contrast to *G. sulfurreducens*, *S. oneidensis* produces just a monolayer biofilm under anaerobic conditions (Rosenbaum et al., 2010). Dolch et al. (2014) reported a 3 to 70 fold decrease in attached *S. oneidensis* cells compared to *G. sulfurreducens* cells under similar conditions. Thicker biofilms are formed under aerobic conditions as shown by Rosenbaum et al. (2010). Furthermore, *S. oneidensis* produces flavins, which are used as a mediator between the electrodes and the microorganism improving the electron transfer (Section 2.1.1) (Canstein et al., 2008). *S. oneidensis* is known for its versatile respiration using soluble and

solid electron acceptors. External mediators (redox active compounds) such as flavins are secreted by the microorganism to enhance extracellular electron transport (Marsili et al., 2008). Similar to *G. sulfurreducens* also cathodic processes are described and also the reduction of fumarate to succinate in the periplasmic space can be performed at low rates (Ross et al., 2011).

Corynebacterium glutamicum

C. glutamicum is the main industrial producer of lysine and is able to produce other products such as organic acids, diamines and biofuels mainly under aerobic conditions (Becker and Wittmann, 2012). The high oxygen demand limits the scale-up of processes into larger scales and leads to high investment costs. One way to overcome this limitation may be to enhance anoxic growth and production of these compounds (Vassilev et al., 2018). The lysine producing strain *C. glutamicum lysC* was characterized and used for anaerobic lysine and organic acid production in a BES using an anode es electron sink (Kim et al., 2006; Vassilev et al., 2018).

Cupriavidus necator

C. necator was formerly known as *Ralstonia eutropha* and is able to grow on a variety of substrates in a heterotrophic and autotrophic way. The microorganism is capable of fixing CO_2 using hydrogen as an electron donor and oxygen as an electron acceptor (therefore it is also called "Knallgas" bacterium). In the 1970s, the strain was mainly investigated due to its efficient polyhydroxybutyrate (PHB) and single cell protein production (Calloway and Kumar, 1969; Repaske and Mayer, 1976; Schlegel et al., 1961). It is a genetically accessible microorganism (Gruber et al., 2015), which is capable of aerobic CO_2 fixation to produce organic compounds such as isopropanol (Grousseau et al., 2014; Marc et al., 2017; Nybo et al., 2015). Besides isopropanol, also the autotrophic production of methyl ketones *via* acetoacetyl-CoA, a precursor of PHB, has been described in a ΔPHB strain (Müller et al., 2013). Therefore, this microorganism is interesting for expanding the product spectrum of MES, because hydrogen and oxygen needed as electron donor and electron acceptor, respectively, can be produced electrochemically *in situ* by water splitting (Li et al., 2012; Liu et al., 2016; Schlegel and Lafferty, 1964; Sydow et al., 2017a; Torella et al., 2015).

The microorganism can not really be categorized into being a cathodic or anodic microorganism, since it is able to grow on a mixture of CO_2, cathodically produced hydrogen and oxygen, which is simultaneously produced electrochemically at the anode (Liu et al., 2016; Schlegel and Lafferty, 1971; Torella et al., 2015). Despite that fact, electrobiotechnological productions with this microorganism should be categorized as MES according to Schröder et al. (2015).

2.2 Reactor concepts for bioelectrochemical systems

In the following section common reactor concepts used as BESs are introduced. Besides the different reactor types also components of the systems like electrode materials, reference electrodes, separators and their positioning is discussed. Important parameters to characterize these systems as well as fluid dynamics in those kinds of reactors are presented.

2.2.1 Requirements on components of bioelectrochemical reactors

Several electrode materials for BESs have been reported so far and were collected and reviewed in Krieg et al. (2014) at the start of this study . The chosen materials depend on the application and can be divided into ones used for cathodic and anodic processes. In general electrodes need to be inert and should not corrode during the process at the used potentials. Engineered composite electrodes consisting of a metal backbone with a carbon coating combining high conductivity with excellent biocompatibility are most attractive towards application (Guo et al., 2015). Besides electrodes further components such as separators (e.g. membranes) are important and used to maintain redox gradients preventing chemical short circuits in BESs.

Anode materials

Carbon based anode materials for MFCs have been extensively screened by Kipf et al. (2013). A carbon fabric called C-Tex 13 (knitted activated carbon cloth) showed the highest current densities of the materials investigated and was superior to graphite foil and felt, carbon paper and other activated carbon clothes. Graphite fiber brush anodes are reported as a highly promising material enabling high power outputs in MFCs (Logan et al., 2007). One of the advantages of carbon based anodes is the fact that they can be derived from natural sources. For instance the use of carbonized kenaf stems and carbonized corrugated cardboard as anodes for MFCs has been reported (Chen et al., 2012a,b).

Besides carbon based anodes also the use of metal anodes has been discussed as being beneficial in terms of specific conductivity and electrode costs (Baudler et al., 2015). Anodes made of different metals such as copper, stainless steel and others were characterized on a mixed acetate grown MFC and *Geobacteracea* dominated the community (Baudler et al., 2015). Copper was identified as metal anode superior to graphite in terms of maximum current achieved and biofilm thickness.

For MES usually graphite sticks and other carbon based materials are used (Marshall et al., 2012; Nevin et al., 2010). Depending on the potential and the material being used the reaction at the anode produces usually oxygen, which can be toxic for strictly

anaerobic microorganisms. Growth and production processes based on *C. necator* depend on oxygen as electron acceptor. In these cases, dimensional stable anodes with iridium catalysts, which catalyzes oxygen evolution can be applied (Sydow et al., 2017a).

Cathode materials

Cathode material choice itself is highly depending on the respective application. In MFCs oxygen reduction is often done using "air-breathing" or more general gas diffusion cathodes. For gas diffusion electrodes all states of matter are important: gas, in most cases oxygen, can diffuse from the surrounding air into the cathode and reacts with a catalyst (often platinum, but also manganese based catalysts can be used) and electrons to water. A detailed overview of gas diffusion electrode applications in BESs can be found in Horst et al. (2015).

For MES, one must distinguish the nature of electron transfer mechanisms: microorganisms need direct contact with the cathode for a sufficient electron supply if they grow as a biofilm. Usually carbon based materials are used for cathodic processes in MES. Modification of the surface with different materials has led to increased productivity due to a higher electrochemically active surface area and a better biofilm growth on these cathodes (Zhang et al., 2013). For MET, an electrode material has to be used on which the mediator does not adsorb and where the mediator can be regenerated effectively (Kipf et al., 2013).

Especially for an IET *via* hydrogen, electrodes with a low overpotential towards hydrogen evolution should be used. Platinum has excellent properties for hydrogen evolution and lowest overpotentials (Kadier et al., 2014). The biggest drawback is its prize, which makes a commercial use unlikely. A substitute for platinum might be cathodes containing nickel, molybdenum and zinc or stainless steel, which have been used for isopopanol production in MES with *C. necator* (Torella et al., 2015).

Reference electrodes

Potentials are a relative measuring unit. International convention is that the electrochemical equilibrium of hydrogen and protons at standard conditions (p=1 bar, T=298.15 K, pH=0) is declared 0 V. The redox system is called standard hydrogen electrode (SHE) and practically set to 0 V at all temperatures. This electrode setup is rather impracticable for the use in experiments. Therefore, electrodes of the second type are used for potential measurements. Metal electrodes have a constant potential towards their corresponding not readily soluble salts (Sawyer et al., 1995). Most common examples are silver/silver chloride (Ag/AgCl, KCl saturated) or calomel (Hg/Hg_2Cl_2, KCl saturated) electrodes, which have a potential of +199 mV and +244 mV, respectively, *vs.* the standard hydrogen electrode (Sawyer et al., 1995). All potentials in this study are given *vs.* Ag/AgCl

(KCl saturated).

Separators

Separators are often necessary to maintain a redox gradient between electrodes in BESs (Harnisch and Schröder, 2009; Leong et al., 2013). Side reactions need to be prevented and separators need to keep anode and cathode solutions from each other in order to prevent crossover reactions. Furthermore, they need to be conductive for ions, because one ion needs to be transferred between the anode and the cathode compartment for each electron transferred *via* the external circuit (Harnisch and Schröder, 2009). Many materials have been proposed as separators in BESs. The most common materials are polymer electrolyte membranes. Nafion® is the most frequently used membrane on the market and thus being used for separation in this study. Drawbacks of separators in BESs are often higher internal resistances of the system. However, membranes can be used for *in situ* product removal in MES implementing the product purification and concentration into the process (Gildemyn et al., 2015).

Positioning and dimensioning

Positioning of the specific BES components, for example, the distance between the anode and the cathode, is crucial for effective characterization and operation (Zhang et al., 2014). Large distances between electrodes, the need of separators, and relatively low conductivities of media (e.g. waste water compared to an electrolyte) lead to ohmic losses, which increase with distance (Janicek et al., 2014). Additionally, maximum power densities decrease with increasing anode surface area in MFCs (Dewan et al., 2008). Therefore, compact reactor designs and the use of multiple electrodes are needed for process intensification (Ahn and Logan, 2012; Rader and Logan, 2010). The specific cathode area (area per liquid volume) is a crucial factor for MFC scale-up (Cheng and Logan, 2011). Under specific conditions, a doubling of the cathode size was predicted to increase the performance by 62%, *vs.* only 12% for doubling the size of the working electrode, where the biological oxidation was conducted. Systems using a double cathode separated by a glass fiber, supported by a plastic mesh encasing a brush anode, showed up to 135% more power production compared with systems using membrane separators (Zhang et al., 2011b). Internal resistances were reduced using this separator electrode assembly even in larger reactors compared with smaller ones (Ahn and Logan, 2012). Membrane-free systems using gas diffusion cathodes showed improved power densities compared to similar systems separated by a membrane (Liu and Logan, 2004). Realized surface-to-volume ratios (up to 100 m^2 m^{-3}) are thoroughly reviewed for reactors larger than 1 L (Janicek et al., 2014). At the laboratory scale, even higher values are possible, but a transfer to bigger scales has not been achieved yet.

2.2.2 H-cell reactors - the workhorse for bioelectrochemistry

H-cell reactors got their name, because they look like an "H" when they are assembled (Figure 3). The two electrode compartments are usually separated by a membrane and are used for basic studies of BESs. In most cases two glass bottles are modified with a flanch, where the membrane is clamped between the bottles. Several studies have been conducted in these types of cells such as the first MES from CO_2 (Nevin et al., 2010) or other basic studies in the field (Lohner et al., 2014). One drawback of these systems is that they are usually not controlled in terms of pH and mixing. Furthermore, rather high internal resistances are caused due to large electrode spacings increasing the overall cell voltage (Giddings et al., 2015). Therefore, the reaction system can not be used for a scale-up of electrobiotechnological processes (Verstraete et al., 2006).

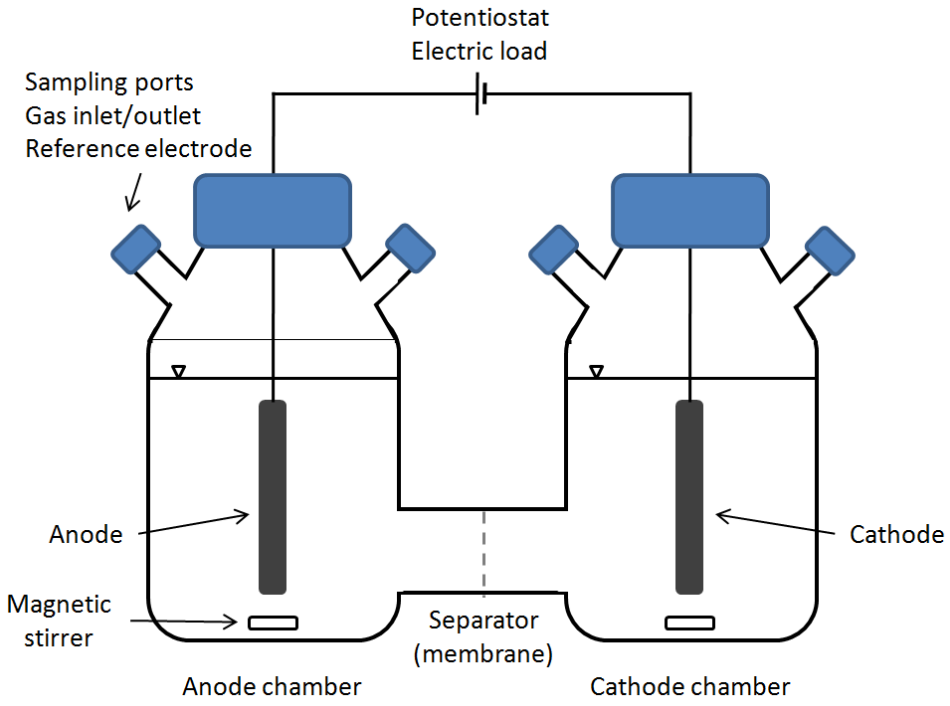

Figure 3: Scheme of an H-cell.

2.2.3 Flat-plate, cubic and other reactors for microbial fuel cells

Flat-plate and cubic reactors (Figure 4) are usually used for MFCs or MECs with an air-breathing cathode (Cheng et al., 2006; Escapa et al., 2015). These reactor types are usually made of plastics such as polyetheretherketone (PEEK) or poly carbonate (PC), which have a good chemical stability (Verstraete et al., 2006). An advantage of PC over PEEK is, that the material is translucent and e.g. biofilm formation can be examined. The advantage of PEEK over PC is its stability and possibility to sterilize the material with an autoclave. Usually gas diffusion electrodes with a catalyst suitable for oxygen reduction

to water are used as cathodes. More details are given in Section 2.2.1. In contrast to H-cells, the electrode spacing is more narrow and by this the internal resistance is reduced. A membrane is not needed in this system, however, it has been shown that the current efficiency increases since oxygen diffusion to the anode is hindered or reduced (Liu and Logan, 2004). It has been shown that the performance of MFCs is limited by the metabolic activity of EAM and electrochemical systematic constraints such as overpotentials at the electrodes or IR losses. Aside from that, increased mass transport seems to increase MFC and MEC performance by altering the flow setups and consequently directing the flow through porous anodes (Cheng et al., 2006; Sleutels et al., 2011, 2009).

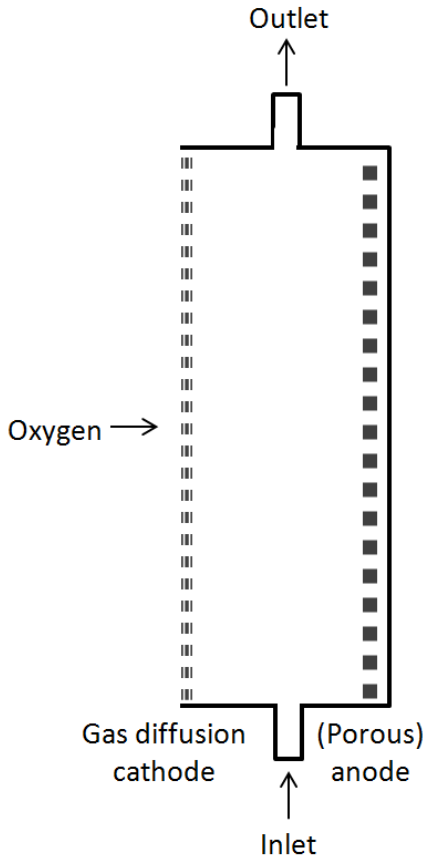

Figure 4: Scheme of a single-chamber MFC with an air-breathing cathode.

2.2.4 Modified bioreactors forming electrobioreactors

Besides the reactor concepts described in the sections before, special reactors for BESs were developed recently (Figure 5). It has been proposed, that for electrochemically influenced cultivations better mixed systems may be needed, especially, if mediators are used and mass transport is limiting (Hintermayer et al., 2016). Furthermore, comparison between studies is improved by the use of more standardized and well-characterized systems such as bioreactors, which can be modified to electrobioreactors (Rosa et al., 2016). Rosa et al. (2016) showed that cultivations in electrobioreactors show smaller standard

deviations compared to cultivations performed in non-controlled three-kneck flasks, which are commonly used in electrochemistry.

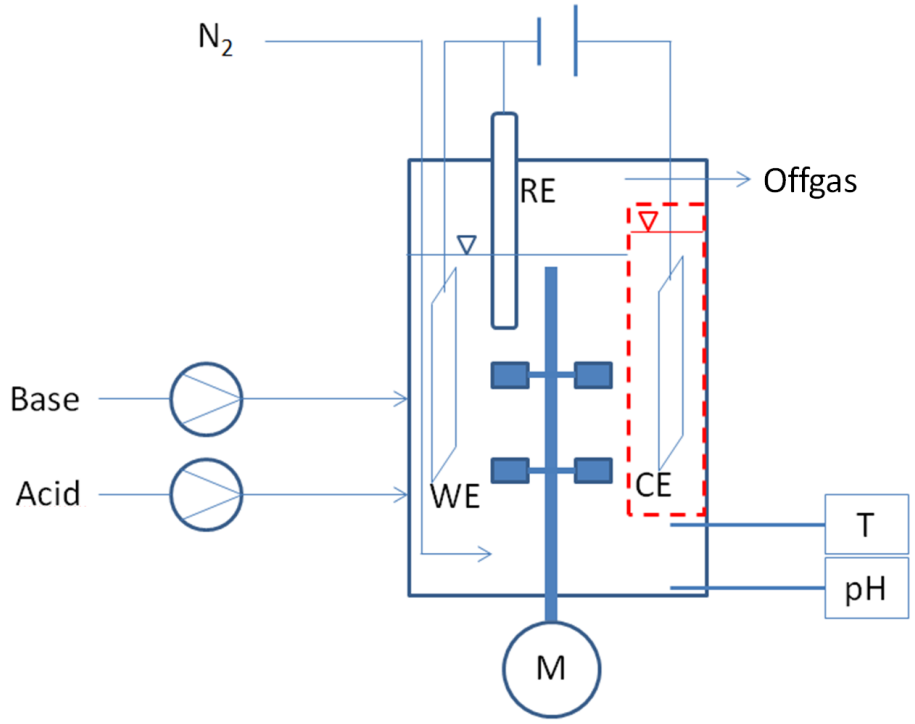

Figure 5: Scheme of a bioreactor modified with inserts to form an electrobioreactor, which can be operated under separated and non-separated conditions. WE: working electrode, CE: counter electrode, RE: reference electrode, T: temperature control, pH: pH control, M: stirring unit.

2.2.5 Characterization and scale-up of bioelectrochemical reaction systems

Bioelectrochemical reaction systems are characterized by different values derived from electrochemistry and biotechnology. For fuel cell applications especially, the power output (P) in W can be calculated from the current (I) in mA and the cell potential (E) in V (Equation 2).

$$P = E \cdot I \tag{2}$$

The power output is often normalized to the active electrode area (or alternatively reactor volume) for calculation of the power density (P_A) in W m^{-2} or W m^{-3}, respectively (Equation 3).

$$\text{a) } P_A = \frac{P}{A_{Electrode}} \qquad \text{b) } P_V = \frac{P}{V_{Reactor}} \tag{3}$$

Coulombic efficiencies (CE) in % is the ratio of the charge actually transferred between

electroactive microorganisms and the working electrode *vs.* the theoretical charge obtained or found in the respective amount of substrate or product n. The amount of actually transferred electrons z and the Faraday constant (F, 96485 C mol^{-1}) are also needed to calculate the CE as shown in Equation 4.

$$CE = \frac{Q_{measured}}{Q_{theoretical}} = \frac{\int_0^t Idt}{nzF} \tag{4}$$

Only few BESs, especially MFC and MEC type ones, are close to industrial applications. Initial commercial systems are distributed by companies such as Emefcy for waste water treatment and subsequent energy production (http://www.emefcy.com). Furthermore, benthic MFCs, which are intended to operate as long-term power sources in aquatic environments to power nautical devices such as moored buoys, have been reported as near commercial operation (Nielsen et al., 2007; Sajana et al., 2014). Other BESs, such as those for enzymatic or microbial electrosynthesis, are still in their infancy, with industrial application far off. General scale-up challenges for MFCs are finding low-cost electrode materials and implementing compact separated reactor designs (Ahn and Logan, 2012). As an alternative to scale-up, an increase of productivities can be achieved by increasing the number of basic cell units (numbering-up) (Gálvez et al., 2009). Connecting them to stacked reactors in series or parallel can lead to improved power output and current generation (Zhuang et al., 2012). However, the last cells in a serial connection will have lower productivities due to decreased substrate concentrations (Janicek et al., 2014). The performance of different reactor designs (e.g. tubular *vs.* flat-plate, separated *vs.* non-separated reactors) and different process modes (batch *vs.* continuous) with a volume from 1 L to 1000 L has been thoroughly reviewed by Janicek et al. (2014). To date, most of the systems investigated are tubular shaped and flat-plate designs. As an alternative, systems with multiple electrodes can be used to ensure good positioning of components. There is also a method to use multiple electrodes for avoiding the ohmic losses and edge effects that disturb the electric field and result in enhanced power densities (Dewan et al., 2008; Jiang et al., 2011). Stackable reactor systems seem to be the most suitable design concept so far, achieving target volumes by increasing the number of stacked units. These individual reactors can have well-characterized performances, which also allows for an easy estimation of overall productivity. One of the largest BES to date is an MEC pilot plant with a volume of 1000 L, which was used to produce hydrogen and methane at the cathode powered by a microbial anode (Cusick et al., 2011). The experience of the most recent tests showed that the process performances at the technical scale are well below that of small-scale devices (Cusick et al., 2011). This may be due to the effects of inoculation and enrichment procedures, as well as process control, variation of natural feedstocks (e.g. varying concentrations, absence of substrates and others) and long-term stability issues of the materials used for separators and electrodes (Cusick et al., 2011; Leong et

al., 2013). For MES applications, the modification of bioreactors to electrobioreactors has been proposed recently (Hintermayer et al., 2016; Rosa et al., 2016). However, the highest volumes are in the low liter range to date and a thorough characterization in terms of fluid dynamics and electrochemical losses needs to be done.

2.2.6 Fluid dynamics in (electro)bioreactors

Characterization and improvement of fluid dynamics has been shown to be a powerful tool to improve biotechnological processes (Sharma et al., 2011). Especially in the field of cell culture and tissue engineering, where shear stress has a great impact on the performance processes, computational fluid dynamics (CFD) helped to optimize these processes (Dusting et al., 2006). In conventional bioreactors where high Reynolds numbers are reached, turbulence is considered high enough to prevent dead zones and a sufficient supply of oxygen in aerobic processes or nitrogen to drive out oxygen in anaerobic processes is ensured. Bioreactors have been equipped with electrodes probably altering the fluid dynamics in these reactors (Hintermayer et al., 2016; Rosa et al., 2016).

For BESs flow dynamics have been especially studied in terms of applying baffles or altering the anode geometry (Kim et al., 2014). The use of porous anodes and a flow through the anode (working electrode) increased the power output in these systems and the internal resistance was reduced by most likely increasing the mass and charge transport speed (Cheng et al., 2006; Sleutels et al., 2011). Hydrodynamics of different anodes (graphite and stainless steel plates, graphite granules and meshs) were simulated using 2D computational fluid dynamic simulations (Vilà-Rovira et al., 2015). Peclet number profiles indicated that mass transfer was achieved by dispersion or diffusion rather than convection. This study shows that spatial heterogeneity in bioanodes exists and is lowered by using meshes or granular setups (Vilà-Rovira et al., 2015). Further studies show that porous bio-electrodes with greater specific surface areas do not necessarily produce more current, as long as convection through the pores is absent (Picioreanu et al., 2010).

2.3 Status quo of microbial terpenoid production

In the following section the theoretical background on the biotechnological production of terpenoids is given. Metabolic details on synthesis starting at different substrates and possible microorganisms of choice are introduced.

2.3.1 Terpenoids

Terpenes are olefinic hydrocarbons with the chemical formula $(C_5H_8)_n$ derived from the organic compound isoprene and therefore assigned to the isoprenoids. Structural properties are described by the ispoprene rule dividing terpenes into classes based on the number of isoprene units (C_5) in the compound (Ruzicka, 1953). Terpenes are distinguished in hemi- (C_5), mono- (C_{10}), sesqui- (C_{15}), di- (C_{20}), tri- (C_{30}), tetra- (C_{40}) and polyterpenes (C_n, $n > 40$). The biologically activated isoprenes isopentenyl pyrophosphate (IPP) and dimethyl-allyl pyrophosphate (DMAPP) are the universal precursors of all terpenes. Derivatives of terpenes with functional groups (OH-, etc.) are called terpenoids. Terpenoids are interesting compounds due to their high biological activity for several industries. They can be used as additives in fragrances due to their smell or drugs due to their high biological activity (George et al., 2015). Especially the latter application is of great interest, because terpenoids are precursors for drugs, which cure several diseases such as malaria with the drug artemisinin or several cancer types using taxol (Chang and Keasling, 2006; Ro et al., 2006). Further terpenoids, e.g. limonene, pinene and farnesene, have been reported to be precursors for possible biofuels or can be even used directly as diesel fuel, respectively (Zhang et al., 2011a).

2.3.2 Biosynthesis and biotechnological production of terpenoids

Terpenes are synthesized in nature *via* two pathways providing the two biologically activated isoprenes IPP and DMAPP: the mevalonate (MVA) and the 1-deoxy-D-xylulose 5-phosphate (DXP) pathway. The MVA pathway is usually found in eukaryotes including plants and some bacteria and the DXP pathway can be found in most bacteria (Kuzuyama, 2002). After IPP and DMAPP are formed, the carbon units can be condensed *via* prenyltransferases to form geranyl pyrophosphate (C_{10}, GPP), farnesyl pyrophosphate (C_{15}, FPP) and geranylgeranyl pyrophosphate (C_{20}, GGPP). Terpene synthases then convert the pyrophosphates into the different terpenes as mentioned before (Zhang et al., 2011b) (Figure 6).

Terpenoids can be produced heterologously using glucose, glycerol and other substrates in several engineered microorganisms such as yeast, *Escherichia coli* or *Pseudomonas putida* (Alonso-Gutierrez et al., 2013; Fischer et al., 2011; Mi et al., 2014). This is usually accomplished by the heterologous expression of the mevalonate pathway or by

upregulation of the native DXP pathway (Ajikumar et al., 2010; Sonntag et al., 2015). The first strategy mentioned is, however, the method of choice due to tight regulations of the native DXP pathways (Zhao et al., 2013). One of the limitations in biotechnological production is the toxicity of terpenoids and/or accumulating intermediates during synthesis towards the host. Especially monoterpenoids can be toxic for many microorganisms, because they intercalate into the membrane (Trombetta et al., 2005). Process engineering and *in situ* product removal to overcome toxicity and product inhibition increased production rates tremendously (Mirata et al., 2009; Schewe et al., 2015; Sonntag et al., 2015).

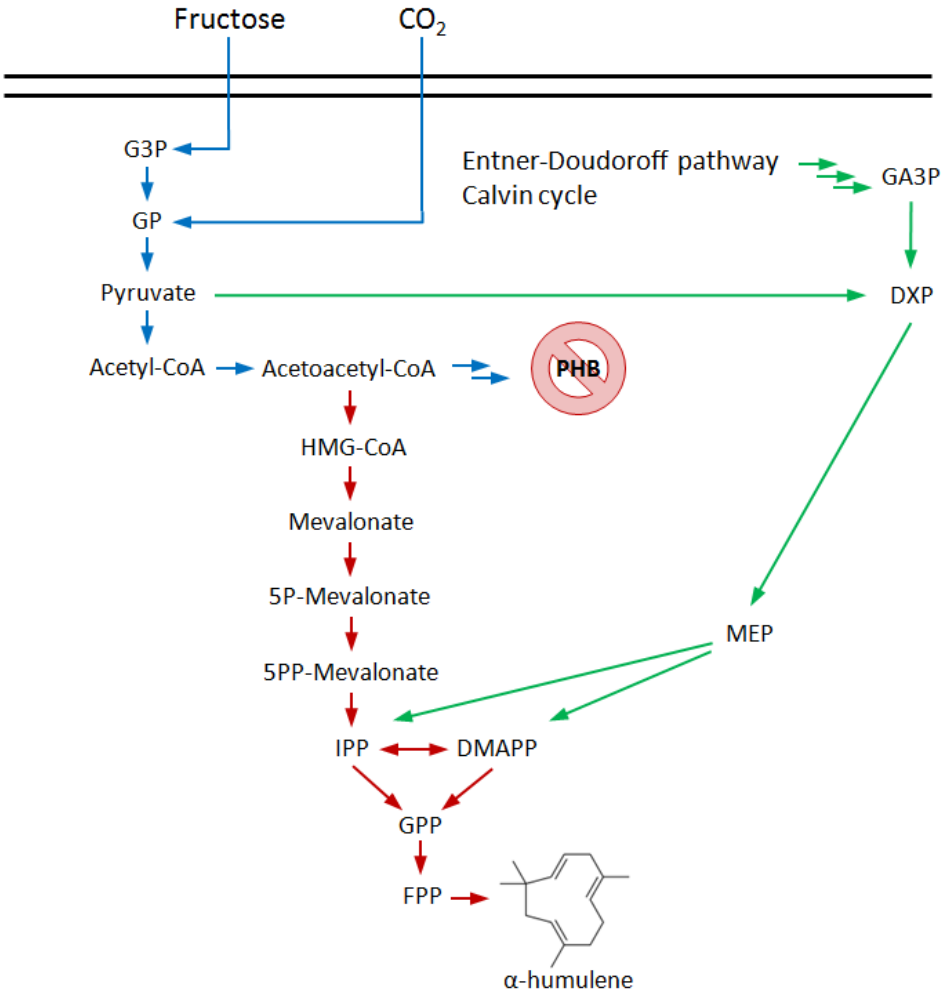

Figure 6: Metabolic pathway of α-humulene production in *C. necator* with the MVA pathway (red) and the DXP pathway (green) adapted from Grousseau et al. (2014) and Sonntag et al. (2015). CO_2 is assimilated *via* the Calvin cycle, which leads to glycerate-3-phosphate (GP). Fructose is catabolized through the Entner-Doudoroff pathway, which leads to glyceraldehyde-3-phosphate (G3P) and pyruvate. Carbon is usually stored in polyhydroxybutyrate (PHB) or may be used for terpenoid production starting at acetoacetyl-CoA. Enzymes of the mevalonate pathway operon are from *Myxococcus xanthus* (red), farnesyl pyrophosphate (FPP) synthase ERG20 (blue) is from *Saccharomyces cerevisiae* and terpene synthase ZSSI (green) is from *Zingiber zerumbet* as described by Sonntag et al. (2015).

2.3.3 Properties of the sesquiterpene α-humulene

The terpene α-humulene, also known as α-caryophyllene, is built from three isoprene units (precursor: FPP, $C_{15}H_{24}$) and therefore categorized as sesquiterpene (Figure 6). Sesquiterpenes belong together with hemi- and monoterpenes to the low molecular, very volatile terpenes. The high volatility is caused by their low volumetric enthalpy of evaporation. α-Humulene has anti-microbial properties by intercalating in membranes due to its high hydrophobicity (Trombetta et al., 2005). Hydrophobicity is often described by the octanol-water partition coefficient (log P_{OW} value). Compounds with log P_{OW} values between 1 and 5 are considered toxic for microorganisms (Heipieper et al., 1994). The solubility of α-humulene in water is poor (0.014 mg L^{-1} at 25°C) and it has a rather high log P_{OW} value of 6.6 (material safety and data sheet, Sigma Aldrich, St. Louis, MO, USA).

Potential applications of α-humulene are in medicine due to its anti-inflammatory, antibacterial, anti-cancerogenic and appetite-suppressing properties (Fernandes et al., 2007; Passos et al., 2007). Furthermore, it is a precursor for zerumbone, which has potent anti-cancerogenic activities. Zerumbone can be obtained by a simple one-step oxidation from α-humulene (Alemdar et al., 2017). To date zerumbone and α-humulene are produced commercially by extraction of plants (Alemdar et al., 2017). It is mainly found in the essential oil of *Humulus lupulus* (hops), *Zingiber zerumbet* (shampoo ginger) and *Eugenia caryophyllata* (clove) (Bernotienë et al., 2004; Yu et al., 2008). Besides extraction from plants, chemical synthesis routes have been developed. Oftentimes terpenoids such as farnesol are substrates for these routes and need to be extracted from plants anyway (Corey et al., 1993). Rather toxic catalysts are used for the extraction and need to be replaced in order to create a sustainable bioeconomy (Hu and Corey, 2002; McMurry et al., 1987; Miyaura et al., 1984; Takahashi et al., 1983). Therefore, alternative routes analogously to nature from sustainable substrates such as CO_2 need to be established. This can be achieved by the heterologous production in microorganisms using biotechnological methods.

Recently, α-humulene was produced with *Methylobacterium extorquens* from methanol as sole carbon and energy source (Sonntag et al., 2015). Introduction of a codon optimized α-humulene synthase from the ginger plant *Zingiber zerumbet* in combination with a farnesyl pyrophosphate (FPP) synthase from *Saccharomyces cerevisiae* and a prokaryotic mevalonate pathway from *Myxococcus xanthus* providing the precursors led to concentrations up to 18 mg L^{-1}. Process engineering in a bioreactor with methanol-limited fed-batch cultivation further increased the maximum concentration to 1.65 g L^{-1} by simultaneously increasing the cell dry weight, which indicated a biomass dependent production of α-humulene. One of the advantages in using compounds such as methanol as a substrate is that this carbon source does not compete with food such as sugars (Sonntag

et al., 2015). Alternative anorganic substrates to methanol such as CO_2 may be also interesting to increase the flexibility in processes based on C_1 compounds. A scheme of the mevalonate pathway and a brief overview of the DXP pathway including heterologous genes are shown in Figure 6 on the basis of *C. necator*.

2.3.4 Terpene production with *Cupriavidus necator* in microbial electrosynthesis

C. necator is an interesting microorganism for biotechnological processes due to its versatility towards various substrates and its flexible production routes (Figure 6) to produce recombinant proteins or bioplastic (PHB) (Kahar et al., 2004; Schlegel and Lafferty, 1971; Srinivasan et al., 2003). Its genome is sequenced and several genetic tools are published making a genetic modification of the microorganism possible (Gruber et al., 2014; Pohlmann et al., 2006). *C. necator* has a great potential as bioproduction platform of interesting products such as isopropanol, alka(e)nes and methyl ketones from various substrates including CO_2 (Crépin et al., 2016; Grousseau et al., 2014; Müller et al., 2013). Acetoacetyl-CoA is the precursor of all the mentioned products (Figure 6) and is also the starting point for the mevalonate pathway from which terpenes are derived.

In the 1970s, an interesting polyhydroxybutyrate-negative phenotype of *C. necator* PHB^- was reported and characterized in detail recently (Raberg et al., 2014; Schlegel and Lafferty, 1971). PHB is synthesized with three enzymes located in the *phaCAB* operon. *C. necator* PHB^- has a mutation in the first *phaC* gene, which is essential for PHB synthesis in contrast to the two other enzymes involved (Raberg et al., 2014). PHB deficient *C. necator* strains served as starting point for several engineering strategies for heterologous protein production and the precursor acetoacetyl-CoA is efficiently rerouted to alternative products. In addition to the down regulation of the PHB production, the pathway to PHB *via* acetoacetyl-CoA can be up regulated under nutrient limiting conditions, especially by limiting the nitrogen source (e.g. ammonium sulfate, Grousseau et al. (2014)).

3 Objectives of this study

There are many open questions to be solved to implement stable and economically feasible processes into a future bioeconomy. BES may be key for a transition and therefore this study was initiated to get more insight into different reactor concepts and process design for BESs. Improvement strategies have to include aspects of biotechnology, electrochemistry and engineering to break down and investigate influencing factors. At the beginning of this study, a flow scheme (Figure 7) with four stages for a knowledge-based rational process design for BESs was proposed in Krieg et al. (2014). Key issues of different BESs were identified at the start to gain more insight into relevant parameters.

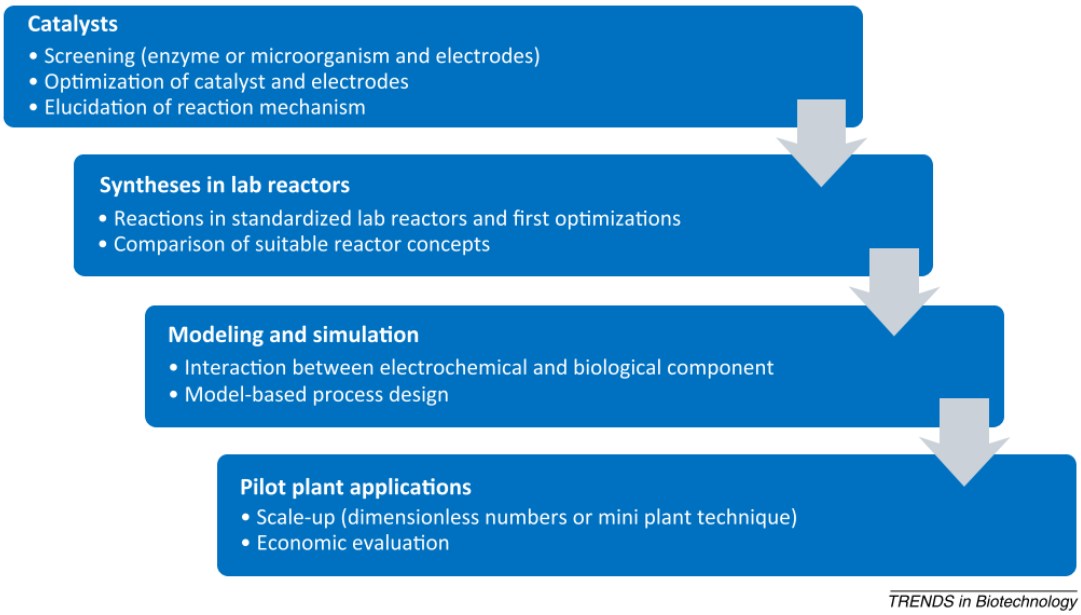

Figure 7: Flow scheme for a knowledge-based rational process design for BESs (Krieg et al., 2014).

The focus and goals of this study are set to the first three stages:

i) Catalysts

- comparison of different electroactive microorganisms in various BESs
- elucidation of catalyst and electrode interaction using the designed MFC as model system

ii) Synthesis in lab reactors

- design of a flat-plate microbial fuel cell (MFC) reactor
- development and characterization of an electrobioreactor based on a conventional bioreactor
- comparison of EAM in different reactor concepts

iii) Modeling and simulation

- modeling and simulation of flow regimes in the reactors to elucidate dead zones and flow distributions
- use simulation results to help interpret and explain experimental results

The tasks mentioned in the last stage in Figure 7 were no objective of this study and have been performed just recently (Christodoulou and Velasquez-Orta, 2016; Harnisch et al., 2015). For stages i) to iii), the following challenges of the respective BESs are defined to be addressed in this study. By this purpose, different aspects of biotechnology, electrochemistry and engineering should be investigated and parameters for improved overall BES performance should be defined.

In order to run a "proof of principle" BES for later characterization H-cells need to be characterized at the start of this study. As H-cells are available and commonly used for BESs, no design is needed for this reactor concept. However, as a first goal of this study a thorough electrochemical and bioelectrochemical characterization should be performed using the "standard" electroactive bacteria *Shewanella oneidensis* and *Geobacter sulfurreducens* in order to compare the later developed and characterized reactors to the standard BES H-cell as described in step ii) of the process design.

Performance of MFCs can be increased by altering the flow setups in flat-plate and cubic reactor types as described in Section 2.2.3. In this study, the described phenomena should be investigated in-depth in the light of the proposed knowledge-based rational process design (Figure 7). Such a flexible reactor should be designed allow variations of the inlet setup and evaluate the influence of directing the flow through a porous carbon fabric anode. *G. sulfurreducens* should be used as EAM for investigation of the MFC performance as it is the dominant bacterium in MFCs based on mixed cultures isolated from waste water streams. Finite element method (FEM) simulations should be used to help interpret the experimental results as described in Figure 7 (step iii)).

Biotechnological processes are usually conducted in stirred tank reactors (STRs), which are standardized and therefore comparable between laboratories (Section 2.2.4). To date every working group in the field of electrobiotechnology designs and engineers their own electrobioreactors, which makes comparison of experimental results hard. As a further goal of this study a STR should be modified reversibly with electrodes being then able to perform BESs in these standard reactor concepts of biotechnology taking their advantages into the field of electrobiotechnology. Therefore, assemblies hosting electrodes should be designed made of a non-conductive material such as polyetheretherketone (PEEK). Furthermore, the lid should be modified to allow electrical contact of the electrodes and the insertion of a reference electrode (RE). The formed electrobioreactor should be characterized electrochemically, bioelectrochemically with *S. oneidensis* and in terms of fluid dynamics (mixing times and flow profiles) according to step iii), which may be altered

due to the inserted assemblies. A comparison of the performance of electrobioreactors to membrane-separated reactor concepts commonly used in BESs such as H-cells is also still missing and should be therefore investigated in this study. During the process of this study other working groups proposed modification kits for STRs (Hintermayer et al., 2016; Rosa et al., 2016; Vassilev et al., 2018). This allows a good comparison and discussion of the electrobioreactors. Furthermore, the anoxic production of lysine and organic acids from glucose with *Corynebacterium glutamicum* should be investigated to further proof the applicability of the modified STR and to compare it with an externally developed electrobioreactor in smaller scale (Vassilev et al., 2018).

For the process stage "Catalysts" i) the main goal is the engineering of (electroactive) microorganisms being able to produce more valuable products. To date, the products of MES are rather limited to simple organic compounds up to three C-atoms such as acetate or isopropanol. In this study a proof of principle synthesizing complex and valuable compounds such as terpenoids from CO_2 should be demonstrated. The work from Sonntag et al. (2015) served as a starting point for the investigations to produce α-humulene from CO_2 by MES using *C. necator* (Section 2.3.1). The heterologous pathway described in Sonntag et al. (2015) should be integrated into *C. necator* PHB^- (further referred to as *C. necator* for simplicity). Characterization of heterotrophic, autotrophic and electroautotrophic production of α-humulene with *C. necator* should be performed to compare production rates of a conventional cultivation with MES to identify bottlenecks of the process.

The overall aim of this study is to provide more knowledge in the first three stages of a knowledge-based rational process design for BESs as illustrated in Figure 7 and link the results to gain improved BESs.

4 Materials and Methods

All chemicals were purchased from VWR, Sigma-Aldrich and Fisher Scientific with a purity of 99 % or higher if not stated otherwise.

4.1 Materials

Materials used in this study including microorganisms, buffers and cultivation media are listed in this section.

4.1.1 Microorganisms

Shewanella oneidensis MR-1 (ATCC 700550, obtained from the American Type Culture Collection, Manassas, VA, USA) was used for the characterization of the different electrobioreactors in this study.

MFC experiments were done with *Geobacter sulfurreducens* DSM 12127 obtained as an active culture from the Leibnitz-Institut Deutsche Sammlung von Mikroorganismen und Zellkulturen GmbH (Braunschweig, Germany).

The lysine-producing strain *Corynebacterium glutamicum lysC* was kindly provided by Prof. Dr. Christoph Wittmann (Institut für Systembiologie, Universität des Saarlandes, Saarbrücken, Germany). This mutant has a single nucleotide exchange (S301Y) in the gene encoding the aspartokinase, resulting in the biosynthesis of lysine being uncoupled from feedback inhibition (Kim et al., 2006). The strain was used in the designed electrobioreactor for anaerobic organic acid production.

Escherichia coli S17-1 λpir (Biomedal, Sevilla, Spain) was used for the cloning and conjugation of the plasmids into *Cupriavidus necator*.

Cupriavidus necator PHB$^-$ DSM-541 was obtained from the Deutsche Sammlung von Mikroorganismen und Zellkulturen GmbH (Braunschweig, Germany). The strain is named as *Cupriavidus necator* in the study for simplicity and was used for the heterologous production of α-humulene.

4.1.2 Buffers and solutions

All media and media stock solutions were autoclaved at 121°C for 20 min if not stated otherwise. Sterile filtered (0.2 µm) antibiotics were added to the media if needed.

Agar plates

For agar plates a total concentration of 15 g L^{-1} agar-agar was used and added to the respective medium. Plates for selection were done by adding 1.5 mL L^{-1} of the tetracycline stock solution at a temperature below 65°C prior casting to obtain plates with a final concentration of 15 µg mL^{-1}.

Gibson master mix

Gibson master mix contained in mM: 500 Tris-HCl, 50 $MgCl_2$, 50 Dithioerythrole (DTT), 5 $NAD^+ + H^+$, 10 dNTPs and 25 % (v/v) PEG-8000 and was prepared on ice and either used directly after preparation or was immediately frozen and stored at -20°C.

Lysogeny broth (LB) medium

LB-medium contained the following components in g L^{-1}: 5 yeast extract, 10 NaCl, 10 tryptone. Media for selection were done by adding 1.5 mL L^{-1} of the tetracycline stock solution prior use to obtain media with a final concentration of 15 µg mL^{-1}.

Minimal medium for the cultivation of *Shewanella oneidensis*

Lactate Shewanella basal medium (LSBM) contained the following compounds in g L^{-1}: K_2HPO_4 0.225, KH_2PO_4 0.225, NaCl 0.46, $(NH_4)_2SO_4$ 0.225, $MgSO_4$ x 7 H_2O 0.117, HEPES 23.81, Na-lactate (50 % solution) 22.41 (final concentration 100 mM), 5 mL L^{-1} vitamin solution, 5 mL L^{-1} trace mineral solution. The vitamin solution contained in mg L^{-1}: biotin 2, folic acid 2, pyridoxine hydrochloride 10, thiamin hydrochloride 5, riboflavin 5, nicotinic acid 5, DL-calcium pentothenate 5, cyanocobalamine 0.1, 4-aminobenzoic acid 5 and lipoic acid 5. The trace mineral solution had the following composition in g L^{-1}: $C_6H_9NO_6$ 1.5, $MgSO_4$ x 7 H_2O 3, $MnSO_4$ x 2 H_2O 0.5, NaCl 1, $FeSO_4$ x 7 H_2O 0.1, $CoCl_2$ 0.1, $CaCl_2$ x 2 H_2O 0.1, $ZnCl_2$ 0.13, $CuSO_4$ x 5 H_2O 0.01, $AlK(SO_4)_2$ 0.01, H_3BO_3 0.01, Na_2MoO_4 x 2 H_2O 0.025, $NiCl_2$ 0.024 and Na_2WO_4 x 2 H_2O 0.025. Vitamin solution and trace mineral solution were sterile filtered and stored at 4°C until further use.

Minimal medium for the cultivation of *Corynebacterium glutamicum*

For cultivation of *C. glutamicum* a defined mineral medium was used, containing per liter: glucose 11 g, KH_2PO_4 3.7 g, K_2HPO_4 15.53 g, $(NH_4)_2SO_4$ 10.64 g, $MgSO_4$ 0.26 g, $CaCl_2$ 16.96 mg, 3,4-dihydroxybenzoic acid 31.91 mg, 1 mL vitamin solution, which contains per liter: cobalamin 0.11 mg, thiamine 0.32 g, pyridoxal phosphate 0.02 mg, biotin 0.11 g and 1 ml trace element solution, which contains per liter: $FeSO_4$ x $7H_2O$ 10.64 g, $MnSO_4$ x H_2O 10.64 g, $ZnSO_4$ x 7 H_2O 2.13 g, $CuSO_4$ x 5 H_2O 0.21 g, $NiCl_2$ x 6 H_2O 21.28 mg and $Na_6Mo_7O_{24}$ x 2 H_2O 21.28 mg (Krömer et al., 2004).

Minimal medium for α-humulene production in *Cupriavidus necator*

The medium for *C. necator* was developed and optimized for electroautotrophic growth from Sydow et al. (2017a). It contained in g L^{-1}: 2.9 Na_2HPO_4, 3.06 $NaH_2PO_4 \cdot 2\ H_2O$ (a 2x stock solution was prepared for these components), 0.17 K_2SO_4, 0.097 $CaSO_4 \cdot 2\ H_2O$ (a 20x stock solution was prepared for these components), 0.8 $MgSO_4 \cdot 7\ H_2O$ (625x stock solution), 0.943 $(NH_4)_2SO_4$ (212x stock solution), 0.016 $FeSO_4$ (298x stock solution). Trace elements were prepared in a 20,000x stock solution and medium contained in mg L^{-1}: 15 $FeSO_4 \cdot 7\ H_2O$, 2.4 $MnSO_4 \cdot H_2O$, 2.4 $ZnSO_4 \cdot 7\ H_2O$, 0.48 $CuSO_4 \cdot 5\ H_2O$ (these components were solved in 0.1 M HCl and sterile filtered), 1.8 $Na_2MoO_4 \cdot 2\ H_2O$, 1.5 $Ni_2SO_4 \cdot 6\ H_2O$, 0.0402 $CoSO_4 \cdot 7\ H_2O$ (these components were solved in ddH_2O and sterile filtered). Equal volumes of the solved components (20,000x) were mixed together to obtain the stock solution and added to the medium after sterilization. For heterotrophic cultivations 4 g L^{-1} fructose (from a 100x stock solution) and for plasmid containing *C. necator* 5 mg mL^{-1} tetracycline (667x stock solution) was added to the medium, respectively. After mixing the stock solutions water was added to obtain a 1x medium. The iron and trace element stock solutions were sterilized by filtration.

Potassium phosphate buffer

Potassium phosphate buffer consisted of 15 g L^{-1} KH_2PO_4 and 30 L^{-1} K_2HPO_4. The pH was adjusted to 7.0 by adding NaOH or HCl and stored at 4°C until further use.

L-rhamnose solution for induction

2 g L^{-1} L-rhamnose were dissolved in water and autoclaved. *C. necator* cells contaning plasmids with the $rhaP_{SR}$ promoter were induced with the solution.

SOC-medium for regeneration of transformed cells

SOC medium contained the following components in g L^{-1}: 20 tryptone, 5 yeast extract, 0.5 NaCl, 0.186 KCl, 2.47 $MgSO_4 \cdot 7\ H_2O$. The pH was adjusted to 7.0 by adding NaOH and the medium was autoclaved at 121°C for 20 min. A 1 M stock solution (50x) of glucose (final concentration in the medium 3.6 g L^{-1}) was autoclaved separately and added after sterilization to prevent maillard reactions.

Tetracycline solution

Tetracycline was used as an antibiotic for selection of clones. A 667x stock solution of 10 mg mL^{-1} tetracycline hydrochloride was prepared, sterile filtered through a 0.2 µm sterile filter and stored at -20°C until further use.

Transfer buffers I and II

Transfer buffer I contained 3 mL 1 M CH_3COOH, 10 mL 1 M KCl, 1 mL $CaCl_2$, 12 mL glycerin and was filled up with ddH_2O to 80 mL and pH was adjusted to 6.1 with NaOH and HCl if needed. Transfer buffer II contained 1 mL 0.2 M MOPS (3-(N-morpholino)propanesulfonic acid), 0.2 mL 1 M KCl, 1.5 mL 1 M $CaCl_2$, 2.4 mL glycerine and was filled up with ddH_2O to 20 mL.

Tris base, acetic acid, EDTA (TAE) buffer

The TAE buffer contained for a 1 L 50x stock solution: 242 g Tris base, 57.1 mL glacial acetic acid and 100 mL of a 500 mM EDTA solution. The pH was adjusted to 8.0 by adding NaOH or HCl and diluted to 1x before further use.

4.2 Methods

All electrode potentials mentioned in this study refer to a Ag/AgCl reference electrode containing saturated potassium chloride, which equals to +199 mV *vs.* the standard hydrogen electrode.

4.2.1 Cultivation methods

Strains, media and cultivation conditions of the electroactive microorganisms used in this study are described in this section.

Shewanella oneidensis

For biological experiments with *S. oneidensis*, a tube containing 5 mL Luria-Bertani (LB) medium was inoculated with *S. oneidensis* cells as a preculture from cryo stocks and cultivated in an orbital shaking incubator (Minitron HT, Infors, Bottmingen, Switzerland) at 180 rpm and 30°C for 8 h. Three 1,000 mL Erlenmeyer flasks containing 200 mL LSBM each were inoculated to an optical density ($OD_{600\ nm}$) of approximately 0.02 and the cells were grown over night to an $OD_{600\ nm}$ of 1.0 to 1.2 under same conditions and harvested by centrifugation at 3,220g for 30 min (Hau et al., 2008).

Geobacter sulfurreducens

G. sulfurreducens was cultivated in DSM 826 medium, which was made as described by the DSMZ, at 30°C. For strain maintenance 1 % (v/v) of the cells were routinely subcultured in 50 mL fresh anaerobic DSM 826 medium every 7 d in 200 mL septum flasks under a 80:20 (N_2:CO_2) gas atmosphere (Aligal 12, Air Liquide, Paris, France).

Corynebacterium glutamicum

Colonies of *C. glutamicum* were grown on lysogeny broth agar plates at 30°C and individual colonies were transferred afterwards into 500 mL baffled shake flasks containing 100 mL of cultivation medium for aerobic overnight cultivation in an orbital shaking incubator (Minitron, Infors, Bottmingen, Switzerland) at 200 rpm and 30°C. When the cells had reached an $OD_{600\ nm}$ between 5 and 6 (log phase) the cells were harvested by centrifugation (10,000g, room temperature, 3 min).

Cupriavidus necator

Cultivation of *C. necator* is extensively described in Section 4.2.18 for heterotrophic, autotrophic and electroautotrophic growth.

4.2.2 Design of an air-breathing microbial fuel cell

A reactor for the MFC experiments was designed based on a flat-plate design using Solid Edge® (Siemens PLM Software, Plano, TX; USA). End plates of the reactor (outside measurements: width=100 mm, height=150 mm, depth=5 mm) and reaction chamber (outside measurements: width=100 mm, height=150 mm, depth=10 mm; inside measurements of the actual reaction chamber: width=60 mm, height=10 mm, depth=10 mm) were made of polyetheretherketone (PEEK) due to its chemical and mechanical stability (Section 2.2.3). Electrodes were contacted using a graphite foil as a current collector (d=0.25 mm, #009077, MaTecK GmbH, Jülich, Germany), which was pressed onto the electrodes in between two silicon rubber foils (d=1 mm, Schulz & Souard, Frankfurt am Main, Germany) sealing the reactor by the end plates to the reaction chamber. End plates were fixed with screws and nuts. The end plate for the gas diffusion cathode was open to the air to allow oxygen to reach the catalyst. A scheme with the investigated flow setups is shown in Figure 8.

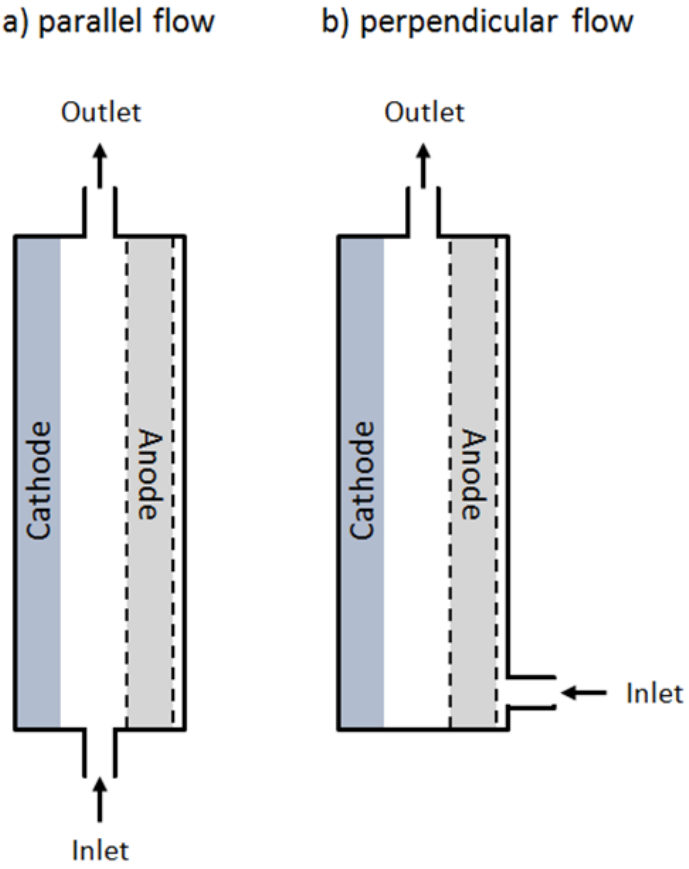

Figure 8: Scheme of the designed air-breathing microbial fuel cell (side view) for parallel flow a) and perpendicular flow through the anode b).

For perpendicular flow through the anode the corresponding end plate at the anode side was opened up by drilling to fit a hollow screw, which served as inlet (Figure 8 b). For a flow parallel over the anode the reactor chamber was opened up by drilling at the

side to fit a hollow screw, which served as inlet in this case (Figure 8 a).

4.2.3 Setup of the microbial fuel cells and cultivation

The reactor contained a gas diffusion cathode (mixed manganese oxide on a PTFE layer contacted with a nickel net (82011, Gaskatel GmbH, Kassel, Germany) and a carbon fabric anode (ACC-5092-15, Kynol, Hamburg, Germany). The electrodes were assembled and contacted with graphite foil as described before. The carbon fabric anode was desorbed at 100°C for 24 h, wetted in isopropanol for 1 h and washed three times with ddH_2O prior use. After assembling the reactor, 225 mL of autoclaved DSM 826 medium was purged with a 80:20 (N_2:CO_2) gas mixture (Aligal 12, Air Liquide, Paris, France) at a flow rate of 30 mL min^{-1} to ensure anoxic conditions in a feed vessel for 1 h. Then the reactor (V=90 mL) was filled with a peristaltic pump and the retention time was set to 1.7 h and the medium was recirculated back into the feed vessel to ensure anaerobic conditions.

G. sulfurreducens cells in stationary phase (after 3 to 7 d) were washed in an equal volume of DSM 826 medium omitting fumarate as a soluble electron acceptor and the feed vessel of the MFC was inoculated with 10 % (v/v) of the culture. The vessel was purged with a 80:20 (N_2:CO_2) gas mixture (Aligal 12, Air Liquide, Paris, France) at a flow rate of 30 mL min^{-1} to maintain anoxic conditions. Medium was pumped with a retention time of 1.7 h in loop-mode and recirculated through the MFCs for 76 h, afterwards it was switched to continuous mode with the same retention time and fresh DSM 826 medium containing 0.5 g L^{-1} acetate was fed continuously in the MFC. The external circuit was closed using a 1 kΩ resistance as an electrical load. The potential drop was measured using a Keithley 2000 Multimeter (Keithley Instruments, Cleveland, OH, USA) and current was then determined using Ohm's law.

4.2.4 Analysis of biofilm distribution using fluorescence microscopy

After 14 d of cultivation, the MFCs were opened up and 1 cm x 1 cm samples of the anode at different locations (from top left to bottom right, in total 9 samples) were taken to investigate the biofilm distribution. Biofilm organisms were stained by DNA binding 4',6-diamidino-2-phenylindole (DAPI). Samples were incubated for 1 min in 1 µg mL^{-1} DAPI in phosphate-buffered saline protected from light (PBS; 8 g L^{-1} NaCl, 0.2 g L^{-1} KCl, 1.42 g L^{-1} Na_2HPO_4, 0.27 g L^{-1} KH_2PO_4). After incubation the samples were washed in PBS for 1 min and pictures were taken using a Axio Imager Z1m fluorescence microscope equipped with a HBO 100 laser, transmission light HAL 100 and a DAPI filter (Zeiss, Oberkochen, Germany). Excication/emission wavelengths were set to 358/461 nm. Pictures were taken and analyzed using the software Axiovision Rel. 4.6. (Zeiss, Oberkochen, Germany).

4.2.5 Characterization of the flow regime in microbial fuel cells with varied electrode setup and inlet

In order to understand the nature of the flow profiles for the different inlet configurations, models of each system were constructed in COMSOL Multiphysics® 5.2 (Boston, MA, USA). For each model, the fluid flow and concentration profiles for substrate were simulated. To describe the fluid flow in the bulk (non-porous) environment, the Navier-Stokes equations were solved for the momentum balance (Equation 5) and continuity equation (Equation 6).

$$\rho(\vec{\boldsymbol{u}} \cdot \nabla\vec{u}) = -\nabla p + \mu\nabla^2\vec{u} \tag{5}$$

$$\nabla \cdot \vec{\boldsymbol{u}} = 0 \tag{6}$$

In Equation 5 and Equation 6, $\vec{u}$ is the velocity vector, p the pressure, ρ the fluid density and μ the fluid viscosity. For the porous domain, the flow profile was solved *via* the Brinkmann formulation (Equation 7) coupled to the continuity equation (Equation 6) (Nield, 1983).

$$\rho\left(\frac{\vec{\boldsymbol{u}} \cdot \nabla\vec{u}}{\epsilon_p^2}\right) = -\nabla p + \frac{\mu\nabla^2\vec{u}}{\epsilon_p} - \left(\frac{\mu}{\kappa}\right)\vec{\boldsymbol{u}} \tag{7}$$

In Equation 7, ϵ_p is the porosity and κ is the permeability of the porous layer.

This velocity profile couples to the concentration profile of substrate in the system, which was determined in a transient fashion. This allowed for determining the effective concentration of substrate within the porous layer as a function of time/effectiveness of substrate distribution in the porous layer, for different porous layer properties (porosity and permeability). In the bulk, the concentration profile is solved as a transient convection-diffusion problem with diffusion governed by Fick's law (dilute conditions, Equation 8),

$$\frac{\partial c}{\partial t} + \nabla \cdot (-D\nabla c + \vec{u}c) = 0 \tag{8}$$

where c is the concentration of substrate (acetate) and D the substrate diffusion coefficient.

For the porous layer, the diffusion is modified by the tortuosity of the porous layer and this is treated by the Bruggemann relationship (Chung et al., 2013; Tjaden et al., 2016). For the Bruggemann relationship, tortuosity (τ) is given as $\tau = 1/\epsilon_p^{1/2}$ and the diffusion coefficient in the porous layer (D_{pl}) is then given as $D_{pl} = D\frac{\epsilon_p}{\tau}$ (Chung et al., 2013).

Dispersion and adsorption into the porous layer were neglected in this simple model, where the goal was purely to determine the effect of changing the carbon cloth permeab-

ility/porosity on the predicted flow profiles for the two MFC configurations (Figure 8). This then leads to the final Equation 9.

$$\epsilon_p \frac{\partial c}{\partial t} + \nabla \cdot (-D_{pl} \nabla c + \vec{u} c) = 0 \quad (9)$$

For boundary conditions, the inlet was considered an inflow for fluid (under laminar conditions) and a constant concentration representing the inflow of substrate for the concentration profile. The outlet was considered a constant pressure condition for fluid (set at an arbitrary value of zero to specify the pressure within the domain) and an outflow condition for concentration (no-gradient). All other exterior boundaries were set as no-slip (zero wall velocity) and no-flux (impermeable walls).

The liquid density is assumed to be that of pure water, i.e., ρ=10^{-3} kg m^{-3} with a viscosity of μ=10^{-3} Pa s. The properties of the carbon fabric anode (ACC-5092-15, Kynol, Hamburg, Germany) were provided by the supplier, the porosity was ϵ_p=0.86 and the permeability κ=10^{-10} m^2. The equations were solved numerically using COMSOL® Multiphysics 5.2 with a relative tolerance of 0.001. P2+P1 discretization (second-order Lagrange elements for velocity and first-order elements for pressure) was used to solve the Navier-Stokes equations and first-order Lagrange elements for the concentration profile. The mesh was refined near the walls and independency was checked. The complete mesh consisted of approximately 600,000 domain elements. The distribution of the organic compound used as a substrate, i.e. acetate, was simulated with the equations listed above for a diffusion coefficient of approximately $0.9 \cdot 10^{-9}$ m^2 s^{-1} for both perpendicular flow and parallel flow through the porous anode (Chen et al., 2012b).

4.2.6 Characterization of H-cells using electroactive microorganisms

H-cells were characterized bioelectrochemically using carbon fabric electrodes (A=6 cm^2, 2 cm x 3 cm) as working and counter electrodes. H-cells were investigated in a non-separated and a separated setup, where working and counter electrode were separated by a membrane (Nafion® 117, Dupont, Wilmington (DE), USA, A=4.9 cm^2). LSBM for *S. oneidensis* and DSM 826 for *G. sulfurreducens* omitting trace element and vitamin solutions was added to a working volume of 120 mL to the anode chamber. The cathode chamber was filled with 120 mL of potassium phosphate buffer (Section 4.1.2). A Luggin capillary filled with 0.5 M Na_2SO_4 for the reference electrode was added *via* a septum and then the H-cells were sterilized at 121°C for 20 min. Afterwards all electrodes (including the silver/silver-chloride reference electrode SE21, Meinsberg Sensortechnik, Waldheim, Germany) were connected to a potentiostat and a potential of +400 mV was applied for 12 to 24 h prior inoculation with cells to equilibrate the medium and enable constant start conditions. Vitamins and trace element solutions were added 30 min before inoculation of the H-cells.

For inoculation of *S. oneidensis* and *G. sulfurreducens*, a preculture was harvested and cell pellets were resuspended in 2 mL of "equilibrated medium", which was taken sterile from the pre-equilibrated electrobioreactor and inoculated into the reactor to the desired optical density. Optical density of *S. oneidensis* was converted into cell dry weight according the following equation (R^2=0.956, Mayer et al. (2018)).

$$c_{CDW} = OD_{600nm} \cdot 0.057 \quad (10)$$

The potential was maintained by a potentiostat (Interface 1000, Gamry Instruments, Warminster, PA, USA) and current density was measured over a period of 50 to 75 h. The electrochemical characterization of the H-cell is described in Section 4.2.10.

4.2.7 Design and construction of electrode assemblies for conventional bioreactors

For first tests, baffles of a 3.7 L KLF 2000 fermenter (Bioengineering, Wald, Switzerland) were equipped with a polytetrafluoroethylene (PTFE) mounting hosting the working and the counter electrode (assembly 1, Figure 9 A). Silicon rubber foil (d=0.1 mm, size: width=2.5 cm, length=12.5 cm, Schulz & Souard, Frankfurt am Main, Germany) was used to isolate the electrodes from the stainless steel baffles (Figure 9 A). Carbon fabric (ACC-5092-15, Kynol, Hamburg, Germany), the electrode material of choice was desorbed at 100°C for 24 h, wetted in isopropanol for 1 h prior use, washed three times with ddH_2O and various layers were placed around the baffles of the bioreactor and clamped onto it using the PTFE mounting fixed by four screws at each side.

One layer of carbon fabric equals a geometric surface area of 120 cm^2 with a mass of 2.42 ± 0.05 g, BET (Brunauer-Emmett-Teller) surface area is 1,450 $m^2\ g^{-1}$ (calculated from the I_2 adsorption, which was 1500 mg g^{-1}, using a correlation graph provided by the supplier) or approximately 3,500 m^2 per layer. The carbon fabric was electrically contacted by weaving a platinum wire (d=0.5 mm) through the layer(s) winding it afterwards to the platinum wire of the contact fitting. A fitting with a diameter of 0.5 mm was used to insert a glassy Luggin capillary with silicone rubber to ensure tightness through the reactor lid for the reference electrode (Figure 9 C). Prior to sterilization, the port was closed by a clamped tube for sterilization at 121°C for 30 min. The Luggin capillary was sterilized using 70 % ethanol for approximately 5 min and added to the bioreactor containing the silver/silver-chloride reference electrode (SE21, Meinsberg Sensortechnik, Waldheim, Germany) after hitting the operating temperature of 30°C using a flame to ensure sterility. The pH was controlled with an electrode (405-DPAS-SC-K8S 325 mm, Mettler-Toledo, Gießen, Germany) and an external addition of 2 M NaOH or 2 M HCl as required maintaining the set pH.

In assembly 2, working and counter electrode were separated by a membrane (Nafion®

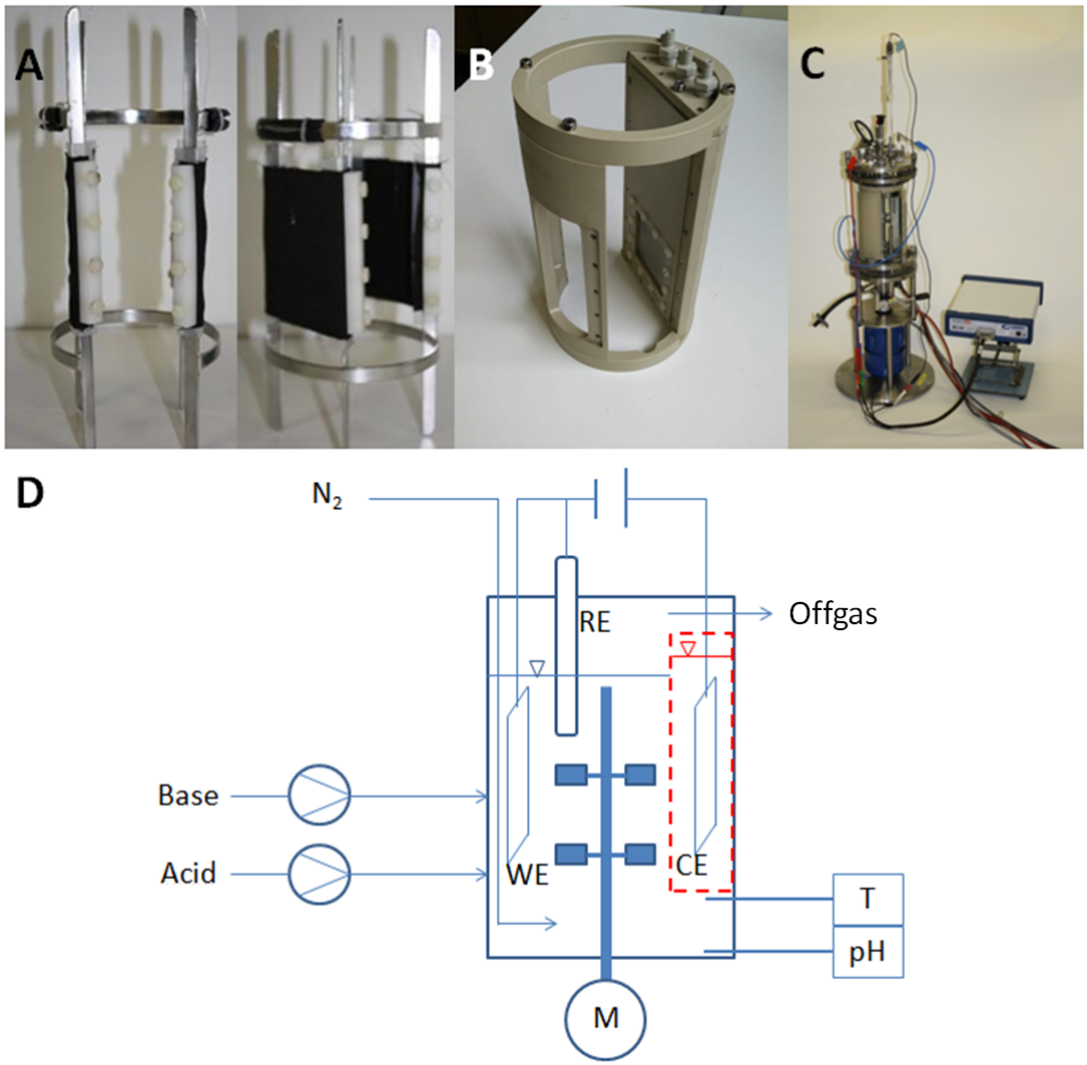

Figure 9: Different possibilities to equip a conventional bioreactor with electrodes. A: Modified baffles with carbon fabric electrodes for non-separated bioelectrochemical processes (assembly 1). B: Designed assembly 2 to allow separated bioelectrochemical processes (assembly 2). C: Equipped electrobioreactor with assembly 2, pH-electrode, thermo element, stirring unit and potentiostat. D: Scheme of the electrobioreactor with controls and possible separation of the counter electrode (dashed red line) with temperature (T), pH control and stirring unit (motor M).

117, Dupont, Wilmington (DE), USA, A=20.3 cm²). The assembly was made of polyetheretherketone (PEEK) and designed and manufactured to host the working electrode, the membrane and the counter electrode in separate compartments (Figure 9 B). PEEK was chosen due to its adequate mechanical, chemical and temperature stability, which allows sterilization at 121°C (Section 2.2.3). The counter electrode compartment consisted of a cylindrical part, with a silicone sealed lid to prevent catholyte and anolyte from mixing. One layer of carbon fabric was folded in the middle two times, placed into the counter electrode compartment and contacted by a platinum wire as described before. Fittings (SS-8-HRN-4, Swagelock, Schönefeld, Germany) were added for the perfusion of the cathode with catholyte from a stock bottle placed outside of the reactor, which was

open to air. Identical fittings were used to contact the working and counter electrode by integration of a glass cylinder (d=6 mm) with a platinum wire (d=0.5 mm, manufactured from Fischer Labortechnik GmbH, Frankfurt am Main, Germany) melted into the glass cylinder. Various layers of pretreated carbon fabric were placed at the working electrode side into the gadget, in which the carbon fabric layers were clamped one above the other using a bar fixed with screws analogue to assembly 1. The reactor was set-up with assembly 1 or assembly 2 for the non-separated and separated cultivation, respectively (Figure 9 A-C).

4.2.8 Characterization of the electrobioreactor using *Shewanella oneidensis*

The reactor was set up with the assembly 1 or assembly 2 for the non-separated and separated cultivation, respectively, as described before (Figure 9 A-D). LSBM omitting trace element and vitamin solutions was added to a working volume of 2.5 L and 2 L for the non-separated (assembly 1) or the separated system (assembly 2), respectively. The cathode chamber was filled with potassium phosphate buffer (Section 4.1.2) and then sterilized at 121°C for 20 min. After cooling down, the reference electrode was sterilized using 70 % ethanol (aq.). All electrodes were connected to a potentiostat and a potential of +400 mV was applied for 12 to 24 h prior inoculation with cells to equilibrate the medium and enable constant start conditions. Vitamins and trace element solutions were added 30 min before inoculation of the electrobioreactor. For inoculation, *S. oneidensis* preculture was harvested and cell pellets were resuspended in 25 mL of "equilibrated medium", which was taken sterile from the pre-equilibrated electrobioreactor and inoculated into the reactor to the desired optical density. The optical density of *S. oneidensis* was converted into cell dry weight concentration (c_{CDW} in g L^{-1}) according to Equation 10.

The potential was maintained by a potentiostat (Interface 1000, Gamry Instruments, Warminster, PA, USA) and current density was measured over a period of 50 to 75 h. A scheme of the electrobioreactor is given in Figure 9 D.

To compare the electrobioreactor to H-cells the specifc charge (q_{spec} in C cm^{-2}) was defined according to Equation 11 to rule out influences of the electrode surface area and allow a better comparison of the systems. The charge ($Q_{measured}$ in C) of the respective runs was calculated according to Equation 11 and divided by the geometric electrode surface area ($A_{Electrode}$ in cm^2).

$$q_{spec} = \frac{Q_{measured}}{A_{Electrode}} = \frac{\int_0^t I dt}{A_{Electrode}} \tag{11}$$

For the characterization and discussion of the coulombic efficiencies the oxygen transfer through the membrane j (in mol h^{-1}) over the process time was calculated according to

Equation 12 with a mass transfer coefficient of oxygen K_{O2} of 2.8 x 10^{-4} cm s^{-1} (Chae et al., 2008), an oxygen concentration c_{O2} in the catholyte of 0.235 mM at 30°C calculated by Henry's law and a membrane surface area A_M of 25 cm^2.

$$j = K_{O2} \cdot c_{O2} \cdot A_M \tag{12}$$

4.2.9 Investigation of the effect of electrode potential on the pH measurement in the modified electrobioreactor

Assembly 1 was used to investigate the influence of electrochemical measurements on the pH measurement. Assembly 1 was inserted, 2 L of LSBM was added and graphite rods were used as working and counter electrodes in a classical three-electrode setup with a surface area of 28.6 cm^2 each (Figure 10). Measurements of pH were performed with the same positioning of the electrode as in the bioreactor and added to the setup. First, pH was measured before a potential was applied as a blank and to validate that the pH values are constant without electrochemical measurements. Next, the diaphragm of the pH electrode was moved to face towards the electrochemical field and the measurement at a certain potential was started (Figure 10).

The pH value was taken when the signal was constant (typically less than 5 min). Afterwards, the diaphragm of the pH electrode was faced away from the electrical field and again pH was measured as described. The procedure was repeated in a potential range of -1,500 mV to +900 mV. Circuits of the electrochemical and the pH measurement were electrically isolated and the experiments were repeated to prevent possible circulating currents using an isolation transformer (LTT 003, VEB Technisch-Physikalischen Werkstätten, Thalheim, Germany).

4.2.10 Electrochemical characterization of bioreactor assembly and H-cells

Assembly 2 was characterized using the same experimental setup as described for the pH measurement effects to perform a cell voltage analysis (Figure 11). However, three reference electrodes were placed in the system: in front of the working electrode, in front of the membrane and behind the membrane directly in front of the counter electrode (distance to the corresponding component approximately 5 mm). Electrochemical losses were analyzed galvanostatically with currents in the range of 5 mA to 75 mA (0.14 mA cm^{-2} to 2.6 mA cm^{-2}) for positive and negative currents. Current was applied to the system until a steady state potential in front of the working electrode was reached (approximately 30 to 120 min). The potential drops between the reference electrodes were measured using a Keithley 2000 Multimeter (Keithley Instruments, Cleveland, OH, USA). H-cells were

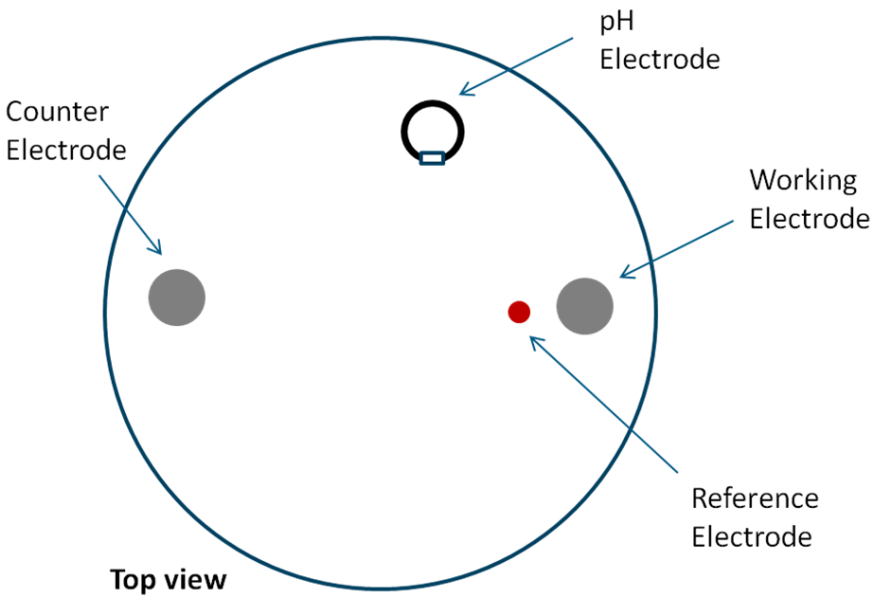

Figure 10: Experimental setup investigating the effect of electrochemical measurements on pH measurements.

characterized the same way using graphite rods (d=6 mm, length=10 cm with 5 cm being in the electrolyte) as working and counter electrodes with a surface area of 9.7 cm^2. LSBM containing 100 mM lactate, the medium omitting lactate (SBM) and 0.5 M Na_2SO_4 as an ideal electrolyte were characterized.

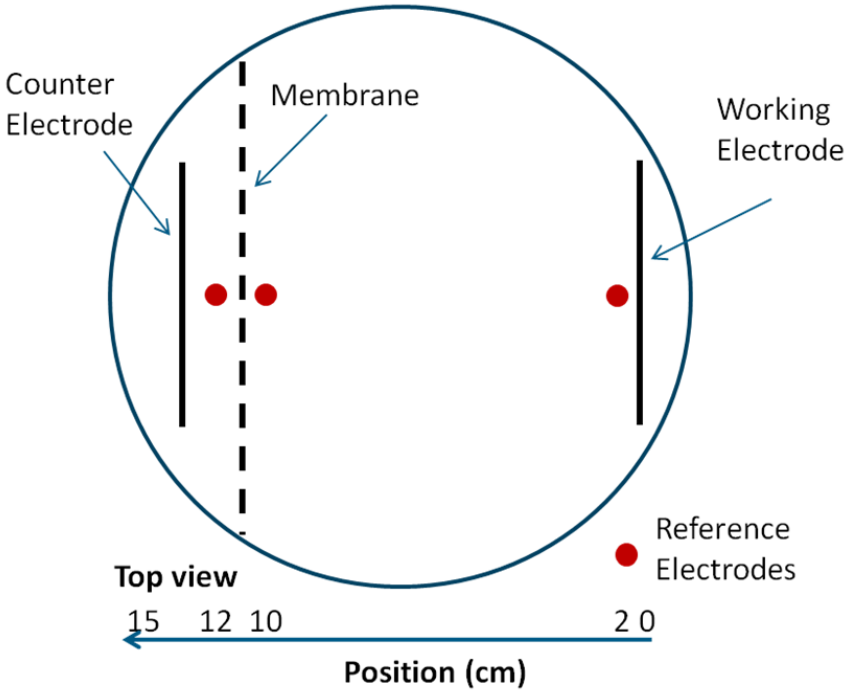

Figure 11: Experimental setup investigating electrochemical losses using assembly 2.

4.2.11 Computational fluid dynamic analysis on the turbulence and mixing times

Flow in both the conventional and designed electrobioreactor with assembly 2 was simulated using the mixer module in COMSOL Multiphysics® 5.2 (Boston, MA, USA) to estimate mixing due to turbulence (eddy viscosity) and to estimate if possible deadzones will arise due to the applied assemblies. Geometric and operating values of the used bioreactor are listed in Table 2. Furthermore, a simplified geometry of assembly 2 was drawn and meshed, which is shown in Figure 12.

Table 2: Parameters of the simulated bioreactors in COMSOL Multiphysics® 5.2. Both bioreactors were equipped with a big rushton turbine and a smaller rushton turbine on top.

Parameters (unit)	Values
Vessel height (m)	0.2
Vessel diameter (m)	0.127
Clearance from the bottom (mm)	37.5
Number of baffles	4
Baffle width (m)	0.127
Baffle offset from bottom (m)	0
Impeller diameter big rushton (mm)	45
Blade length for a rushton turbine (mm)	13.5
Blade width for big rushton turbine (mm)	12
Clearance between the big and small rushton turbine (mm)	84
Impeller diameter small rushton (mm)	39
Blade length for small rushton turbine (mm)	10
Blade width for small rushton turbine (mm)	6.5
Shaft diameter (mm)	12
Stirrer speed (rpm)	400

The Reynolds number of the reactor systems is calculated with Equation 13, where ρ is the density of the fluid, d is the diameter of the stirrer, n is the stirrer rotation speed and μ the dynamic viscosity (Khang and Levenspiel, 1976). With ρ=972 kg m^3, d=45 mm, n=400 rpm and μ=10^{-3} Pa s, Re is calculated to be 13,130 and consequently the flow is assumed to be turbulent (Potter et al., 2012).

$$Re = \frac{\rho \cdot n \cdot d^2}{\mu} \tag{13}$$

Velocity fields in both bioreactor configurations were determined through solving the incompressible Navier-Stokes equations with the k-ϵ model for turbulence in a frozen rotor framework and the conventional bioreactor was compared to the designed electrobioreactor with assembly 2. Mesh independence and resolution was confirmed by successful refinement of the mesh and relative changes of the solution were checked, as well as the

wall lift-off (Kuzmin et al., 2006). Mixing times were compared in the two configurations and diffusion times t_D at different lengths x were calculated with Fick's second law, which gives Equation 14, where D_T is the estimated turbulent kinematic viscosity from simulations.

$$t_D = \frac{x^2}{2 \cdot D_T} \tag{14}$$

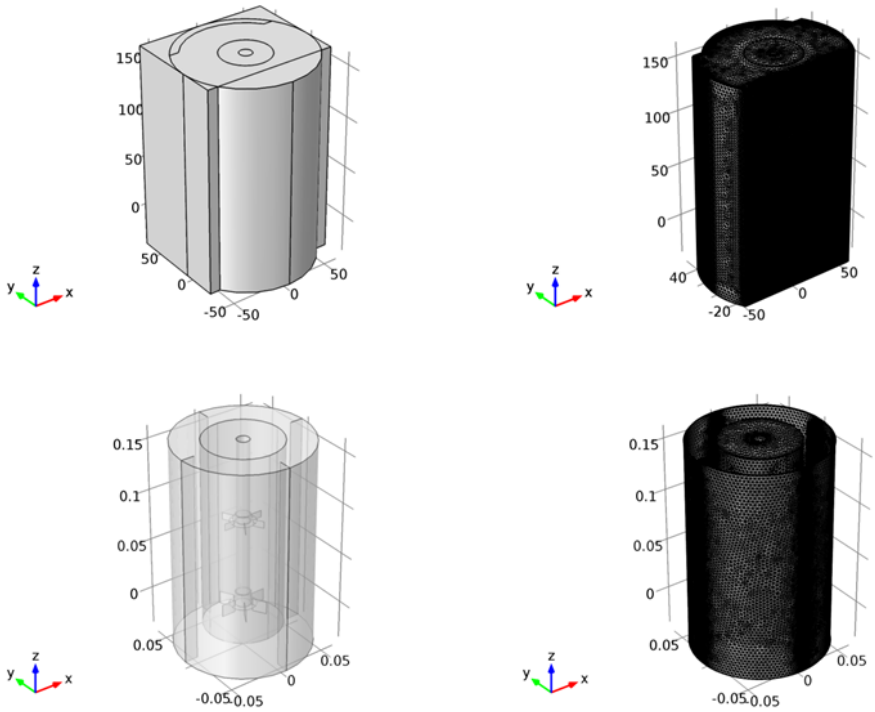

Figure 12: Drawings of the electrobioreactor with assembly 2 (top row) and a conventional bioreactor (bottom row) and their corresponding meshes in COMSOL Multiphysics® 5.2. The mesh of the conventional bioreactor consists of 1,266,093 elements with a minimum quality of $7.9 \cdot 10^{-4}$ and an average quality of 0.62. The mesh of the electrobioreactor with assembly 2 consisted of 1,995,627 elements with a minimum quality of $4.2 \cdot 10^{-4}$ and an average quality of 0.62.

4.2.12 Anaerobic production of lysine and organic acids with *Corynebacterium glutamicum*

The procedure was described in detail elsewhere (Vassilev et al., 2018). Briefly, the electrobioreactor was equipped with assembly 2 and operated as described above. Ferricyanide was added to the medium in the anode chamber as a mediator to enable mediated electron transfer (1.5 mM). The electrobioreactor was inoculated to a start OD_{600nm} of 4. Optical density of *C. glutamicum* was converted into cell dry weight concentration (c_{CDW} in g L^{-1})

according to Equation 15 (Vassilev et al., 2018).

$$c_{CDW} = OD_{600nm} \cdot 0.255 \tag{15}$$

The pH was controlled at 7.2 ± 0.2 as described before by adding HCl or NaOH to the medium as required. The potential of the working electrode was set to a value of +500 mV. The cathode chamber of assembly 2 was filled with potassium phosphate buffer (Section 4.1.2). Specific productivity (SP in $mol_{Product}$ g_{CDW}^{-1} h^{-1}) is calculated by Equation 16, where n is the amount of the respective product in mol, m_{CDW} the cell dry weight in g, which is calculated by $m_{CDW} = c_{CDW} \cdot V_{Anolyte}$ and t is the cultivation time.

$$SP = \frac{n}{m_{CDW} \cdot t} \tag{16}$$

4.2.13 Polymerase chain reactions to produce pKR-hum and derivatives

PCR conditions

Starting plasmids for pKR-hum were pFS62b (Sonntag et al., 2015) and pKRrha (Sydow et al., 2017b). General PCR mix was as shown in Table 3.

Table 3: PCR mix for fragment amplification. Templates were obtained from plasmid preparations, primer were designed and synthesized by Sigma Aldrich (St. Louis, MO, USA). All the other components were obtained from New England Biolabs, Ipswich, MA, USA.

Contents	Volume (total 50 µL)	Final concentration
H_2O	21.5	
Q5 reaction buffer (5x)	10	1x
dNTPs (10 mM)	1	10 µM
Primer fw (10 µM)	2.5	0.5 µM
Primer rev (10 µM)	2.5	0.5 µM
Template	2	1 ng to 1 µg L^{-1}
High GC Enhancer	10	
Q5 polymerase (1 U)	0.5	

PCRs were performed in a thermocycler (T3000, Biometra, Göttingen). General PCR conditions were as shown in Table 4.

Primers

All primers used in this study are shown in Table 5.

Table 4: General PCR conditions to amplify the fragments. Steps denaturation 2, annealing and elongation are repeated for 35 cycles. Elongation time t is calculated from the fragment size and equals t=25 s kb^{-1}. Annealing temperature T_A was calculated for each primer pair using the Tm calculator from NEB (tmcalculator.neb.com).

Step	t (s)	Temperature (°C)	Cycles
Denaturation 1	30	98	
Denaturation 2	7	98	35
Annealing	15	T_A	
Elongation	t	72	
Final elongation	120	72	

Plasmids

pKR-hum: pKRrha was used as a backbone with a L-rhamnose inducible promotor (Sydow et al., 2017b). Two fragments were amplified by PCR with primers pKRrha1_fw and pKRrha1_rev, pKRrha2_fw and pKRrha2_rev leading to fragment sizes of 5,216 bp and 6,767 bp for fragment 1 and 2, respectively. α-Humulene pathway was taken from plasmid pFS62b developed by Sonntag et al. (2015) using primers pFS62b_fw and pFS62b_rev leading to fragment 3 with a size of 9,563 bp.

pKR-hum ΔMVA: pKR-hum was used as a starting point and all MVA genes, except of the gene coding for the isomerase fni, the α-humulene synthase ZSSI and the FPP synthase ERG20 were cut out of the plasmid to investigate the natural production of precursors *via* the DXP pathway in *C. necator*. Three fragments were amplified by PCR with the primers delMVA1_fw and delMVA1_rev, delMVA2_fw and delMVA2_rev, delMVA3_fw and delMVA3_rev leading to fragment sizes of 1,076 bp, 9,547 bp and 5,195 bp, respectively.

pKR-hum ΔZSSI: pKR-hum was used as a starting point and the α-humulene synthase ZSSI was cut out of the plasmid to investigate whether *C. necator* produces any terpenes naturally. Two fragments were amplified by PCR with the primers delZSSI1_fw and delZSSI1_rev, delZSSI2_fw and delZSSI2_rev leading to fragment sizes of 10,763 bp and 10,684 bp, respectively.

PCR products were analyzed in terms of fragment length and specificity (unwanted fragments) with DNA gel electrophoresis. Gels were casted using Tris base, acetic acid, EDTA (TAE) buffer (Section 4.1.2). TAE stock was diluted to a 1x working solution, agarose 1% (w/v) was added and solved using a microwave prior casting. PCR products (5 µL) were mixed with 1 µL of 6x DNA loading dye and GeneRuler 1 kb plus DNA ladder (Thermo Scientific, Waltham, MA, USA) was used to compare the length of the fragments. Afterwards the gel was stained for 30 min using GelRED staining solution (Biotium, Fremont, CA, USA) and analyzed in a transilluminator (Bio-Doc-Analyze Ti5,

Table 5: Overview of the primers used in this study.

Primer	Sequence (5' to 3')
pFS62b_fw	TTAGACTGGTCGTAATGAACAATTG ATAAAGAAGGAGGTAAAACAT GGAACGCCAGTC
pFS62b_rev	TCTTCTCTCATCCGCCAAAACAGCC AAGCTTCAGCTCAGCGCGC GCAC
pKRrha2_fw	TTGGTACTCACGCCTGTTATACTATG
pKRrha2_rev	AATTGTTCATTACGACCAGTCTAA
pKRrha1_fw	AGCTTGGCTGTTTTGGC
pKRrha1_rev	CCTTCTGTGCGTGAGTACTCAT
delMVA1_fw	GTTCTAGGAGGAATAATATGGGCGAC
delMVA1_rev	CTACAGCGCCGCCAAC
delMVA2_fw	TTGGTACTCACGCCTGTTATACTATG
delMVA2_rev	CCTGCGCTCCTCTCTAGATAAAG
delMVA3_fw	AAGCTTGGCTGTTTTGGCG
delMVA3_rev	CCTTCTGTGCGTGAGTACTCAT
delZSSI1_fw	GCACTTATGACTGTCTTC
delZSSI1_rev	CATTACGACCAGTCTA
delZSSI2_fw	ATCGATACATCAAACCAAAG
delZSSI2_rev	TGTCCTACGAGTTGCATG
Seq1_fw	GCATCACATCACCACAATTC
Seq1_rev	GTTCCCTACTCTCGCATG
Seq2_fw	GTGTCGCTGTTCCTCGAGAC
Seq3_fw	CGAAGATCCTCAAGTCGTGC
Seq4_fw	ACCATGTTGGTACAAGGTTC
Seq5_fw	ATAGATTAATCCTCCTCTAC
Seq6_fw	GGCTGGTCCGCTGGTCGGAC
Seq7_fw	GACCTGTCCACGGCCTTCCT
Seq8_fw	GCATGGCGCTGCCGTTGTTC
Seq9_fw	CGAGGTTCGCGTGCTGCCGG
Seq10_fw	GTGGAGAAGATCGCCAACCT
Seq11_fw	AGGCTCGCTGGCCGTCGC
Seq12_fw	GAGTACGCCGTGCTGTGG
Seq13_fw	GCCATGCGATTGAGGACG

Biometra, Göttingen).

For unspecific PCRs, the DNA fragment with the correct length was cut out of the gel and a gel extraction using NucleoSpin® Gel and PCR Clean-up-Kit (Macherey-Nagel, Düren, Germany) was performed for purification. If no unwanted DNA fragments were showing on the gels, a PCR purification using the same kit was performed prior Gibson assembly according to the manufacturers manual with the optional washing steps.

4.2.14 Cloning of plasmids using Gibson assembly

PCR products were assembled to the plasmids (Figure 39) using the method introduced by Gibson et al. (2009). PCR fragments in molar ratios of 1:1:1 for pKR-hum and pKR-hum ΔMVA were digested and 1:1 for pKR-hum ΔZSSI, respectively, using DpnI for 50 min at 37°C to cleave any methylated template DNA prior use. Afterwards the enzyme was inactivated for 20 min at 80°C. A volume of 2.4 µL of the DpnI digested PCR fragments was mixed with 8 µL Gibson master mix on ice and incubated for 1 h at 50°C (Section 4.1.2). Furthermore, the following enzymes were in the mix in U μL^{-1}: 10 5'-T5 exonuclease, 2 Phusion® polymerase and 40 Taq DNA-ligase.

The exonuclease creates single stranded 3' overhangs by chewing away the 5' strand of the double-stranded template DNA. This facilitates the annealing of fragments that share previously designed complementary regions of approximately 20 to 40 base pairs at these overlap regions. Afterwards the polymerase fills in the gaps in each annealed fragment and subsequently the ligase seals nicks in the assembled DNA strain. The result is a double-stranded DNA (in this case a plasmid) that can be transformed into *E. coli* S17-1 λpir as a host.

4.2.15 Transformation of plasmid DNA into chemical competent *E. coli* S17-1 λpir cells

Transformation of plasmid DNA into *E. coli* S17-1 λpir was done by applying the $CaCl_2$ method described by Hanahan (1983). LB-medium (3 mL) inoculated from a cryo stock was incubated over night (approximately 12 to 16 hours) at 37°C at 250 rpm. LB-medium (50 mL) containing 10 mM $MgSO_4$ in a 1 L Erlenmeyer flask was inoculated with 500 µL of the preculture and grown to an optical density of 0.3 to 0.5. The cells were centrifuged at 5,000g for 5 min at 4°C and resuspended in transfer buffer I. After 1 h of incubation on ice cells were centrifuged again and the sediment was gently resuspended in transfer buffer II (Section 4.1.2). The cells were then aliquoted in 100 µL suspension per 1.5 mL reaction tube, immediately shock frozen in liquid nitrogen and stored at -80°C until use.

For transformations of plasmid DNA into *E. coli* S17-1 λpir, competent cells were thawed for 10 min on ice. Gibson assembly solution (5 µL) was added to the cells and incubated for 30 min on ice. Afterwards the cells were heat shocked at 42°C for exactly 30 s and cooled down immediately on ice for 5 min. Cells were regenerated for 1 h at 37°C at 800 rpm on a heating shaker in SOC-medium (Section 4.1.2). Afterwards 100 µL of the cell suspension was plated on LB-agar plates containing the selection antibiotic. Remaining cell suspension was centrifuged for 5 min at 14,000g at room temperature, supernatant was discarded leaving approximately 100 µL in the reaction tube. The pellet was resuspended in the remaining supernatant and plated on LB-agar plates containing the selection antibiotic.

Different clones of transformed *E. coli* S17-1 λpir were picked and grown in 5 mL LB-medium in test tubes containing tetracycline over night. Plasmids were isolated from the cells and purified using a kit (Roti - Prep Plasmid MINI, Carl Roth, Karlsruhe) according to the manual with an optional washing step. Concentrations of the plasmid DNA was measured using a spectral photometer (NanoDrop 200c, Thermo Scientific, Waltham, MA, USA).

4.2.16 Plasmid transfer by conjugation into *Cupriavidus necator*

Since no satisfactory transformation protocol was available for *C. necator*, all the cloning experiments were done in *E. coli* S17-1 λpir. *E. coli* S17-1 λpir containing the plasmid of interest was then used for conjugation of the plasmid into *C. necator* according to the following protocol. Thick LB-agar plates without antibiotics, a sterile 0.9% NaCl solution and minimal medium agar plates containing tetracycline were prepared as described before prior starting.

Day 1: A liquid culture of *C. necator* was inoculated from the cryo stock in a 100 mL Erlenmeyer flask containing 10 mL LB-medium and incubated over night (approximately 20 h) at 30°C and 180 rpm. A liquid culture of *E. coli* S17-1 λpir was prepared in a 100 mL Erlenmeyer flask containing 10 mL LB-medium and incubated over night (approximately 16 h) at 37°C and 180 rpm.

Day 2: Maiting: Both liquid cultures were centrifuged for 20 min at maximum speed at 25°C and washed with the same volume of 0.9% NaCl after reaching exponential to early stationary growth phase. After a second centrifugation step at the same conditions, every culture was resuspended in 0.5 mL 0.9% NaCl. Culture (0.2 mL) of the donor *E. coli* S17-1 λpir containing the plasmid of interest and 0.2 mL culture of the acceptor *C. necator* were put as a drop on a thick agar plate and incubated at 30°C.

Day 3: Selection was done after at least 24 h of mating. All the cells on the agar plates were washed off using 3 mL 0.9% NaCl. A volume of 100 µL of dilutions (1:10 and 1:100) and the concentrated cell suspension were plated onto minimal medium agar plates containing tetracycline as selection antibiotic. The plates were incubated at 30°C until single colonies showed up (typically 2-3 d). *E. coli* is auxotrophic to proline and thiamine and therefore not able to grow on the provided minimal medium.

Day 5-6: For purification of the cultures, dilution streaks of 6 to 12 colonies on minimal medium agar plates containing tetracycline were done and incubated at 30°C until single colonies showed up. Single clones were streaked on another minimal

medium agar plate containing tetracycline and stored at 4°C. Clones were then analyzed using colony PCR and sequencing.

4.2.17 Cloning control methods

Different clones of transformed *E. coli* S17-1 λpir and conjugated *C. necator* were analyzed with the following methods.

Digestion of the plasmids using restriction enzymes

Enzymes EcoRI and KpnI were used to digest the control plasmids. DNA fragments were analyzed using an agarose gel as described before. A volume of 1 µL CutSmart buffer, 5 µL plasmid-DNA, 0.5 µL EcoRI-HF and 0.5 µL KpnI-HF was incubated for 37°C for 2.5 h in the thermocycler. For pKR-hum ΔMVA three fragments with a length of 1,873 bp, 2,487 bp and 11,485 bp and for pKR-hum ΔZSSI four fragments with a length of 815 bp, 3,659 bp, 3,843 bp and 11,485 bp, respectively, were expected.

Enzymes NheI, DraI and PciI were used to digest pKR-hum. A volume of 1 µL NEB 2.1 buffer, 8.2 µL plasmid-DNA, 0.2 µL NheI, 0.3 µL DraI and 0.3 µL PciI was incubated for 37°C for 2.5 h in the thermocycler. Fragments with a length of 61 bp, 1,047 bp, 5,014 bp, 6,915 bp and 8,410 bp were expected.

Colony PCR

Colonies were scratched from agar plates and solved in 20 µL H_2O. Seq1_fw and Seq2_rev were used as primers and a PCR was conducted as described in Section 4.2.13 but with an extended denature 1 time to 600 s for cell disruption. Fragment sizes were analyzed using an agarose gel as described before.

Sanger sequencing

Plasmids, which showed a correct restriction pattern and the correct fragment size in the colony PCR were sequenced at GATC Biotech (Konstanz, Germany). For pKR-hum a full sequencing of the insert was performed with primers Seq1 to Seq13_fw and Seq1_rev. For pKR-hum ΔMVA and pKR-hum ΔZSSI only the overlaps of the Gibson cloning were sequenced with primers.

4.2.18 α-Humulene production in *Cupriavidus necator*

Transformed *C. necator* strains were analyzed under different cultivation conditions to characterize α-humulene production from fructose (heterotrophic), CO_2 with an external supply of hydrogen and oxygen (autotrophic) as well as electrochemically produced hydrogen and oxygen (electroautotrophic), respectively.

Seed train

A scheme of the seed train for α-humulene production under different cultivation conditions is shown in Figure 13. Every preculture (PC) and main culture (MC) was incubated at 30°C at 180 rpm in a incubator shaker if not stated otherwise. The electroautotrophic main cultures were stirred with a magnetic stirrer bar.

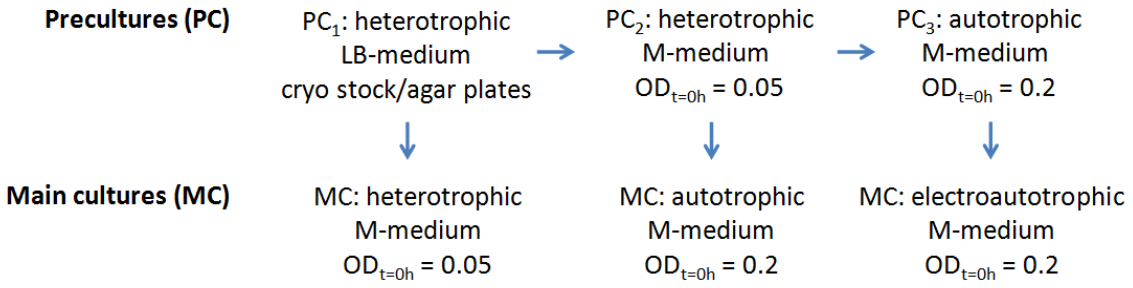

Figure 13: Scheme of the seed train for α-humulene production in *C. necator*. M-medium: Minimal medium.

Preculture 1: LB-medium containing tetracycline was inoculated from cryo stocks or agar plates with the respective *C. necator* strain and grown to stationary phase over night. PC_1 was used to inoculate the heterotrophic cultures to produce α-humulene or to inoculate PC_2.

Preculture 2: Minimal medium (25 mL) containing the corresponding antibiotic was inoculated from PC_1 of the respective *C. necator* strain to a start optical density of 0.05 and cultivated for approximately 24 h. This PC_2 was used to inoculate PC_3 and the autotrophic cultures to produce α-humulene.

Preculture 3: Minimal medium (25 mL) containing the corresponding antibiotic was inoculated from PC_2 of the respective *C. necator* strain to a start optical density of 0.2 in serum bottles (see autotrophic α-humulene production chapter below for more details) and incubated for approximately 24 h. PC_2 was centrifuged at 4,000g for 5 min at room temperature and washed with 0.5 mL minimal medium to get rid of any fructose. PC_3 was used to inoculate electroautotrophic cultures to produce α-humulene.

Optical density of *C. necator* was converted into cell dry weight concentration (c_{CDW} in g L^{-1}) according to Equation 17 (Krieg et al., 2018). Specific productivities (SP) were calculated as described before (Section 4.2.12).

$$c_{CDW} = OD_{600nm} \cdot 0.43 \tag{17}$$

Heterotrophic α-humulene production

Heterotrophic cultivations were performed in 300 mL Erlenmeyer flasks containing 20 mL minimal medium and 5 mL n-dodecane as organic phase for an *in situ* product removal. Seed train was done as described before. Induction of the cells was done at an OD_{600nm} of approximately 0.7. Samples of the aqueous phase (approximately 800 µL) were routinely taken to monitor OD_{600nm}. Concentration of α-humulene was determined by analysis of the n-dodecane phase in a GC/MS (Section 4.2.19). Culture broth was completely harvested after approximately 36 h by centrifugation for 5 min at 3,220g and 4°C.

Autotrophic α-humulene production

Autotrophic cultivations were performed in 200 mL serum flasks containing 20 mL minimal medium and 5 mL n-dodecane as organic phase for an *in situ* product removal. Seed train was done as described before. Medium was filled into the serum flasks and sealed by a butyl septum. Gas phase was set to a ratio of hydrogen to oxygen to CO_2 4.0 to 3.2 to 1.0 (or 64%, 20% and 16% v/v) at a gas station. Gas quality was at least N 3.0. Induction of the cells was done at an OD_{600nm} of approximately 0.9. Samples of the aqueous phase (approximately 800 µL) were routinely taken to monitor OD_{600nm}. Concentration of α-humulene was determined by analysis of the n-dodecane phase in a GC/MS (Section 4.2.19). Culture broth was completely harvested after approximately 48 h by centrifugation for 5 min at 3,220g and 4°C.

Electroautotrophic α-humulene production

Electroautotrophic cultivations were performed in non-separated H-cells containing 100 mL minimal medium and 20 mL n-dodecane as organic phase for an *in situ* product removal. Stainless steel (A=7.84 cm^2, 2.8 cm x 2.8 cm, thickness 0.2 mm, material number 1.4404, Goodfellow, Huntington, England) was used as cathode, a dimensionally stable anode (DSA, Ti expanded metal type 11159, Denorea, Rodenbach, Germany) and a silver/silver-chloride reference electrode (SE21, Meinsberg Sensortechnik, Waldheim, Germany) were used. The reference electrode was integrated *via* a Luggin capillary (Labortechnik Fischer, Frankfurt am Main, Germany) filled with 0.5 M Na_2SO_4 close to the working electrode surface (the cathode). Stainless steel and DSA electrodes were mounted into the reactor and autoclaved. Minimal medium and n-dodecane were filled into the H-cells and the luggin capillary stored in ethanol prior use was also applied under sterile conditions.

Electroautotrophic cultivations were performed in a incubator hood, which was set to 30°C. To ensure comparable starting conditions, H-cells were purged with CO_2 at 0.08 to 0.12 vvm (10 to 15 cm^{-3}) and a potential of -2 V was applied using a potentiostat (Gamry ECM8, Gamry Instruments, Waminser, PA, USA) over night, which ensures sufficient electrochemical production of hydrogen at the stainless steel cathodes and oxygen at

the DSA prior inoculation. Mixing was performed using a magnetic stirrer at 150 rpm. Samples of the aqueous phase (approximately 800 µL) were routinely taken to monitor OD_{600nm}. Concentration of α-humulene was determined by analysis of the n-dodecane phase in a GC/MS. Therefore, a sample of the organic phase (200 µL) was taken and analyzed as described in Section 4.2.19.

4.2.19 Analytical methods

Analysis of organic acids using high performance liquid chromatography (HPLC)

Lactate, succinate and acetate were measured by HPLC (Prominence 20 series, Shimadzu Deutschland GmbH, Duisburg, Germany) equipped with a Rezex ROA-Organic Acid 8% H+ 300x7.8 mm (Phenomenex, Aschaffenburg, Germany) column *via* a photo diode array detector (SPD-M20A, Shimadzu Deutschland GmbH, Duisburg, Germany) at the detection wavelength of 209 nm. Sulfuric acid (5 mM) was used as mobile phase with a flow rate of 0.6 mL min^{-1} at 60 °C over a total run time of 30 min. Quantification was done using a calibration curve with external standards in the range of 0 to 200 mM lactate, succinate and acetate, respectively.

Analysis of lysine and alanine using liquid chromatography with mass spectrometry (LC/MS)

Lysine and alanine were analyzed on an equivalent HPLC system described before equipped with a Kinetex® 2.6 µm XB-C18 100 Å 30x2.1 mm column (Phenomenex, Aschaffenburg, Germany) and coupled to a triple-quadrupole mass spectrometer (LCMS-8040, Shimadzu Deutschland GmbH, Duisburg, Germany) with an electrospray ionization source (Shimadzu Deutschland GmbH, Duisburg, Germany). Column temperature was 30 °C, the mobile phase consisted of solvent A, H_2O + 0.0025% ammonia, and solvent B, acetonitrile, combined following a binary gradient method (0 min 5% B, 1.5 min 5% B, 1.8 min 95% B, 3.2 min 95% B, 3.3-4.5 min 5% B) with a run time of 4.5 min and a total flow rate of 0.3 mL min^{-1}. Electrospray ionization was performed in the positive mode while the interface voltage was set at 4.5 kV. To analyze lysine and alanine, the mass spectrometer was run in the selected ion monitoring mode at m/z 147.1 for the detection of protonated lysine and m/z 90.1 to detect protonated alanine, respectively. A linear calibration curve of external standards in the range of 0 to 200 µM was used for quantification of the amino acids. The samples were diluted 1:25 with double distilled water prior measurement.

Analysis of terpenes using gas chromatography with mass spectrometry (GC/MS)

Concentration of α-humulene was determined using gas chromatography with mass spectrometry (GC17A with Q5050 mass spectrometer, Shimadzu, Kyoto, Japan) equipped

with a Equity 5 column (Supelco, 30 m x 0.25 mm x 0.25 µM) according to the protocol described in Sonntag et al. (2015). Due to injection and evaporation, GC/MS analysis is prone to errors. Therefore, zerumbone was chosen as internal standard due to its structural similarity to α-humulene. Zerumbone (100 mM) was solved in n-dodecane as an internal standard solution. Samples were dried using sodium sulfate and 10% (v/v) of the internal standard solution was added. Quantification was done by a calibration curve of the ratio of measured areas of α-humulene to zerumbone *vs.* the concentration ratios of α-humulene to zerumbone.

Analysis of cell growth using optical density measurements

Cell growth was monitored at 600 nm using a spectral photometer (WPA CO8000 Cell Density Meter, Biochrom, Cambridge, United Kingdom). Volumes of 700 to 1000 µL culture were added to a 1 mL cuvette (Sarstedt AG & Co., Nümbrecht, Germany) and briefly mixed. For values greater than 0.5, the culture was diluted using 0.9% NaCl solution.

4.2.20 Statistical methods

In order to compare two means and decide whether the difference is significant, student's t-test was performed. The null hypothesis states, that the differences of the two populations are purely due to random error and not systematic errors, the alternative hypothesis states the exact opposite. In this case, the null hypothesis would be, that the mean of the compared populations are purely due to random noise. The alternative hypothesis would be, that the differences measured are significant. A confidence level of 95 % to accept or reject the null hypothesis was used in this study (α=0.05). As a first step, the arithmetic mean $\bar{x}$ (Equation 18) and the standard deviation s (Equation 19) of the measurement series to be compared (e.g. A and B) are calculated. Furthermore, standard deviations for measurements performed in $n = 3$ or more are calculated with Equation 19 and are shown as error bars in the figures.

$$\bar{x}_A = \frac{\sum_{i=1}^{n_A}}{n_A} \qquad \bar{x}_B = \frac{\sum_{i=1}^{n_B}}{n_B} \tag{18}$$

$$s_A = \sqrt{\frac{\sum_{i=1}^{n_A} (\bar{x}_A - x_i)^2}{n_A - 1}} \qquad s_B = \sqrt{\frac{\sum_{i=1}^{n_B} (\bar{x}_B - x_i)^2}{n_B - 1}} \tag{19}$$

Then the standard deviations are pooled and estimated with Equation 20.

$$s_{AB} = \sqrt{\frac{(n_A - 1)s_A^2 + (n_B - 1)s_B^2}{n_A + n_B - 2}} \tag{20}$$

Finally, the t-value is calculated with Equation 21 and compared to the critical t-values of the set confidence interval for the given degree of freedom, which is calculated by $DF = n_A + n_B - 2$. In this study the t-test was performed with Microsoft® Excel and the respective p-values are reported. If the calculated p-values were below 0.05, the populations were considered significantly different.

$$t = \frac{|\bar{x}_A - \bar{x}_B|}{s_{AB}\sqrt{\frac{1}{n_A} + \frac{1}{n_B}}} \tag{21}$$

5 Results and Discussion

The objectives of this study were the creation of work packages for a knowledge-based process design according to Figure 7 and the investigation of different aspects thereof. The "Results and Discussion" chapter is divided into three sections. In the first section, a custom designed MFC is characterized with different inflow setups. The experimental results are linked to a finite element method simulation to explain the observed effects. In the second section, H-cells, the workhorse of BESs and the custom designed electrobioreactors are characterized and compared. In the third section, a proof of principle that rather complex compounds can be produced from CO_2 and electrochemically produced hydrogen and oxygen is described with an engineered *C. necator* strain.

5.1 Development and characterization of a flat-plate microbial fuel cell

To investigate MFC performance with different inlet setups, an air-breathing flat-plate based reactor concept was designed as described in Section 4.2.2.

5.1.1 Influence of perpendicular flow through a carbon fabric anode on the current of a flat-plate microbial fuel cell

Experiments with a *G. sulfurreducens* based MFC were done in the developed reactors (see Section 4.2.2 and Section 4.2.3) in order to investigate, how the flow setups (parallel *vs.* perpendicular flow through the anode) influence current and power generation in the flat-plate reactor. Perpendicular flow through the porous anode in batch experiments (pumping the medium in a loop) shortened the lag-time until current production compared to a parallel flow from approximately 12 h to 4 h, respectively (Figure 14). Maximum currents were 0.55 mA and 0.45 mA for perpendicular flow through the porous anode and parallel flow, respectively, in the batch mode. After 76 h of start-up in batch-mode, the MFCs were switched to continuous mode for the following experimental stage.

In continuous mode the maximum currents were reached after 12 d for perpendicular flow through the porous anode *vs.* 7 d for parallel flow and were 0.52 mA and 0.29 mA (45.1 mW m^{-2} and 14 mW m^{-2} using an external resistance of 1 kΩ), respectively (Figure 15). Acetate consumption was comparable between the two reactors and the corresponding inlet setups. *G. sulfurreducens* consumed 16.5 and 17.0 mmol acetate after 14 d, respectively (Figure 15). It can be assumed, that the metabolic activity was not affected by the flow regime in the MFC. Coulombic efficiencies were 3.7 % for the

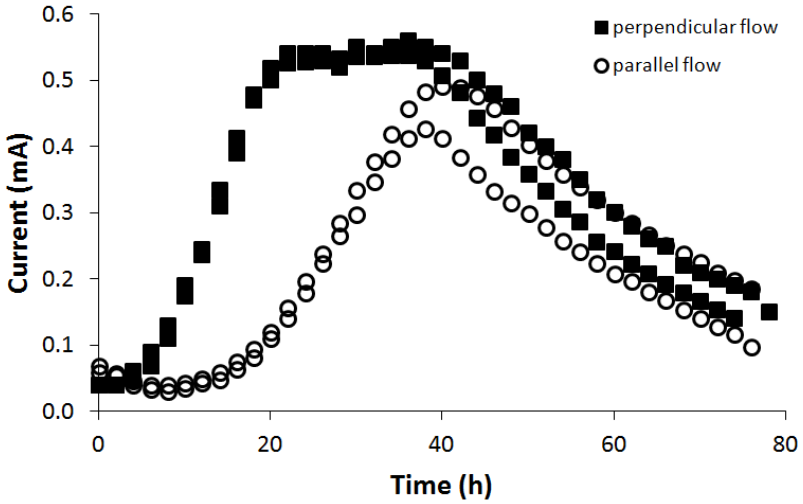

Figure 14: Current production in the flat-plate MFC in the start-up phase conducted in loop mode with a hydrodynamic retention time of 1.7 h, n=2.

perpendicular flow setup and 2.0 % for parallel flow, respectively. This is an increase for the perpendicular flow through the porous anode by a factor of 1.9 and explain the higher current production for this setup. Typical values of current efficiencies are in the range of 10 % for an external resistance of 1 kΩ in literature and thus comparable to the values obtained in this work (Cheng et al., 2006). More acetate is converted by releasing the respirative electrons to the anode rather than to oxygen. This can be explained by the altered flow setup: oxygen, which is introduced by the air-breathing cathode, is kept apart more efficiently from the biofilm due to the perpendicular flow. In this study a current increase by a factor of 1.8 and a power density increase by a factor of 3.2 were measured using a porous carbon fabric anode with an external resistance of 1 kΩ. Cheng et al. have reported a power density increase of approximately 1.1 fold using a plain carbon cloth electrode in a continuous cubic reactor setup with an external resistance of 1 kΩ (Cheng et al., 2006). Differences to this study can most likely be explained by the differences in the used geometries and biological variations.

5.1.2 Comparison of biofilm distribution on electrodes for both inlet applications to the measured biofilm distribution on the anode

Biofilm distribution on different parts of the carbon fabric anode was analyzed and compared after continuous cultivation of 14 d in the reactors provided with the two different inlet setups. DNA of the cells in the biofilm was stained with DAPI and analyzed using a fluorescence microscope (Section 4.2.4). Cells are shown in blue and the porous carbon fabric anode is black. For the perpendicular flow through the porous anode a biofilm is only detectable at the bottom part of the MFC (Figure 16). From these pictures it can be concluded, that more current could be produced in this MFC, because the anode is

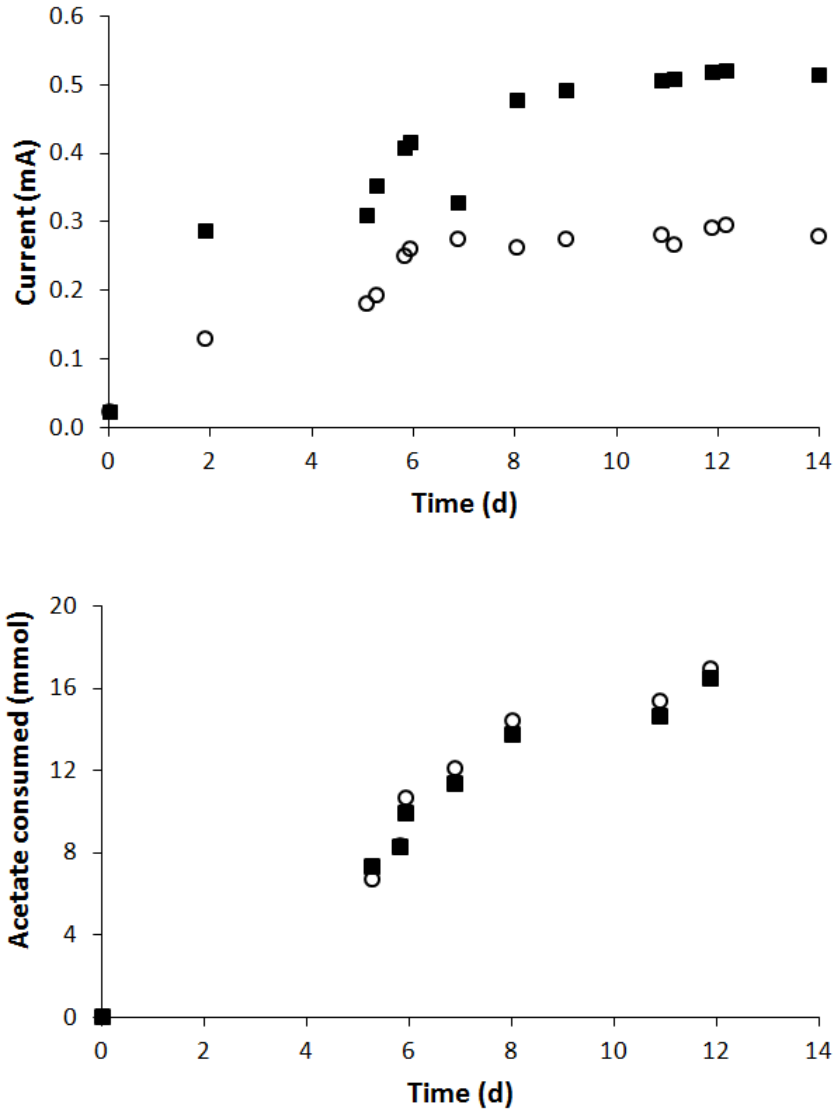

Figure 15: Current output and consumed acetate of a flat-plate MFC with an electrode spacing of 1 cm comparing the perpendicular flow through a porous anode (squares) *vs.* parallel flow (circles) in a continuous flow mode (start-up in loop mode is shown in Figure 14) with 0.5 g L^{-1} acetate as carbon source with a retention time of 1.7 h, n=2.

not fully grown with *G. sulfurreducens* biofilm. This could also be an explanation for the lower coulombic efficiencies in this study compared to literature values (Cheng et al., 2006), because a lot of electrode surface area is not covered by EAM and unwanted reactions may occur at the anode. For the parallel flow in general a lower degree of biofilm is visible (Figure 17). This explains the lower current production of 0.29 mA *vs.* 0.52 mA for parallel flow *vs.* the perpendicular flow through the porous anode. Most likely the cells adsorbed to the carbon fabric directly after entering the reactor since it is known, that the material has autoadsorptive properties (Mayer et al., 2018).

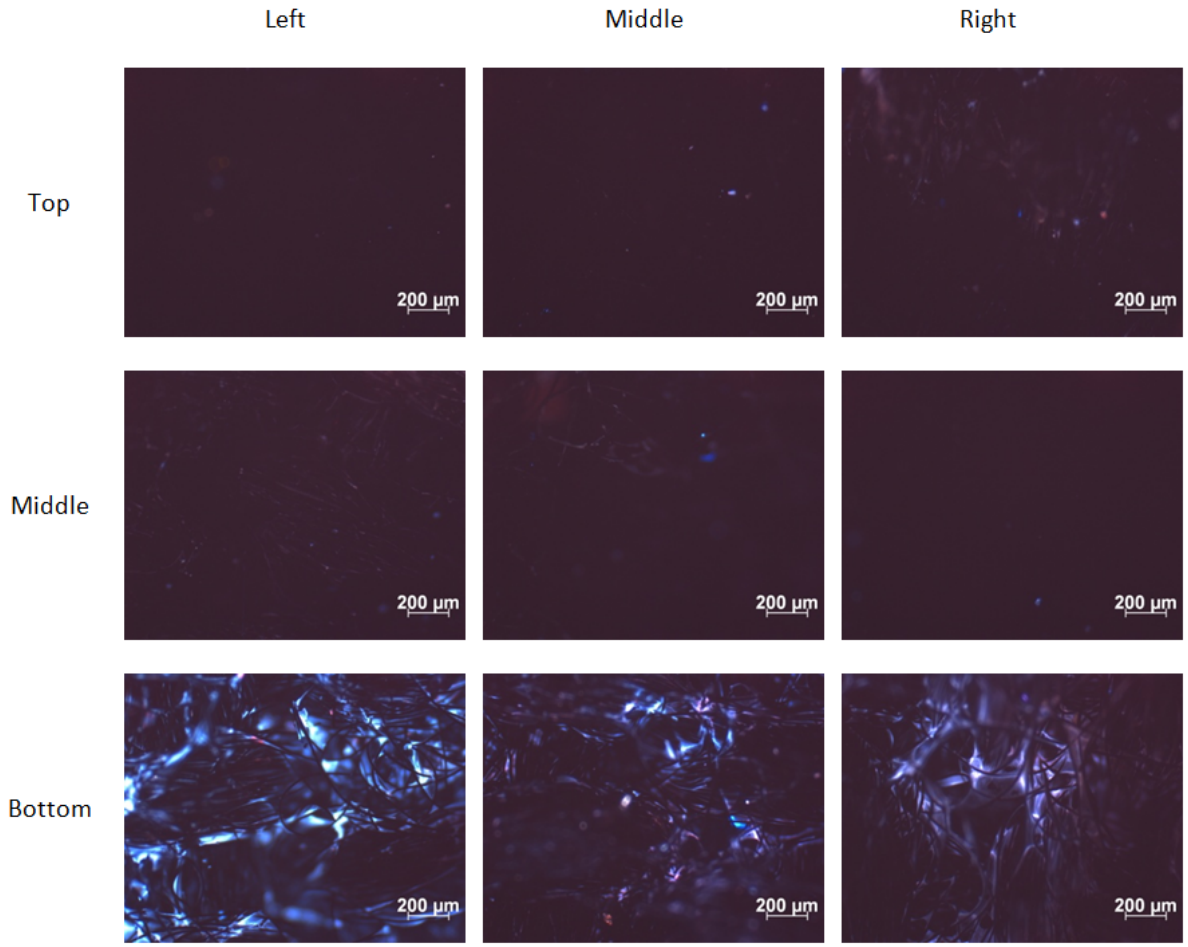

Figure 16: Biofilm distribution of *G. sulfurreducens* at different points in the microbial fuel cell after 14 days of an perpendicular flow through the porous anode visualized by DAPI staining of the cells (blue) and a fluorescence microscope. Inlet position was at the bottom middle.

5.1.3 Finite element method simulation of flow and concentration profiles for different MFC configurations

After observing the increased MFC performance and looking at the biofilm distribution, a finite element simulation was constructed for each flow configuration in order to understand the resulting experimental performance in terms of the mass transport properties of each system. Besides reducing oxygen concentrations, also improved substrate distribution due to a better mass transport has been reported to be responsible for an increased MFC performance (Cheng et al., 2006; Sleutels et al., 2011). Simulations with parametric sweeps of both, porosity and permeability, were performed to assess the impact these parameters could have on the resulting fluid and substrate concentration profiles for each flow configuration. In this study, a carbon fabric with a porosity of 0.86 and a permeability of 10^{-10} m^2 was used. Simulation results were obtained in order to investigate the influence of electrode properties on the substrate distribution, pressure drops and the ratio of advective transport rate and diffusive transport rate (Peclet number), which may

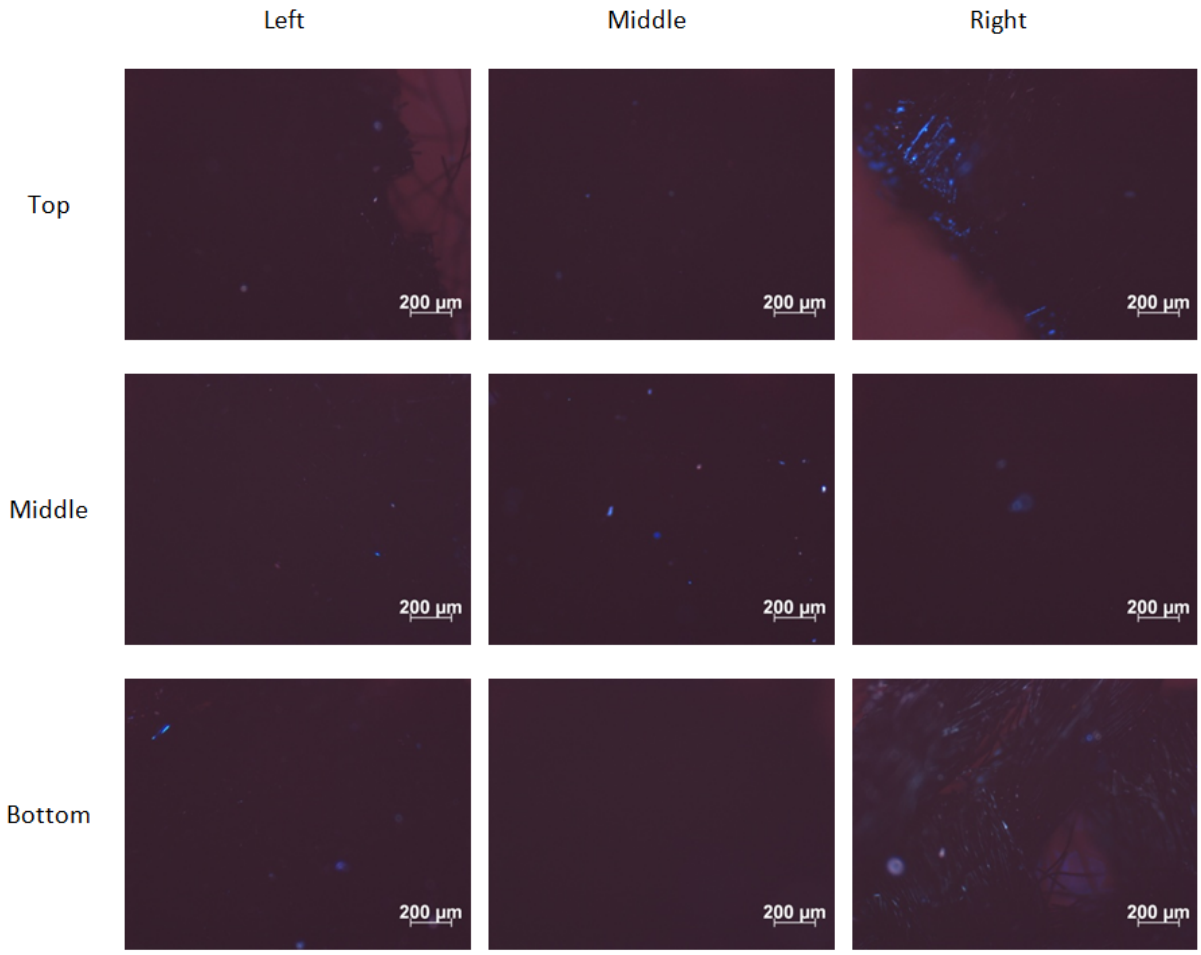

Figure 17: Biofilm distribution of *G. sulfurreducens* at different points in the microbial fuel cell after 14 days of a parallel flow over the anode visualized by DAPI staining of the cells (blue) and a fluorescence microscope. Inlet position was at the bottom right.

have a strong influence on MFC performance. Therefore, an inlet of uniform concentration into a substrate depleted system (the porous anode and the MFC) was simulated with a normalized concentration of 1 as the steady-state. Figure 18 shows the normalized concentration profile of a substrate in the porous layer *vs.* time for the two simulated flow setups. For perpendicular flow, the porous layer achieved steady-state after an operation time of 10 h while for a parallel flow it took close to 30 h (simulated operation times) for a complete distribution of the substrate in the porous layer. These differences in the simulations indicate that the effect on current output as discussed before for the used carbon fabric electrode (ϵ=0.86 and κ=10^{-10} m^2) is due to differences in substrate distribution for the two setups (Section 4.2.5).

The simulations reveal possible substrate limitations for the biofilm in certain areas of the anode for the parallel flow. In this simulations no consumption of acetate by the EAM *G. sulfurreducens* is calculated. Therefore, substrate depletion by the EAM at certain areas of the anode can only be estimated. Caccavo et al. (1994) reported acetate consumption rates of 0.1 mM h^{-1} with ferric phosphate as an electron acceptor calculated

over a cultivation time of 12 d to reach cell concentrations of approximately 10^8 cells per mL.

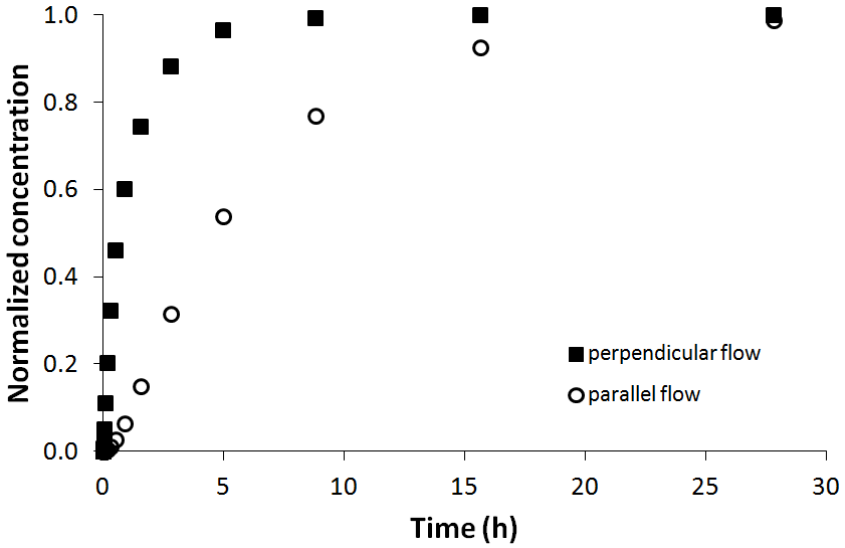

Figure 18: Normalized concentration profiles in the porous layer (i.e. the carbon fabric anode) *vs.* time in the perpendicular flow setup (closed squares) and parallel flow to the anode (open circles).

Looking at the estimated Peclet numbers through the porous layer, which describe the ratio of convective mass transport (fast transport by convection) and diffusive mass transport (slow transport due to molecular diffusion), support this explanation. If Peclet numbers are far below 1 diffusion dominates over convection (Huysmans and Dassargues, 2005). For the perpendicular flow a Peclet number of 1.9 *vs.* 0.004 for parallel flow was estimated over the whole electrode based on the average velocity and substrate diffusion coefficients, indicating a shift from diffusion-dominated transport in the parallel flow system to a slightly more convection-dominated regime in the perpendicular flow MFC. As illustrated in the resulting concentration *vs.* time plots in the porous layer, increasing the rate of convective transport is beneficial to eliminate substrate limitations (Figure 18). One can discuss however, that the advantage of this increased substrate availability is outweighed by an increased pressure drop in the system and possible clogging due to biofilm growth. However, Cheng et al. reported, that there was no blocking of the electrode over a time period of 42 d with glucose as a substrate and over 100 h for real waste water with a perpendicular inlet (Cheng et al., 2006).

In this study as well, no clogging of the electrode was observed over a time period of 14 d. The simulations also showed an increase of the pressure drop from 1 mPa to 34 mPa by changing the inlet flow setup from parallel to perpendicular, respectively, however overall pump power requirements are negligible for both setups given the flow rates involved. Flow rates in MFCs need to be slow due to low decomposition rates of the organic loading leading to high hydraulic retention times and a laminar flow regime.

The increased current output with perpendicular flow through the porous anode can then be explained by increased convective transport and a general improvement in the substrate distribution throughout the entire porous cloth in the case of perpendicular flow (Figure 19). The simulated substrate distribution does also fit to the observed biofilm on the carbon fabric anode as discussed before (Figure 16 and Figure 17).

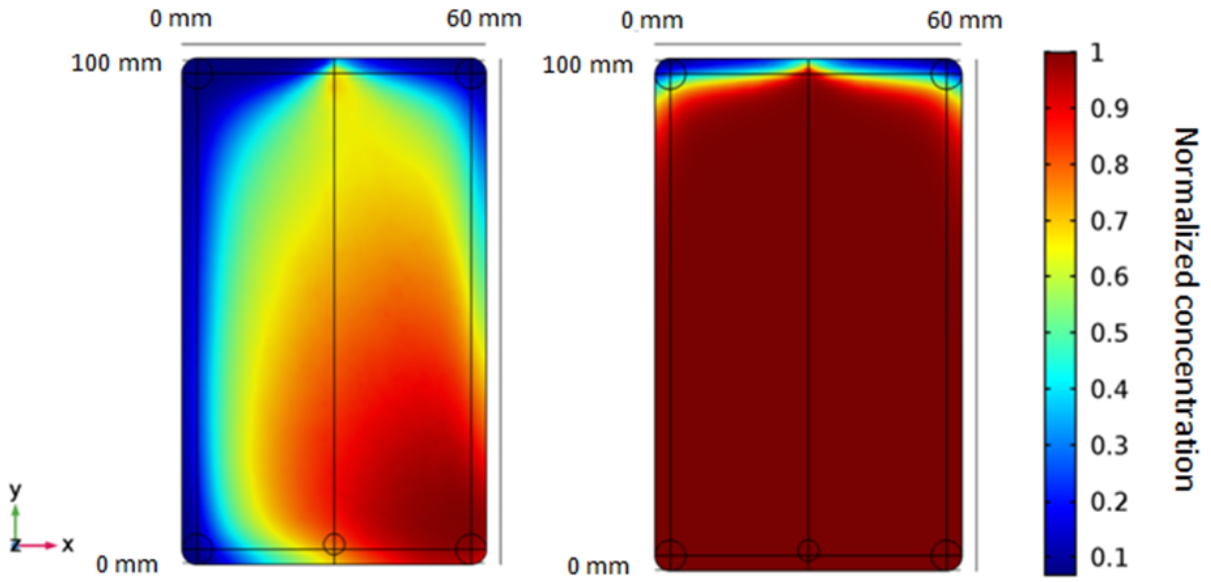

Figure 19: Normalized concentration profiles in the porous layer (i.e. the carbon fabric anode) after 5 h in parallel flow (left, inlet at the bottom right) and perpendicular flow through the anode (right, inlet in the middle at the bottom).

Since the electrode properties seem to be important for the MFC performance, further simulations with changes in porosity and permeability were performed to estimate what properties would be interesting to investigate in future studies. Varying the porosity did not lead to a significant change of the distribution (data not shown).

Figure 20 shows that a further increase in permeability would lead to a faster substrate distribution for the perpendicular flow setup. By increasing the permeability from 10^{-8} m^2 to 10^{-11} m^2 a faster saturation of the porous layer with substrate can be simulated. At permeabilities greater than 10^{-11} m^2 no further increase of saturation speed of the porous layer with substrate is shown in the simulations. Permeability affects the degree of flow dispersion (uniformity through the bottom). The more resistive the cloth (the electrode) is the more flow will spread out to make sure it can go through it. Substrate distribution is not affected by changing porosity and permeability for the parallel flow setup. The distribution is governed by molecular diffusion from the bulk into the porous layer and will not transport through the layer before exiting the reactor. Therefore, only the electrode surface area facing the medium can be accessed by the EAM. For perpendicular flow also deeper parts of the electrode are provided with substrate and can be accessed by the EAM. Therefore it can be concluded, that for the system considered, the inlet flow configuration

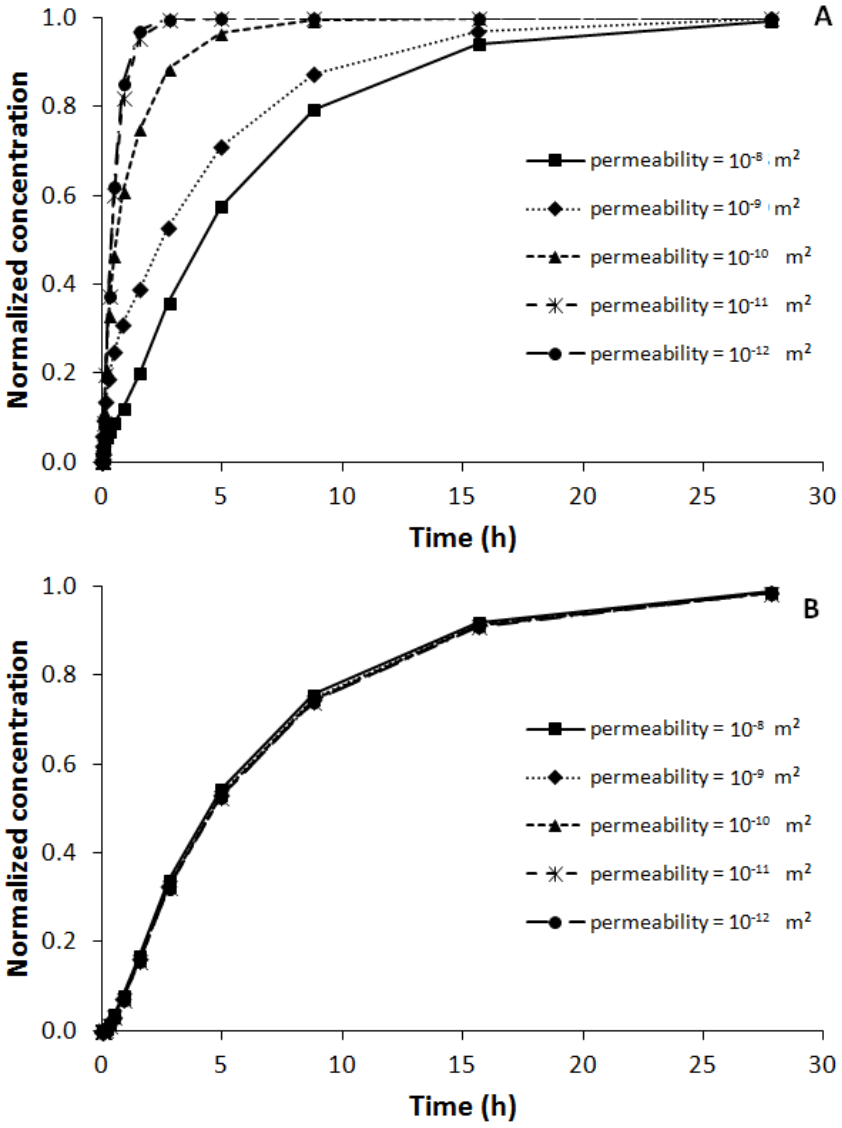

Figure 20: Substrate distribution at different time points for different electrode properties in the perpendicular flow setup (A) and the parallel flow setup (B). Lines are to guide the eye.

is more important than the properties of the cloth for MFC performance. While substrate distribution is increased for the perpendicular flow at higher permeabilities, as mentioned also an increased pressure drop is found (Figure 21). For parallel flow the pressure drop is nearly constant if the permeability is varied. This can be explained due to the fact that the inlet flow does not have to go through a higher flow-resistance area of the electrode itself *vs.* the case of a perpendicular inlet where the flow is forced through the porous layer.

Peclet numbers, which describe the ratio of convection (advection) to diffusion, are influenced by the porosity for the perpendicular flow setup (Figure 22). With decreasing porosities of the electrode from 0.8 to 0.4, the Peclet number increased in an exponential fashion from approximately 2 to 6 and convection dominated, which ensured a fast substrate transport. For the parallel inlet setup in general, the Peclet numbers were sev-

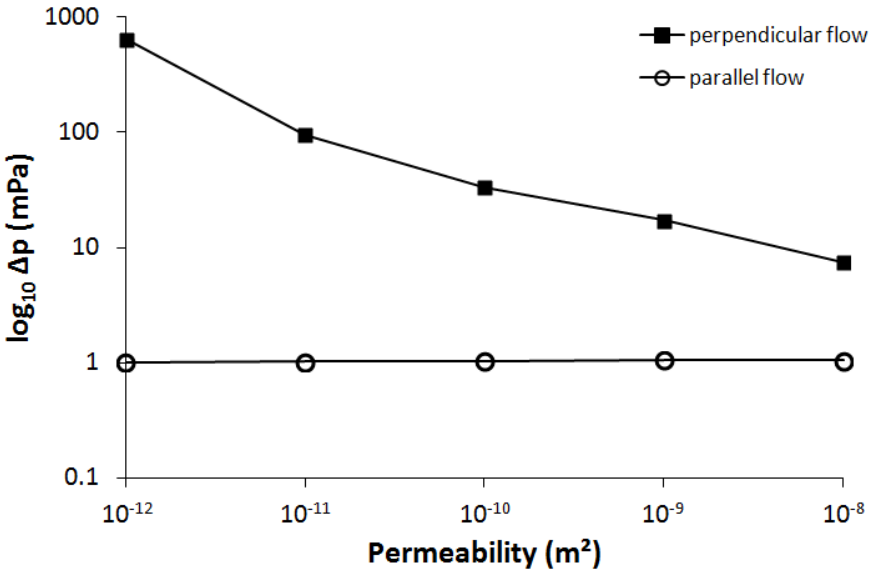

Figure 21: Pressure drops for the perpendicular flow and the parallel flow setup.

eral orders of magnitude lower compared to the perpendicular flow setup. Permeability and porosity influence the Peclet number, which was highest at a porosity of 0.4 and a permeability of 10^{-8} m^2 (Figure 22).

For perpendicular flow there is no significant change in the diffusive contribution compared to the convective contribution, while for parallel flow increasing porosity increases the diffusion coefficient and therefore enhances transport (as it is in a diffusion-dominated regime). Also increasing permeability makes the fluid more likely to transport through the cloth due to a lower resistance. Cheng et al. suggested using greater overall porosities to prevent clogging in real waste water treatment (Cheng et al., 2006). This would prevent clogging, however, the simulations show that an increased porosity could lead to a lower Peclet number which would possibly lead to a lowered convective transport and negate the positive effect.

An alternative for directing the flow through the anode could be the insertion of internal structures to ensure a better distribution of the substrates (Kim et al., 2014). The anode itself also could be altered geometrically to ensure a better substrate distribution (Chen et al., 2012b). Also completely different reactor designs with serpentine flows or flat-plate reactors, where the flow is directed along the anode, have been reported (Feng et al., 2014; Zhuang et al., 2012). However, these strategies have the disadvantage of increased investment costs and complexity of design. Therefore, despite their promising performances in larger scales, these reactor concepts may not be suitable for a scale-up due to high investment costs (Zhuang et al., 2012). Furthermore, penetration of the electrodes with substrate may still not be ideal in the reactor systems and should be investigated in the future.

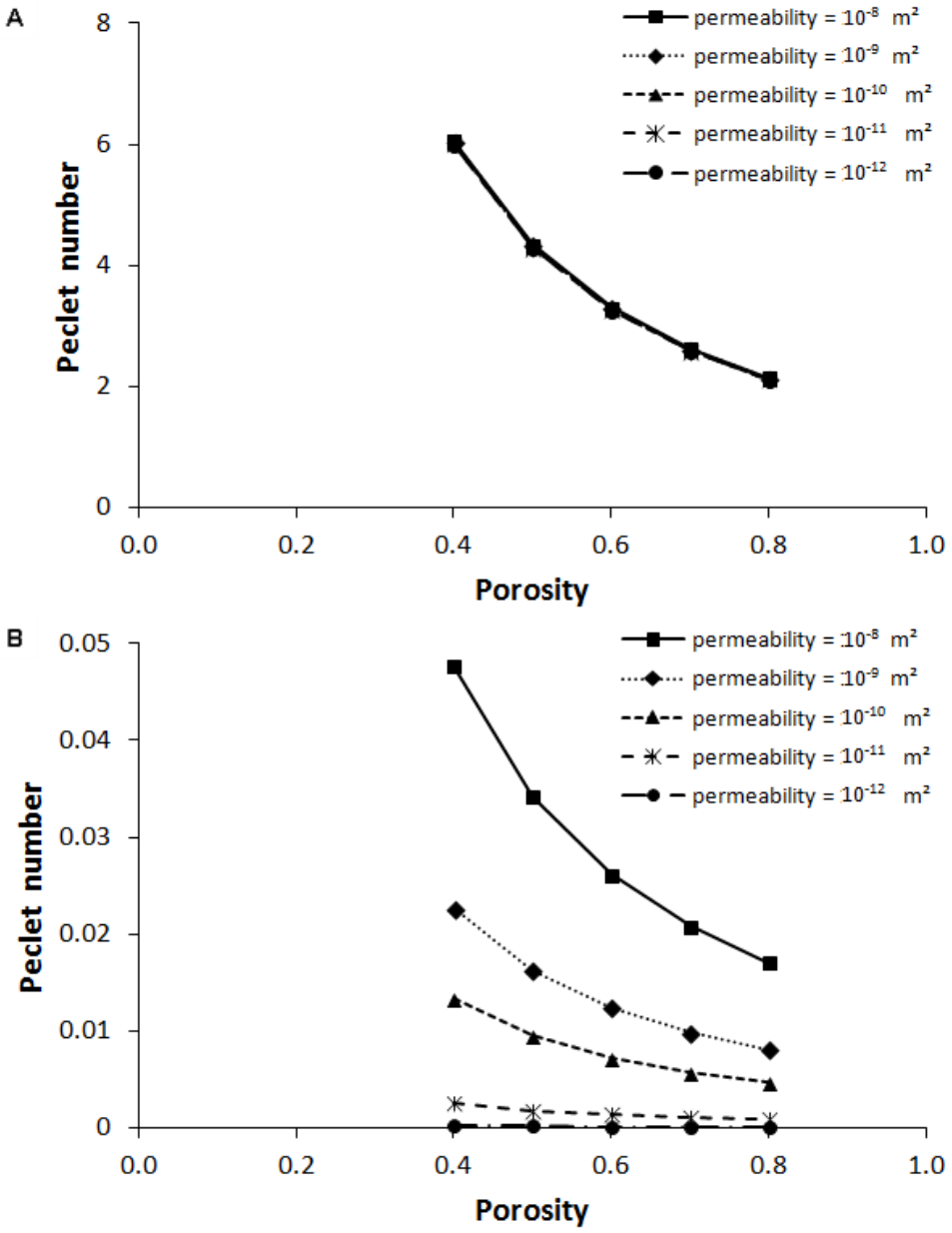

Figure 22: Peclet numbers for the perpendicular flow (A) and parallel flow setup (B).

5.2 H-cells - the workhorse for microbial electrochemical technologies

H-cells are widely used for fundamental investigations in BESs. A deeper characterization and comparison in terms of electrochemical losses and biological performance *vs.* more controlled systems such as electrobioeactors is described in the following sections.

5.2.1 Electrochemical characterization

Figure 23 shows the abiotic characterization based on water electrolysis of an H-cell using graphite sticks as electrodes regarding voltage drops over the distance between the anode and the cathode *via* the membrane. The ideal electrolyte 0.5 M Na_2SO_4 was chosen for characterization due to its relatively high conductivity of 55 mS cm^{-1} (Wolf, 1966). A Nafion® 117 membrane was applied as it is widely used in MFCs (Leong et al., 2013). The conductivity of the membrane has been determined in literature before and is approximately 101 mS cm^{-1} (Affoune et al., 2005). Main losses were observed at the working and counter electrodes and increased with the applied current (Figure 23). If a biofilm or an other catalyst is interacting with the working electrode, a lower potential loss is expected, because the overpotential at the electrodes is reduced. Cell voltages were in the range of 1.5 to 3.8 V, which fits to values reported in literature. Giddings et al. (2015) reported cell voltages of 3 to 5 V depending on the applied potential at the working electrode. For an abiotic hydrogen production in H-cells at a potential of -990 mV, cell voltages of 3.5 V were reported in the same study.

Besides the overpotentials at the anode and the cathode caused by the non-catalyzed oxygen evolution reaction (OER) and hydrogen evolution reaction (HER), respectively, also the membrane and the electrolyte are responsible for losses. The losses increased with the applied current. It did not matter whether a positive or a negative current was applied, the curves mirrored at the y-axis (Figure 24). Compared to the overpotentials measured at the electrodes (Figure 23) the losses caused by the electrolyte and the membrane were rather small with a maximum of 0.24 V and 0.21 V, respectively.

5.2.2 Biological characterization with *Shewanella oneidensis* and *Geobacter sulfurreducens*

Biological characterization of H-cells was done using *S. oneidensis* and its anaerobic anode respiration using lactate as a substrate. Carbon fabric was used as anode and cathode material and the working electrode was poised at +400 mV. To compare the influence of Nafion® 117 membranes, the H-cells were operated without a membrane (non-separated condition) and with a membrane (separated condition). Current production of both con-

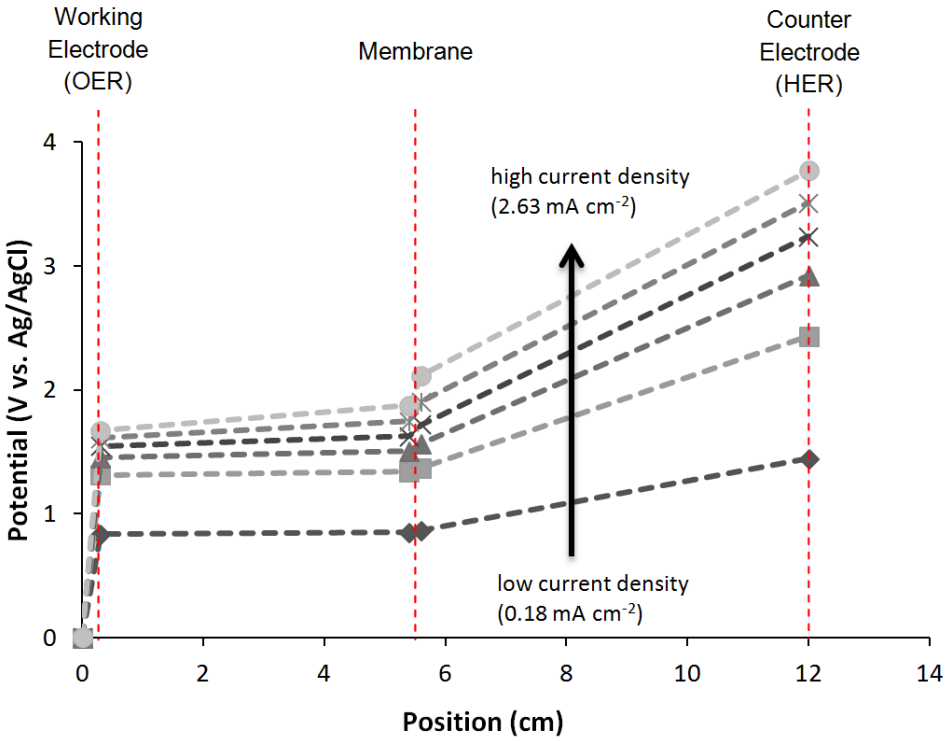

Figure 23: Electrochemical losses of 0.5 M Na_2SO_4 at various current densities in a conventional H-cell electroreactor. Graphite sticks with a surface area of 9.7 cm^2 were used as working and counter electrodes. Position 0.2 cm is the working electrode and position 12.0 cm is the counter electrode potential in the system.

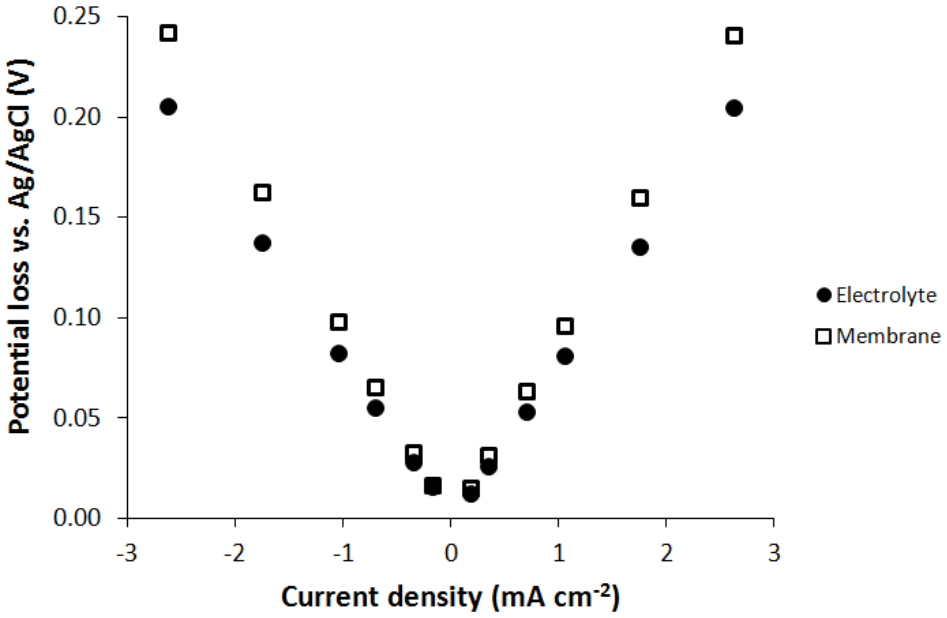

Figure 24: Electrochemical losses over the electrolyte 0.5 M Na_2SO_4 and the membrane (Nafion® 117) in a conventional H-cell electroreactor. Graphite sticks with a surface area of 9.7 cm^2 were used as working and counter electrodes.

ditions is compared in Figure 25. Maximum current densities in both operation modes were comparable, but slightly higher in the non-separated case with 150 ± 49 µA cm^{-2} *vs.* 121 ± 19 µA cm^{-2}. Relative standard deviations were, however, lower in the separated operation mode with 16% *vs.* 32% for the non-separated one, respectively. The lower current densities in the separated H-cells can be explained by the installed membrane and its resistance causing a potential loss as described in Section 5.2.1. Coulombic efficiencies were 4.6% and 12.5% for the non-separated and the separated operation mode, respectively. It can be concluded, that the lower coulombic efficiency may come from oxygen diffusing into the H-cell being responsible for the higher current density in the non-separated operation mode. This effect (higher current production in the presence of oxygen) has been described in literature for *S. oneidensis* based MFCs (Rosenbaum et al., 2010). Rosenbaum et al. (2010) used comparable conditions (separated operation) in H-cells and average current efficiencies of 4.5% were reported. The calculated current efficiencies of 4.6% in this work are fitting well to the values reported.

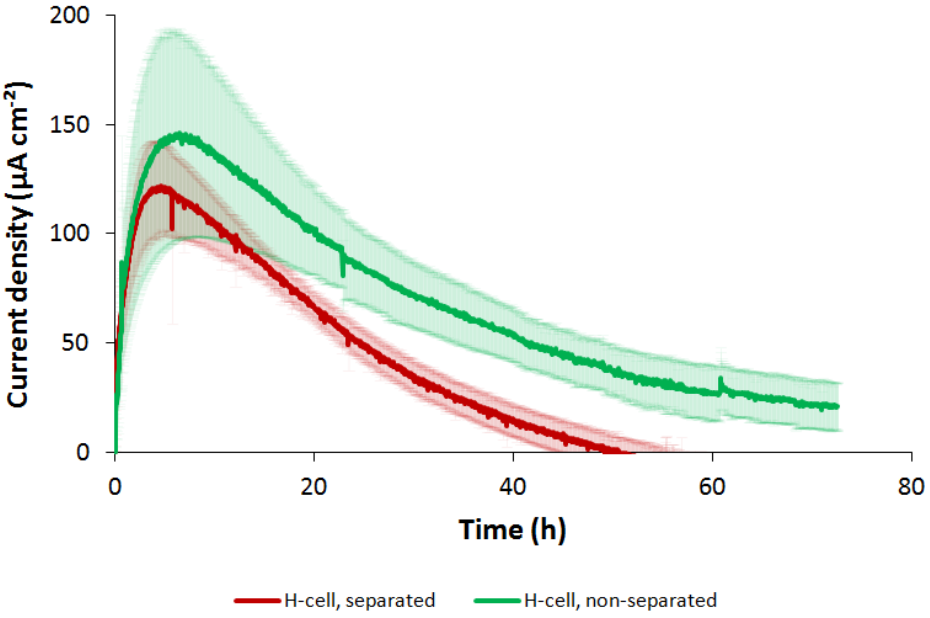

Figure 25: Current generation of 12.2 ± 1.3 mg L^{-1} *S. oneidensis* in a separated (red) and non-separated (green) H-cell, respectively, using 6 cm^2 of the working electrode and counter electrode carbon fabric poised at +400 mV *vs.* Ag/AgCl. The experiments were performed with n=4 repeats in separated and non-separated H-cells, respectively.

G. sulfurreducens was used as a second electroactive model organism in a separated H-cell. The non-separated system was not part of the experiments, because *G. sulfurreducens* is oxygen sensitive. Otherwise, comparable conditions to the experiments as discussed before were chosen, but acetate was used as a carbon source instead of lactate. Maximum current densities of 1,060 µA cm^{-2} were reached increasing the performance of the *S. oneidensis* MFC by 8.8 fold at a coulombic efficiency of 18.6% (Figure 26). These results are in line with literature studies (Section 2.1.2), where the performance of *G. sul-*

furreducens and *S. oneidensis* MFCs were compared in a cubic reactor using comparable electrode materials (Dolch et al., 2014). The results gained in the H-cell are used as a "standard" for the comparison of the developed electrobioreactor, which is highlighted in the next section.

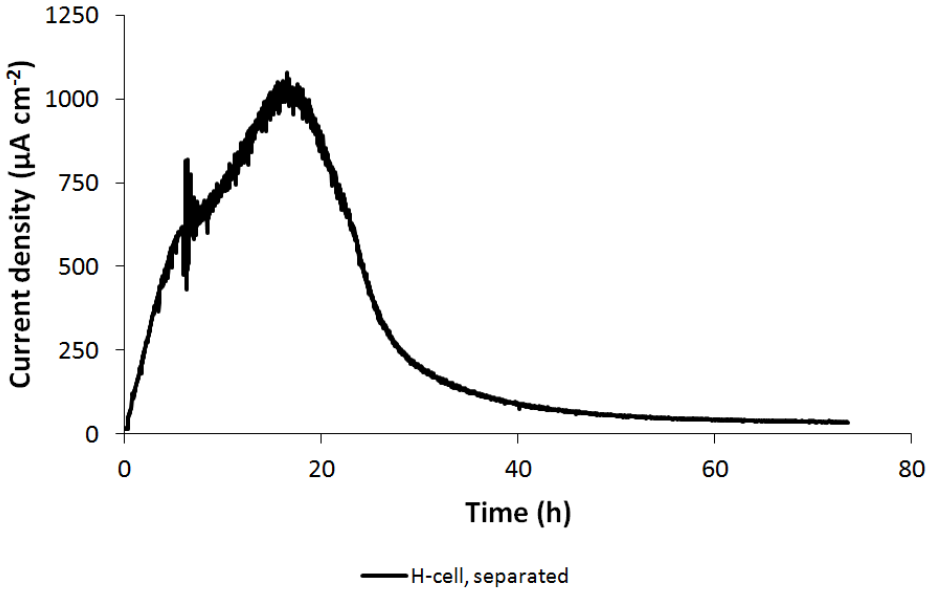

Figure 26: Current generation of *G. sulfurreducens* inoculated at an OD_{600nm} of 0.6 in a separated H-cell using 6 cm^2 of the working electrode and counter electrode carbon fabric poised at +400 mV *vs.* Ag/AgCl in n=1.

5.3 Electrobioreactors - modification of a conventional stirred tank (bio)reactor

Several electrobioreactors have been described so far (Hintermayer et al., 2016; Rosa et al., 2016; Utesch and Zeng, 2018). In this section two assemblies to host carbon fabric electrodes in a conventional bioreactor are designed and characterized electrochemically as well as biologically. Furthermore, flow profiles calculated by computational fluid dynamics simulations are compared to a conventional bioreactor to ensure comparable flow properties and mixing.

5.3.1 Design of inserts for a non-separated and a separated electrobioreactor and their characterization

Design of assembly 1 and assembly 2 for a non-separated and a separated operation mode, respectively, is described in Section 4.2.7.

Electrochemical characterization

To compare assembly 2 with conventional reactor concepts for BESs such as H-cells, electrochemical losses were investigated according to Section 5.2.1 based on water electrolysis using an idealized and simplified electrochemical system with graphite stick electrodes and 0.5 M Na_2SO_4 as electrolyte (Figure 27). Current was applied to the system and potentials were measured using reference electrodes placed next to the electrodes and the membrane to measure losses due to electrolyte and membrane (Figure 11, Section 4.2.10). The potential losses *via* the membrane and the electrolyte increased with the applied current in a linear (ohmic) fashion. As expected from the experiments performed in H-cells (Section 5.2.1), independent of negative or positive current applied, the potential losses were comparable to each other. In agreement with the respective results obtained in H-cells (Section 5.2.1) these results show that the biggest loss in this BES is due to overpotentials at the two electrodes caused by the non-catalyzed oxygen evolution reaction (OER) and hydrogen evolution reaction (HER), respectively. This can be reduced by the use of catalysts (Section 2.1): i) for cathodes platinum or electroactive bacteria catalyzing oxygen reductions can be used ii) for anodes dimensional stable anodes or electroactive bacteria catalyzing oxygen evolution or in general the supply of electrons can be used (Dulon et al., 2006; Huang et al., 2011; Zhou, 2013).

Compared to the potential losses measured at the electrodes in H-cells (Figure 23) the losses caused by the electrolyte and the membrane are much smaller in the electrobioreactor with assembly 2 with a maximum of 0.14 V and 0.10 V, respectively. It was expected, that only the electrode distance influences the potential losses. However, the losses are smaller as indicated for the electrobioreactor although the electrode distance is

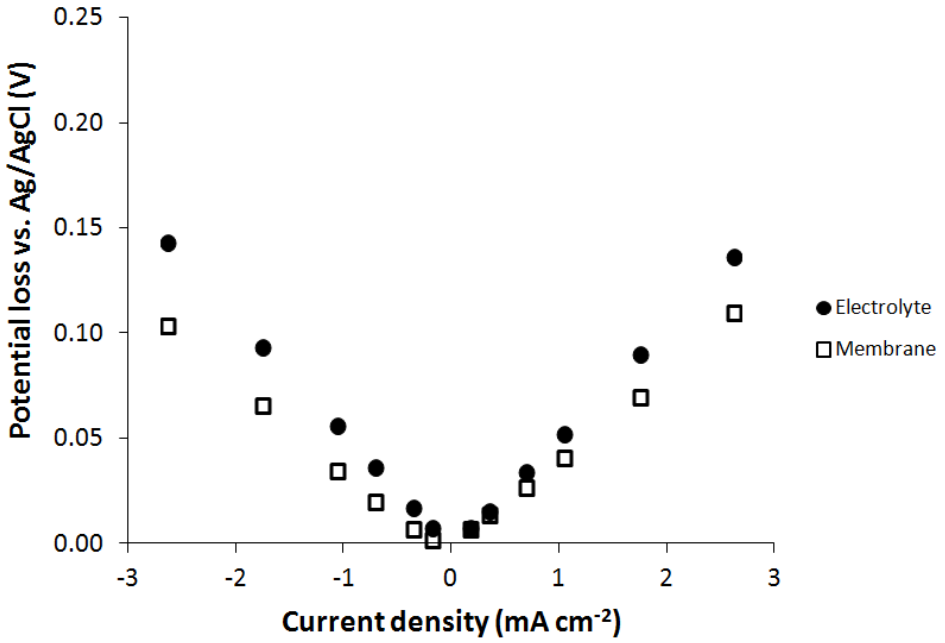

Figure 27: Electrochemical losses over the electrolyte 0.5 M Na_2SO_4 and the membrane (Nafion® 117) in the developed reactor assembly 2. Graphite sticks with a surface area of 28.6 cm^2 were used as working and counter electrodes.

increased from 12 cm in the H-cell to 15 cm in the electrobioreactor (Figure 28). The increased size of the membrane in the electrobioreactor with assembly 2 (H-cell: A=4.9 cm^2, electrobioreactor with assembly 2: A=20.3 cm^2, which is a 4 fold increase) could explain these results, because the resistance caused by the membrane is reduced by increasing the membrane surface area (Leong et al., 2013). A drawback of an increased membrane surface area can be oxygen crossover, which lowers the coulombic efficiency (Leong et al., 2013). It can be concluded that the losses in the electrobioreactor with assembly 2 are 42 % lower for the electrolyte and 52 % lower for the membrane compared to the H-cell measurements.

Overall the losses are negligible when using 0.5 M Na_2SO_4 as an electrolyte due to its high conductivity (55 mS cm^{-1}, Wolf (1966)). For BES, growth media with far lower conductivity need to be used and most likely, the potential losses *via* bulk solution resistance do matter (Sydow et al., 2017a). To test this hypothesis, LSBM and SBM were used to characterize the system. The specific electroactive surface of a graphite rod is fairly low and would not be used in a technical setup. Therefore, a carbon fabric electrode with a higher electrode surface area was used for further characterization to be closer to a technical application. Electrochemical characterization revealed, that the growth media show higher potential losses in comparison to 0.5 M Na_2SO_4 (Figure 28, conductivity of the used buffer system is 10 mS cm^{-1}). Especially the medium omitting lactate showed high potential losses compared to a medium with 100 mM lactate and the “ideal” electrolyte Na_2SO_4. Comparable losses were measured in H-cells using graphite sticks, which are

widely used in BES (Figure 23 and Figure 24).

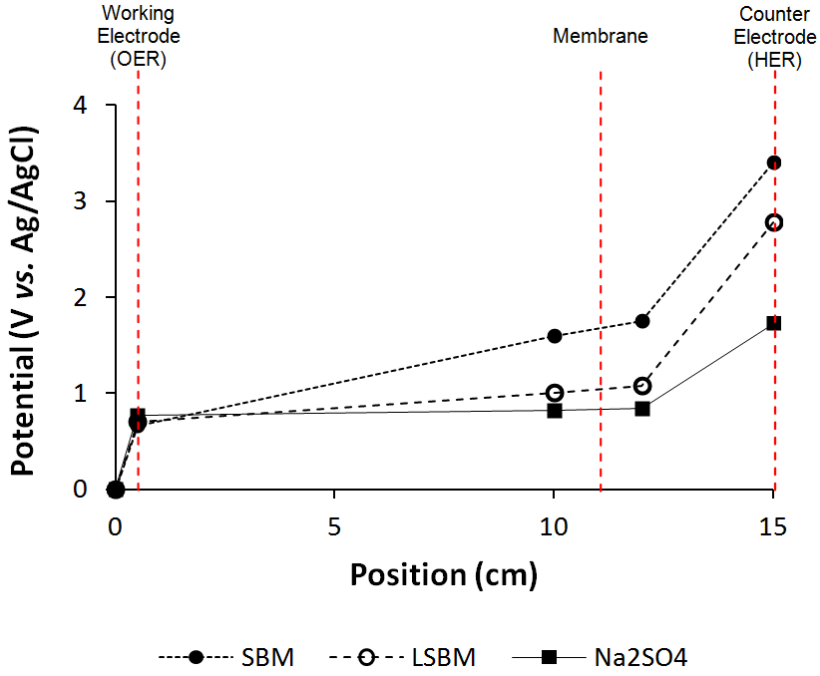

Figure 28: Electrochemical losses of different electrolytes at a current density of 1.05 mA cm^{-2}: SBM, LSBM and 0.5 M Na_2SO_4 and the membrane (Nafion® 117) in the developed reactor assembly 2. Carbon fabric (129 cm^2) contacted with a platinum wire (d=0.5 mm) was used as working and counter electrode.

Current densities reported for unbalanced fermentations are in the range of 55 µA cm^{-2} for a *S. oneidensis* based microbial fuel cell in a modified bioreactor (Rosa et al., 2016). For cathodic processes where current is consumed and acetate or butyrate is produced using pure or mixed cultures, current densities (using the projected geometric surface areas for calculation) range from several µA cm^{-2} up to 3.7 mA cm^{-2} (Campos-Rodrigues and Rosenbaum, 2014; Ganigué et al., 2015; Giddings et al., 2015). However, a *Pseudomonas putida* based anodic respiration process using an external mediator showed higher current densities (up to 12 mA cm^{-2} projected geometric surface area). Here, electrochemical losses at the electrodes play a greater role compared to the processes described before and need to be accounted for the electrochemical measurements (Hintermayer et al., 2016). In general, it can be concluded that electrochemical losses over the electrolyte and the membrane can be neglected in most setups due to the low current densities in the respective BESs. This postulate can be confirmed looking at current densities of BESs, which are limited due to high overpotentials at the electrodes and slow migration of protons or other ions *via* membranes (Clauwaert et al., 2008; Zhou, 2013). These results indicate that the losses are reduced in the electrobioreactor compared to the H-cell and is therefore more suitable for BESs.

5.3.2 Computational fluid dynamic analysis on the turbulence and mixing times by the applied insert

By applying an insert hosting electrodes into a bioreactor the velocity fields may be influenced and dead zones could be generated. To address this postulation the velocity fields were solved in the conventional bioreactor and turbulent kinematic viscosity was calculated and compared (Figure 29). Maximum values were $1.1 \cdot 10^{-4}$ m^2 s^{-1} and minimum values were $2.0 \cdot 10^{-6}$ m^2 s^{-1} for the conventional bioreactor, respectively, indicating that the fluid is well mixed. Assuming a stirrer speed of 400 rpm, which was used in this study, a substance is transferred a distance of 12.7 cm (which is the vessel diameter) at the least mixed zone (nearby the shaft) in 66 min, 1.2 min in the best mixed zone and 2.1 min in average, respectively, in a conventional bioreactor. By using the electrobioreactor with assembly 2, maximum values were $2.9 \cdot 10^{-4}$ m^2 s^{-1} and minimum values were $1.5 \cdot 10^{-6}$ m^2 s^{-1}, respectively. Assuming a stirrer speed of 400 rpm a substance is transferred a distance of 12.7 cm at the least mixed zone (nearby the shaft of the electrobioreactor) in 89 min, 0.5 min in the best mixed zone and 1.2 min in average, respectively. This implies a fairly minimal change in the mixing intensity between the two investigated configurations. Values in the electrobioreactor hosting assembly 1 as an insert are to be expected in the same range due to geometric similarity. It can be concluded that both modified systems are well mixed and no significant dead zones are caused by inserting electrodes into the bioreactor.

5.3.3 Electrochemical measurements affect the pH measurement in the electrobioreactor

During first tests of assembly 1, differences between pH values (up to 0.2 units) measured with the reactor probe *vs.* external measured values occurred frequently and were consequently investigated. Figure 30 shows the measurement of the pH with different positioning of the pH probe. In the range of -1,000 mV and +600 mV the measured pH values were stable, if the diaphragm of the pH electrode did not face towards the electric field, which allows a pH measurement without interference. A slight increase of the pH values from negative potentials to positive potentials was observed in the range, if the diaphragm was facing towards the electric field (Figure 10).

An electronic separation of the two measurement systems, i.e. electrochemical and pH measurement, was done using an isolating transformer to isolate the circuits but did not reduce the pH shift during electrochemical measurements. Parasitic currents, which are unwanted and circulate between devices of integrated circuits, may be responsible for this behavior. Functionality of the pH probe was ensured with calibrations prior to every cultivation and potential values of the probe did not drift over 20 cultivations.

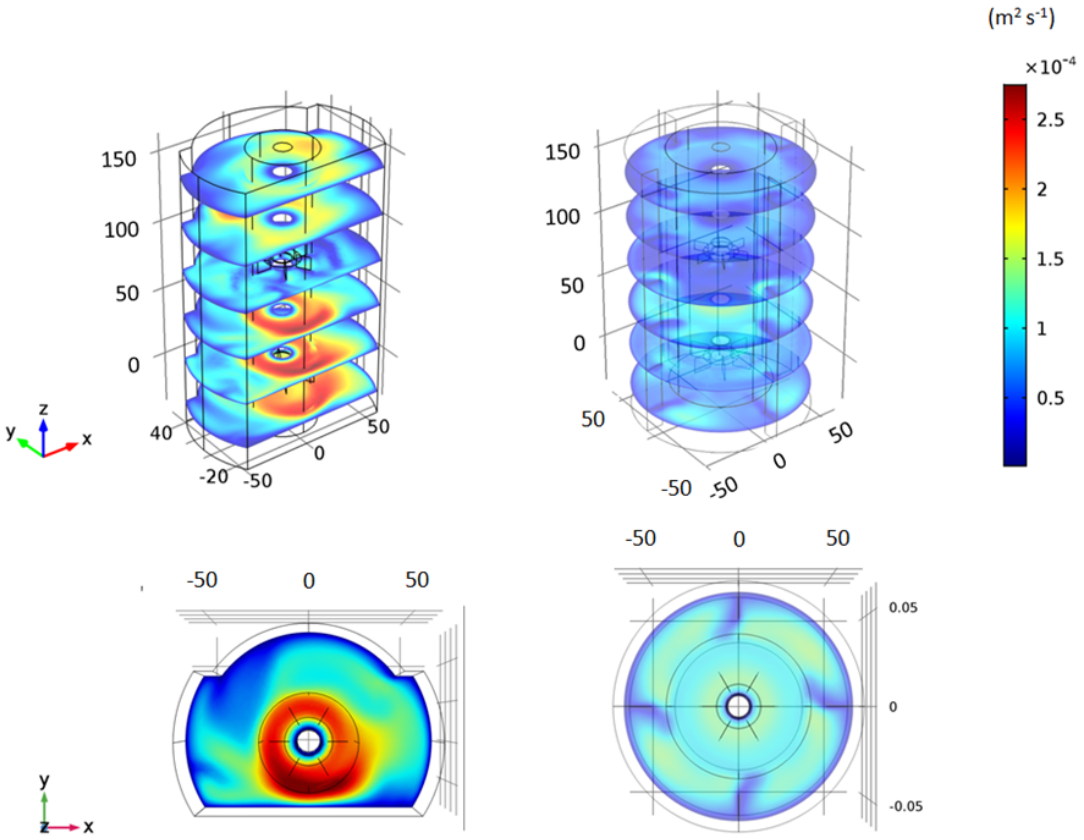

Figure 29: Comparison of the turbulent kinematic viscosity in the bioreactor equipped with assembly 2 (left image) and a standard bioreactor (right image) simulated by computational fluid dynamics in COMSOL®. Dimensions in x, y and z direction are given in mm. The figures show slices in xy-planes at different heights throughout the different reactor configurations, with the magnitude of turbulent kinematic viscosity plotting on each slice.

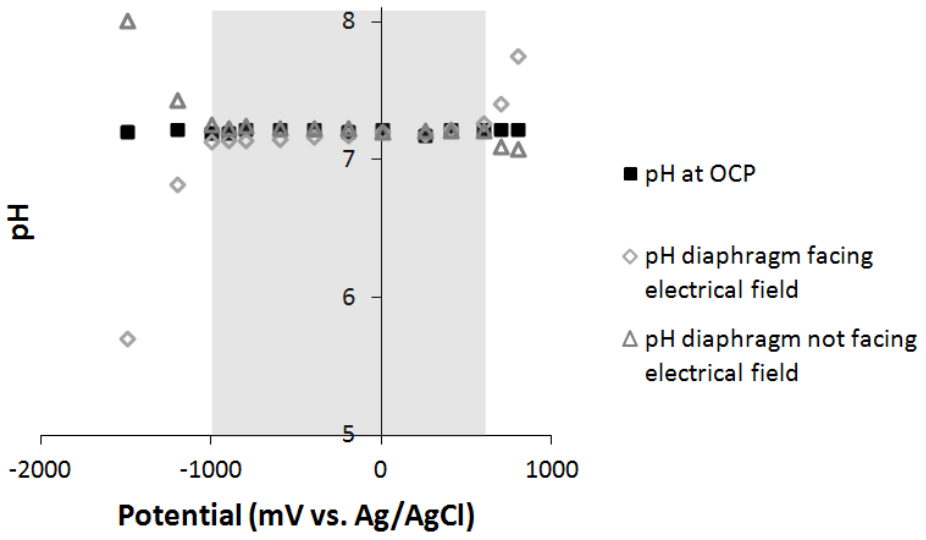

Figure 30: pH values during an electrochemical measurement and at the open circuit potential (OCP) with different positions of the pH electrode diaphragm towards the electric field. Graphite sticks with surface area of 28.6 cm^2 were used as working and counter electrodes at varied potentials. Potential range of reliable operation is marked in grey.

The identified operation range of -1,000 to +600 mV *vs.* Ag/AgCl is fitting most BES. However, BES using higher or lower potentials are excluded (e.g. H_2 evolution for indirect electron transfer) (Sydow et al., 2017a). Therefore, other pH measurement techniques need to be considered for these applications like optical measurements, which already have been described for pH control in bioreactors (Hanson et al., 2007; Kusterer et al., 2008).

5.3.4 Bioelectrochemical characterization of the electrobioreactor with *Shewanella oneidensis*

Bioreactor cultivation of *Shewanella oneidensis* in the non-separated assembly 1

First, characterization and proof of principle of electrode integration into a conventional bioreactor was done by a simple modification of vortex breakers (assembly 1). The first runs were carried out at a constant potential of +400 mV without inoculation of any cells into the reactor to prove sterility and stability in the used bioreactor and evaluate the capacitive current caused by the high BET (Brunauer–Emmett–Teller) surface of the electrodes. A current of 5.2 mA (corresponding to a current density of 43.1 µA cm^{-2}) was measured after 24 h and without inoculation of cells current maintained at this level for over 100 h. After 100 h medium was sampled under sterile conditions and plated onto an LB-agar plate. No colonies arose during a 7 d incubation period at 30°C. It was concluded from this result that the electrobioreactor was sterile over this time period. In the next step, the bioreactor hosting assembly 1 was inoculated with different concentrations of *S. oneidensis* cells (5.1, 6.8 and 14.3 mg L^{-1}) in order to investigate the current measured in the electrobioreactor. Immediately after inoculation an increased current was measured, showing that the electrobioreactor hosting assembly 1 can be used for BESs. Surprisingly, no dependency between the current production and the inoculated biomass concentration was observed as a higher current output was expected by a higher biomass (Figure 31).

It was concluded that the working electrode surface was limiting the current production in the system. The working electrode surface was therefore increased by inserting additional layers of carbon fabric into assembly 1. A linear dependency between the maximum current and the working electrode surface area was observed up to a geometric surface area of 960 cm^2 (Figure 33). The current density between 1 and 8 layers (120 to 960 cm^2) was at a constant level of 157 ± 11 µA cm^{-2}, decreasing to 110 µA cm^{-2} at 12 layers of carbon fabric (1,440 cm^2). A substrate limitation was excluded by measuring the lactate concentration by HPLC. Only 13 mM of the supplied 100 mM lactate were consumed over the time-course of the experiment. To exclude the possibility due to limitation of the counter electrode surface area the cathode dimension was increased by 4 fold. No increase of current was observed under these conditions (Figure 32). Experiments with 120 cm^2 were done in duplicate and showed rather small deviations (19.6 mA *vs.* 17.1 mA

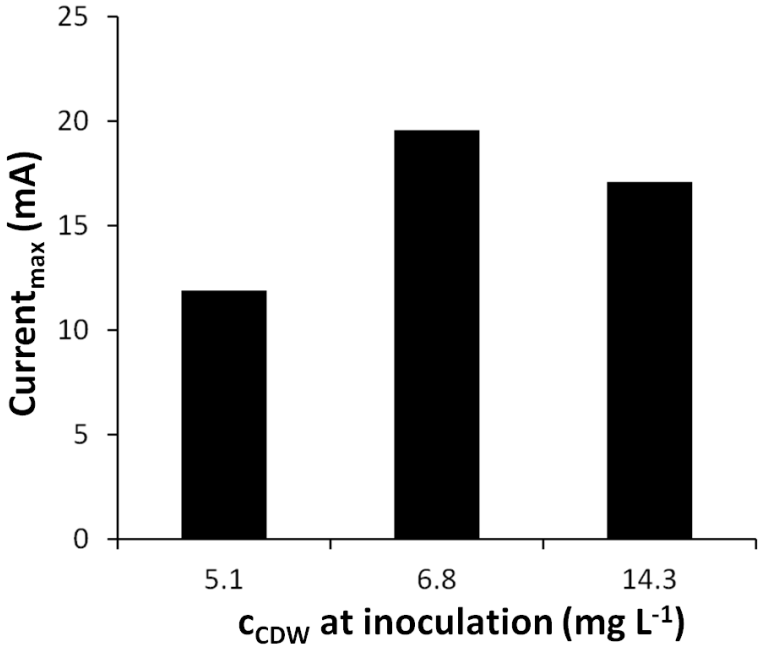

Figure 31: Maximum current generation using different *S. oneidensis* biomass concentrations for inoculation. One layer of carbon fabric (A=120 cm^2) was used as counter electrode and working electrode material, n=1.

measured peak current, see Figure 32).

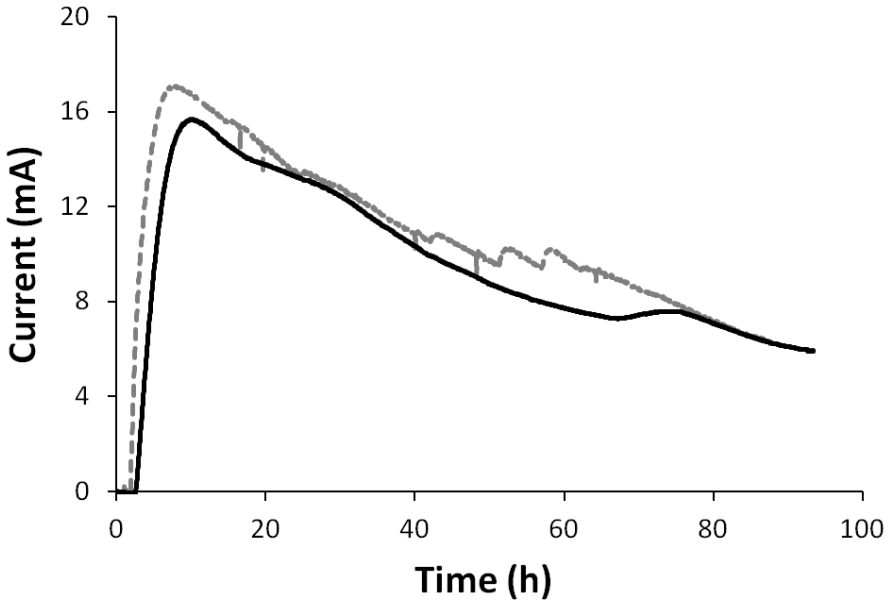

Figure 32: Current generation of 10.5 mg L^{-1} and 9.8 mg L^{-1} *S. oneidensis* cells, respectively, using one layer of carbon fabric (grey, A=120 cm^2) as counter electrode *vs.* four layers of carbon fabric (black, A=480 cm^2) as counter electrode material.

It can be concluded that the experimental conditions are robust and one experiment per electrode surface area was performed for further characterizations. Coulombic efficiencies increased from 38 % using 1 layer of carbon fabric up to around 73 % using more layers

of carbon fabric (Figure 33). These values are rather high compared to reported current efficiencies for *S. oneidensis* based MFCs, which are usually around 10 % (Rosa et al., 2016; Rosenbaum et al., 2010). However, Rosa et al. used an aerobic growth phase for biomass generation and Rosenbaum et al. used a continuous process in H-cells. Here, the electrobioreactor was purged with nitrogen and the inoculum was washed in pre-equilibrated (nitrogen purged) medium.

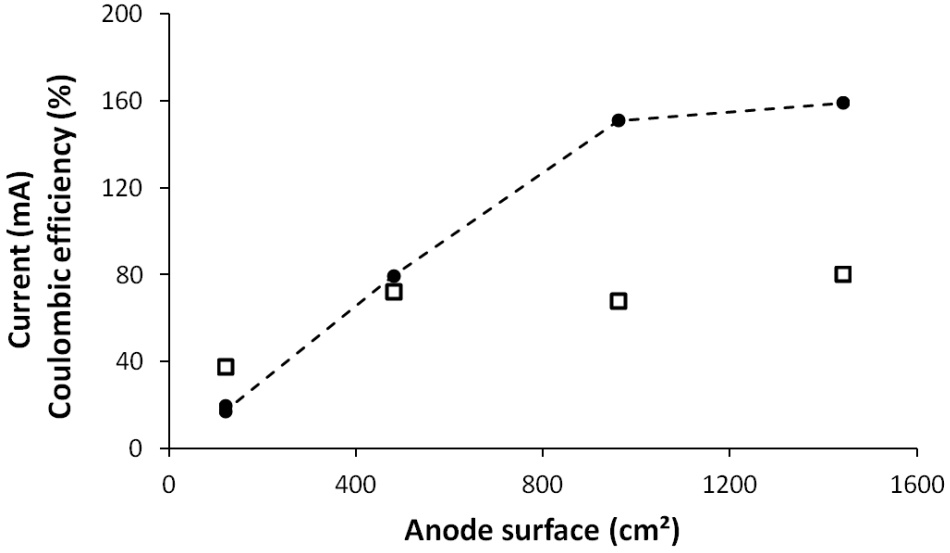

Figure 33: Closed dots show the maximum current generations of 11.5 ± 4.3 mg L^{-1} *S. oneidensis* using assembly 1 (non-separated). The working electrode consisted of 1 to 12 layers (120 to 1,440 cm^2 of carbon fabric) poised at +400 mV *vs.* Ag/AgCl. Open squares are the corresponding current efficiencies.

The designed assembly can host flexible electrode surface areas by simply applying different layers of carbon fabric and can be tailored for the respective electrobiotechnological process. However, the ability to separate the working from the counter electrode is often needed in BESs to prevent cross-reactions (e.g. oxygen produced at the anode diffusing into the anaerobic cathode chamber). Therefore, a new electrode holder was developed and constructed to host a membrane separating the two electrodes (assembly 2, Figure 9 B and C). A Nafion® 117 membrane was chosen to separate the system, as it is widely used in BESs (Leong et al., 2013).

Comparison of the current production of *S. oneidensis* using the different assemblies in the electrobioreactor

An electrobiotechnological process using the model electroactive bacterium *S. oneidensis* was performed in both assemblies to compare the performance between a separated and a non-separated operation as described in Section 4.2.8. Current densities of up to 154 ± 13 µA cm^{-2} were achieved in the non-separated electrobioreactor (Figure 33). In comparison, the highest current densities using the separated system were at 96 ±

14 µA cm^{-2} and thus lower (Figure 34). The highest current densities in electrobioreactors with *S. oneidensis* previously reported were 55 µA cm^{-2} (Rosa et al., 2016). Cells were first cultivated aerobically and gassing with nitrogen started after 24 h of cultivation, which may have led to rather small current efficiencies due to oxygen in the system in the reported electrobioreactor. Furthermore, the used carbon fabric anode has autoadsorptive properties, which also may have increased the current densities compared to the literature values (Mayer et al., 2018).

Higher internal resistances were not responsible for the difference between the separated and non-separated electrobioreactor (Figure 34), as the electrochemical characterization showed only low electrochemical losses due to the membrane (Figure 28). Current profiles shown in Figure 34 may be explained by mass transport limitations through the Nafion® 117 membrane, which limit the performance (Chae et al., 2008). The authors reported that the membrane size should be approximately the size of the electrode (geometric surface area of the used electrode was 120 cm^2) to reduce the internal resistance. One drawback of an increased size is that oxygen diffusion is facilitated. In this study a membrane size of 20.3 cm^2 was used due to stability constraints. Membranes with larger surface areas bulged and interfered with the stirrer. To overcome this problem different, more stable membrane materials should be used for future studies.

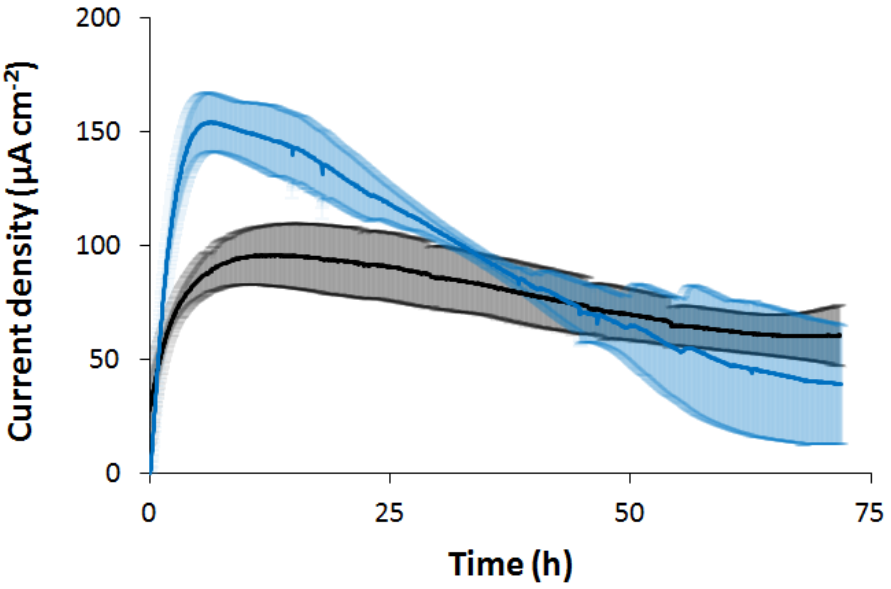

Figure 34: Current generation of 12.5 ± 2.8 mg L^{-1} *S. oneidensis* in the separated (black) and non-separated (blue) electrobioreactor, respectively, using one layer of the working electrode carbon fabric poised at +400 mV *vs.* Ag/AgCl. The experiments were performed in n=3 in the electrobioreactor with assembly 1 and assembly 2.

Besides maximum current densities, the specific charges of the reactor systems were compared and calculated to exclude the impact of the different anode surface area sizes of the reactor systems (Figure 35). Both setups showed comparable specific charges transferred. Despite showing a lower maximum current density, the separated electrobioreactor

with the designed and characterized assembly 2 was the best performing system in terms of long-term stability (meaning constant current densitiy over time), indicated also by the intersection point of current densities shown in Figure 34. Coulombic efficiencies were highest with 66 ± 12 % in the non-separated electrobioreactor and 27 ± 8 % in the separated electrobioreactor. This is an increase of 2.7 to 6.6 fold compared to values reported in literature (Rosa et al., 2016). The differences between the operation modes may be explained by chemical short circuits in the non-separated electrobioreactor and/or limitations caused by the membrane. Substances may react at the different electrodes leading to false positive current measurements (Harnisch and Schröder, 2009).

The difference between the two setups can not be explained by oxygen diffusion from the cathode chamber through the Nafion® 117 membrane to the anode chamber, which has been reported before (Leong et al., 2013). Theoretical total oxygen flux through the membrane was 444 µmol during the measured time of 75 h and was calculated as described before (Section 4.2.8, Chae et al. (2008)). It can be concluded, that oxygen diffusion through the membrane accounts for only 1 % of the consumed lactate over the process time.

5.3.5 Performance comparison of the electrobioreactors to H-cells

Highest current densities up to 150 µA cm^{-2} were achieved in the non-separated electrobioreactor and H-cell, respectively, followed by the separated H-cell at 125 µA cm^{-2} (Figure 25 and Figure 34). The separated electrobioreactor shows current densities up to 100 µA cm^{-2} still being in the same range as the other systems (Figure 34). This was not expected as the electrochemical characterization of the electrobioreactor showed a 42 % and 52 % lower potential loss for the electrolyte and the membrane, respectively, compared to the H-cells (Section 5.2.1). The differences between the separated and non-separated reactor concepts can not be explained by higher internal resistances, because the electrochemical characterization showed only low electrochemical losses due to the membrane.

Besides maximum current densities, the specific transferred charge of the reactor systems was calculated. Since the separated H-cell stopped producing current after 58 h the transferred charges were calculated until this time to compare the reactor systems. Again the non-separated electrobioreactor performed best, however, current density was decreasing over time most likely due to the lack of an electron acceptor at the cathode (no oxygen was present in the system). The separated electrobioreactor and the non-separated H-cell transferred about the same amount of charge and the separated H-cell was trailing. Best performing system in terms of long-term stability was the separated electrobioreactor with the designed and characterized assembly 2 as the current density was stable over a longer time compared to the other systems. Specific charge does not

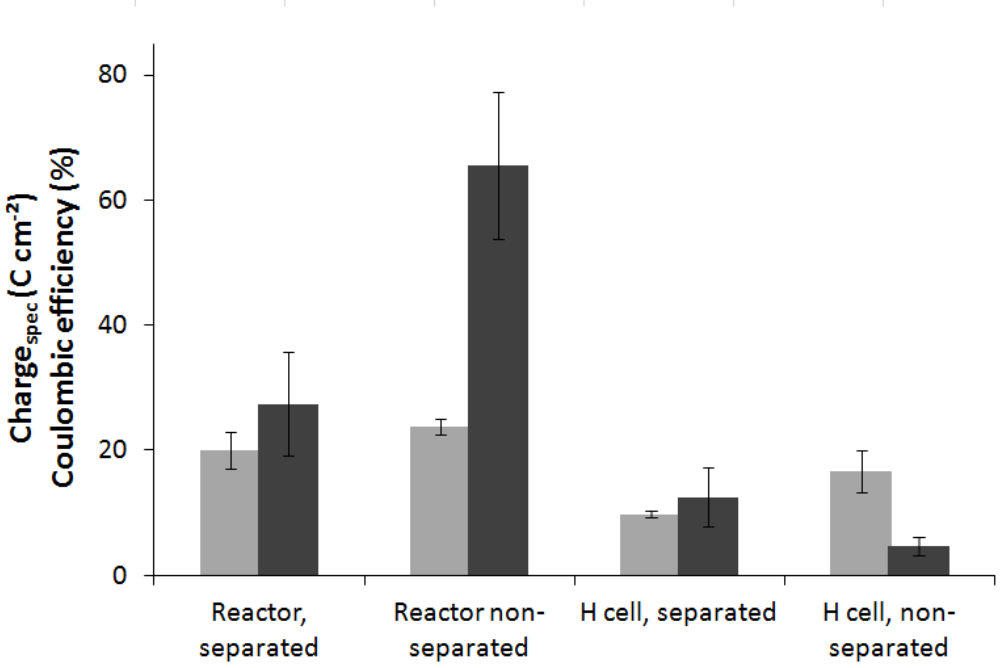

Figure 35: Transferred specific charge (light grey) and current efficiencies (dark grey) of 12.5 ± 2.8 mg L^{-1} *S. oneidensis* in the separated and non-separated electrobioreactor and 12.2 ± 1.3 mg L^{-1} *S. oneidensis* in the separated and non-separated H-cells, respectively. Carbon fabric contacted with platinum wire (d=5 mm) was used as working and counter electrode material in the electrobioreactors (120 cm^2, one layer) and the H-cells (6 cm^2) poised at +400 mV *vs.* Ag/AgCl. The experiments were performed in n=3 in the electrobioreactor with assembly 1 and assembly 2 and n=4 in the H-cells.

differ significantly between the non-separated (assembly 1), the separated (assembly 2) electrobioreactor (p=0.06) and the non-separated H-cell (p=0.2) according to the t-test. The other combinations differ significantly from each other since the p-values are below 0.05 (Figure 35).

To compare the coulombic efficiencies it is important to also consider the gassing setups in the reactors used in this study Table 6. Coulombic efficiencies were highest with 66 % in the non-separated electrobioreactor followed by the separated electrobioreactor with 27 % and the separated H-cell with 12.5 %, respectively. The coulombic efficiencies were lowest with 4.6 % for the non-separated H-cell, which fits to literature values in a comparable system (Rosenbaum et al., 2010). It was expected that the values are in accordance to differences between the two reactors caused by the setup, i.e. separated *vs.* non-separated. This is in agreement with the results obtained in the non-separated electrobioreactor and thus a general phenomenon. Most likely oxygen diffusion into the system is responsible for the value measured in the non-separated H-cell as bioreactors are sealed tighter compared to H-cells.

Table 6: Overview of the gassing setups in the different reactor concepts.

Reactor concepts	$Gassing_{Anolyte}$	$Gassing_{Catholyte}$
Electrobioreactor (assembly 2), separated	N_2/O_2 (80:20)	Air
Electrobioreactor (assembly 1), non-separated	N_2/O_2 (80:20)	-
H-cell, separated	N_2/O_2 (80:20)	Air
H-cell, non-separated	N_2/O_2 (80:20)	-

5.3.6 Bioelectrochemical anaerobic production of lysine and organic acids using *Corynebacterium glutamicum*

To show the broad applicability of the developed reactor system, a second biological system was investigated in assembly 2. Previous works showed that anaerobic conversion of glucose to lactate, succinate and lysine with an engineered *C. glutamicum* is enhanced by the application of an anode as an external electron acceptor and 1.5 mM ferricyanide used as a mediator (Vassilev et al., 2018). These investigations were done in self-made electrobioreactors with a working volume of 350 mL (Lai et al., 2016; Vassilev et al., 2018). The counter electrode was separated by a cation exchange membrane and products were in the bulk phase (anolyte) of the electrobioreactor. A scale-up of this process was realized from 295 mL to 2 L with the designed electrobioreactor using assembly 2. Mediator concentrations and specific electrode surface areas of the used carbon cloth electrodes were kept constant at 0.07 cm^2 cm^{-3}. Specific membrane area per working volume was 10.2 cm^2 dm^{-3} in this work *vs.* 0.96 cm^2 dm^{-3} in the previous work by Vassilev et al. (2018). A control experiment without applying a potential was omitted in this work, because the process was extensively characterized before (Vassilev et al., 2018).

Current production started immediately after inoculation and reached current densities of up to 115 µA cm^{-2}, which is in the same range compared to the *S. oneidensis* experiments described in Section 5.3.4 (Figure 36 A). Glucose was consumed over a period of 25 h and concentrations of up to 70 mM lactate, 10 mM succinate and 2 mM lysine were produced in the system (Figure 36 B). Specific production rates were 1.7 mmol g_{CDW}^{-1} h^{-1} lactate, 0.25 mmol g_{CDW}^{-1} h^{-1} succinate and 0.047 mmol g_{CDW}^{-1} h^{-1} lysine, which are in the same range as in the 350 mL system (1.5 mmol g_{CDW}^{-1} h^{-1} lactate, 0.25 mmol g_{CDW}^{-1} h^{-1} succinate and 0.076 mmol g_{CDW}^{-1} h^{-1} lysine) previously reported by Vassilev et al. (2018). These results prove that the designed electrobioreactor with assembly 2 is suitable for bioelectrochemical production of chemicals. Despite using a defined and well characterized modified electrobioreactor with optimal mixing conditions of the medium *vs.* a electrobioreactor with non-defined mixing by a magnetic mixer, no increased production rates were measured. This indicates that anodic electro-fermentation of lysine and organic acids might not be limited by the BES setup but rather by the biocatalysis of the cells.

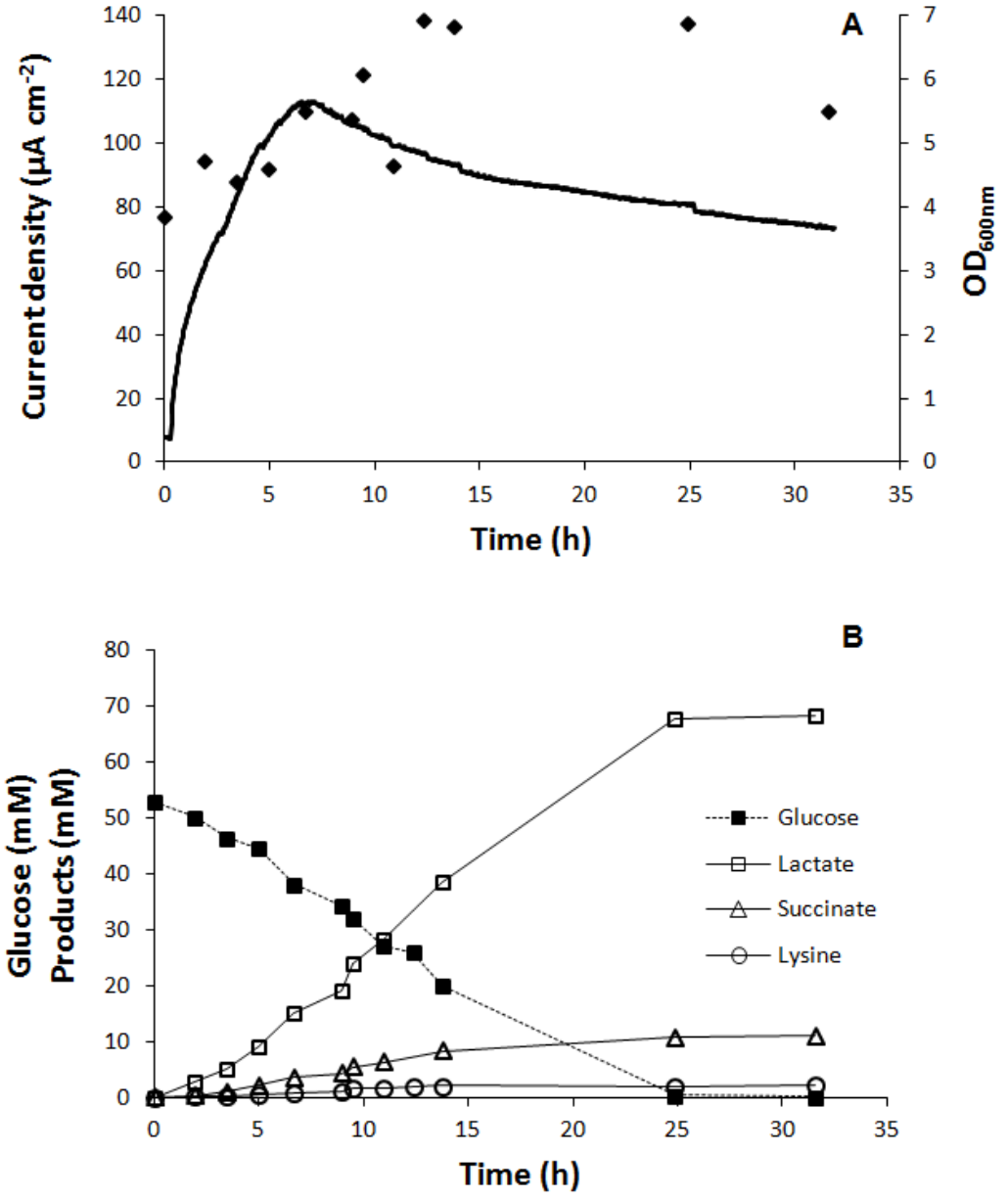

Figure 36: Electrochemically influenced conversion of glucose to lactate, succinate and lysine in *Corynebacterium glutamicum*. A: Current density (line) and OD_{600nm} (diamonds) during the conversion. B: Concentrations of the substrate glucose and the products lactate, succinate and lysine.

5.4 Terpenoid production in genetically modified *Cupriavidus necator*

Products from microbial electrosynthesis (MES) from CO_2 are mostly rather simple such as acetate, isopropanol and butyrate (Nevin et al., 2011, 2010; Torella et al., 2015). In this section, a *C. necator* strain was genetically modified to produce the terpenoid α-humulene. This investigation serves as a proof of concept, that also products of more complex pathways can be made from CO_2 and electrical energy.

5.4.1 Cloning strategy for α-humulene production

Sonntag et al. (2015) introduced the mevalonate pathway into *M. extorquens* to produce α-humulene from the sole C_1 carbon source methanol. Besides methanol, also CO_2 is of great interest as a starting point for the production of chemicals such as terpenoids and *C. necator* was chosen as a host for a proof of concept of this idea. The α-humulene pathway was taken from the plasmid pFS62b (Sonntag et al., 2015) (see Figure 37, which would enable a metabolic pathway as shown in Figure 6).

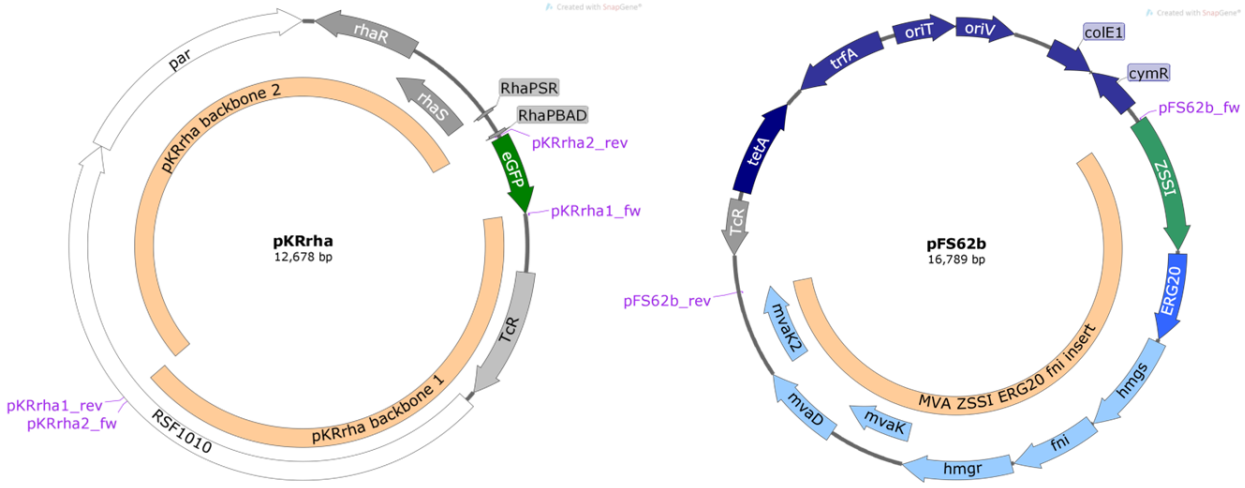

Figure 37: Backbone of pKR-hum and α-humulene pathway were taken from pKRrha and pFS62b, respectively. Plasmid maps show the location of primers and the location of fragments used in this study: *par* (partitioning system), RSF1010 (origin of replication), *rhaR* and *rhaS* (genes coding for activator proteins), $rhaP_{SR}$ (promoter for *rhaS* and *rhaR*), $rhaP_{BAD}$ (L-rhamnose inducible promotor), genes coding for *eGFP* (enhanced green fluorescent protein), Tc^R (tetracycline resistance casette), ZSSI (α-humulene synthase from *Z. zerumbet*), ERG20 (FPP synthase from *S. cerevisiae*) and the *M. xanthus* MVA pathway genes: *hmgs* (3-hydroxymethylglutaryl-CoA synthase), *hmgr* (3-hydroxymethylglutaryl-CoA reductase), *mvaK* (mevalonate kinase), *mvaK2* (phosphomevalonate kinase), *mvaD* (pyrophosphomevalonate reductase) and *fni* (IPP isomerase) (Sonntag et al., 2015; Sydow et al., 2017b).

If toxic intermediates are expected in a biotechnological process, plasmids hosting inducible promotors need to be developed for a tunable expression of proteins. First tries

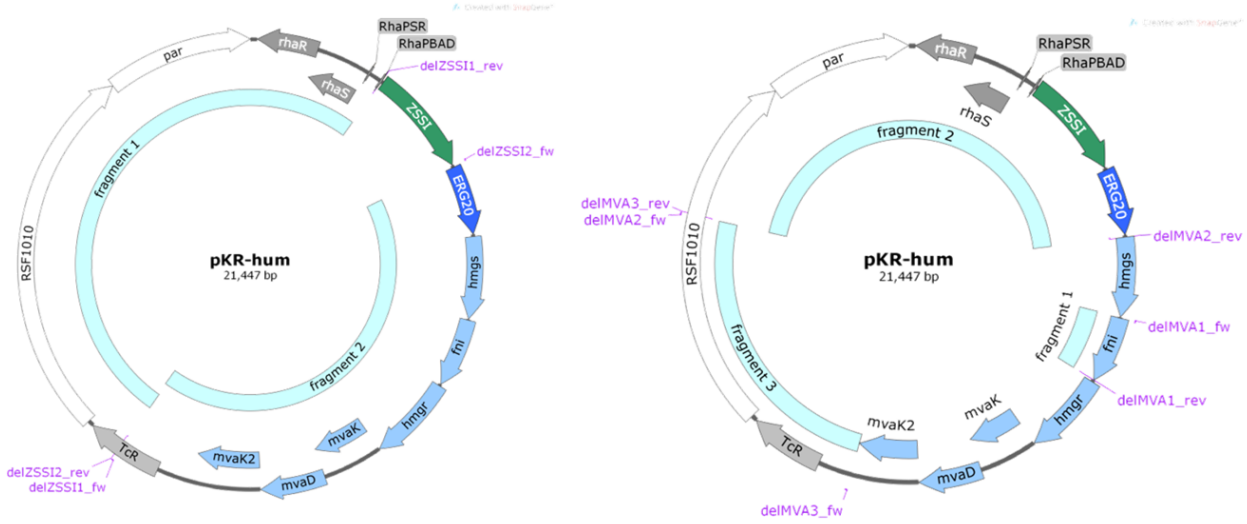

Figure 38: Cloning strategy of the control plasmids pKR-hum ΔZSSI and pKR-hum ΔMVA from pKR-hum (Figure 39). See Figure 37 for the description of genes and other elements.

to express the α-humulene pathway using the constitutive promotor P_{j5} (Gruber et al., 2014), which is active in *E. coli* and *C. necator* were not successful. It was not possible to isolate a plasmid with the correct size in *E. coli*. Most likely toxic compounds such as pyrophosphates or other intermediates of the MVA pathway accumulated in the cells, which have been reported to be toxic for microorganisms in unbalanced pathways (Peralta-Yahya and Keasling, 2010). Therefore, a plasmid system with a L-rhamnose inducible promotor has been developed recently by Sydow et al. (2017b) named pKRrha, which is a derivative of the plasmid pKRSF1010 (Gruber et al., 2014) and suitable for *C. necator* (see Figure 37).

From pFS62b and pKRrha, pKR-hum was constructed and contained the mevalonate pathway, FPP synthase and α-humulene synthase (see Figure 39). A sufficient cloning was ensured by sanger sequencing of the α-humulene pathway using the primers Seq1_-fw to Seq13_fw and Seq1_rev (Section 4.2.13 primer list) as shown in Figure 39. To get more insight into the mechanism of α-humulene production, two more plasmids were constructed (see Figure 38). *C. necator* posses a native DXP pathway, which ends up at acetoacetyl-CoA like the MVA pathway. Therefore, the plasmid pKR-hum ΔMVA containing the FPP synthase, the isomerase and the α-humulene synthase omitting the mevalonate pathway to analyze the activity of the native DXP pathway was constructed. Small amounts of α-humulene production are expected using *C. necator* pKR-hum ΔMVA. Furthermore, pKR-hum ΔZSSI omitting the α-humulene synthase was constructed to analyze whether any native terpene synthases are present in *C. necator* (see Figure 39). No α-humulene production is expected using *C. necator* ΔZSSI.

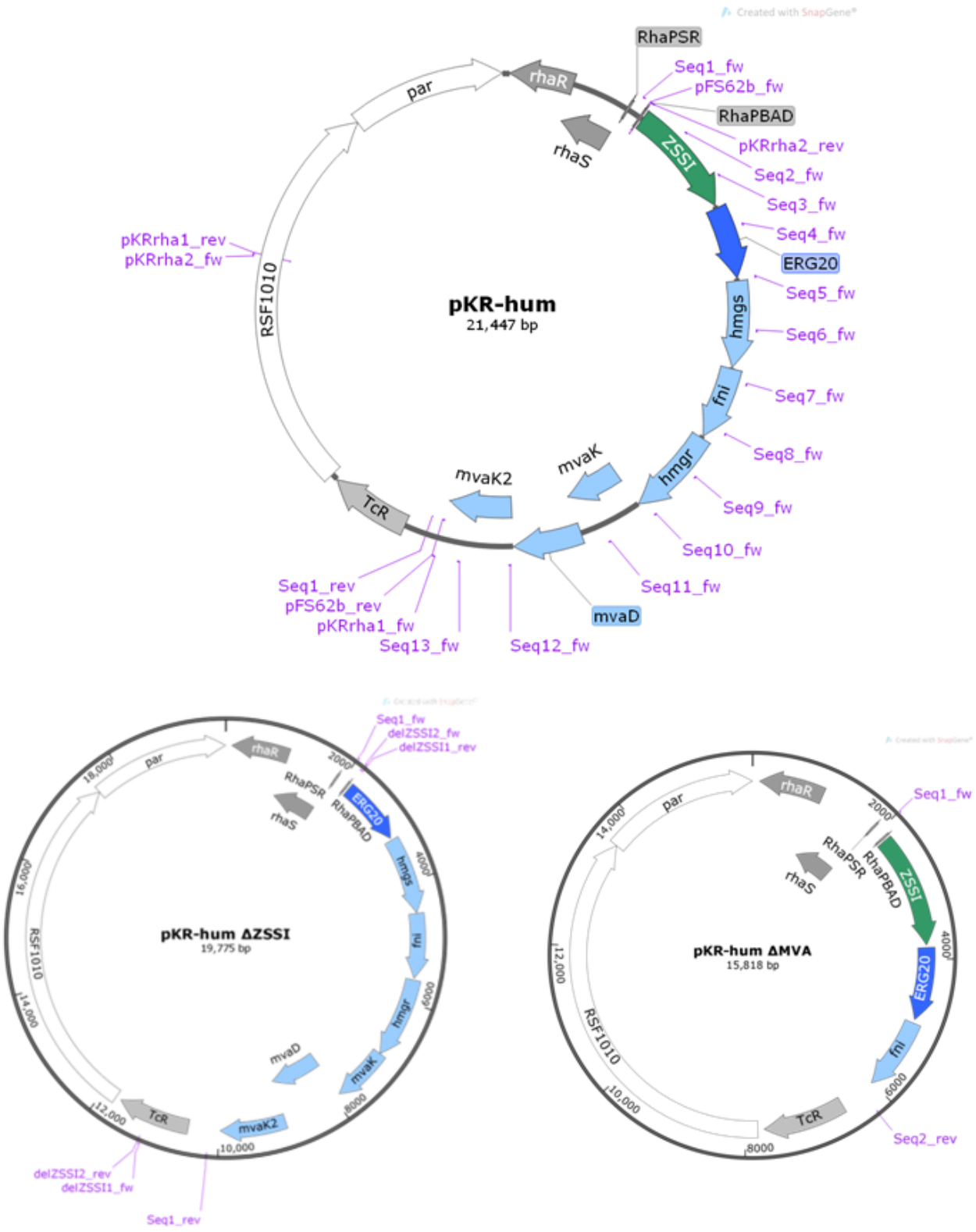

Figure 39: Plasmid maps of pKR-hum and its derivatives pKR-hum ΔMVA and pKR-hum ΔZSSI. Location of PCR and sequencing primers is also shown (Section 4.2.13). See Figure 37 for the description of genes and other elements.

5.4.2 Heterotrophic production of α-humulene

C. necator pKR-hum clones with positive restriction patterns and sequences were tested under heterotrophic conditions using minimal medium with fructose as a substrate. N-dodecane was added as organic phase for an *in situ* product removal to prevent α-humulene evaporation. N-dodecane has been used in studies before and did not influence growth of *M. extorquens* (Sonntag et al., 2015). This was also verified for *C. necator* in an advanced test and no influence on growth was observed. α-Humulene did not affect growth up to a concentration of 1,000 mg L^{-1} using 20% n-dodecane as organic phase in which α-humulene was solved (see Appendix Figure 44). Growth of *C. necator* pKR-hum is shown in Figure 40. *C. necator* pKR-hum grew up to a cell dry weight concentration of 1.6 g L^{-1}. The culture was harvested after 48 h. N-dodecane phase was analyzed with a GC/MS. A concentration of 4.6 ± 0.4 mg L^{-1} α-humulene, corresponding to a productivity of 2.3 mg L^{-1} d^{-1} was found related to the aqueous production phase. No byproducts or other terpenoids were found in the samples.

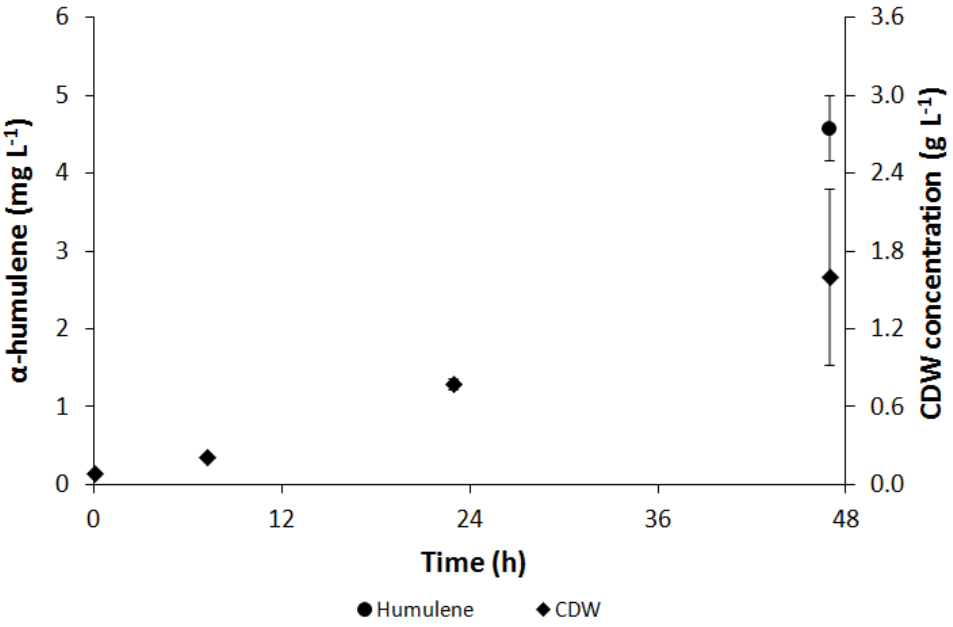

Figure 40: Heterotrophic production of α-humulene with *C. necator* pKR-hum in 300 mL Erlenmeyer flasks at 30°C with fructose as a carbon source on a rotary shaker at 180 rpm, n=3. Minimal medium (20 mL) was used for growth and 5 mL n-dodecane were used as organic phase for an *in situ* product removal. Cells were induced with 2 g L^{-1} L-rhamnose after a cultivation time of 10 h.

5.4.3 Autotrophic production of α-humulene

To proof that α-humulene can also be produced with CO_2 as sole carbon source under autotrophic conditions, experiments in serum flasks were conducted. *C. necator* pKR-hum cultures were induced 6.25 h after inoculation and grew up to a cell dry weight concen-

tration of 0.7 g L^{-1} within 2.3 d (see Figure 41). A relevant production of α-humulene started after 1.25 d and a maximum concentration of approximately 5 mg L^{-1} was measured after 3 d related to the cultivation phase. The values are in the same range as in the heterotrophic production of α-humulene, where 4.6 ± 0.4 mg L^{-1} were measured (Figure 40). Productivity was lower for the autotrophic production with 1.7 mg L^{-1} d^{-1} compared to 2.3 mg L^{-1} d^{-1} under heterotrophic conditions, which was caused by a slower growth on CO_2 as sole carbon source *vs.* fructose.

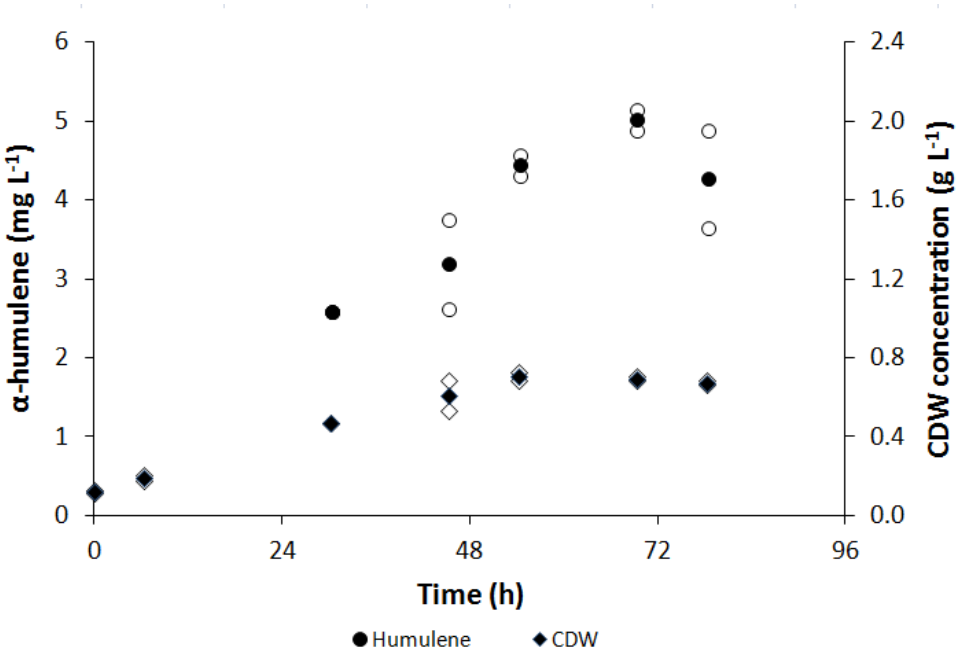

Figure 41: Autotrophic production of α-humulene with *C. necator* pKR-hum in 200 mL serum bottles at 30°C with a gas atmosphere of $CO_2/H_2/O_2$ (16/64/20 % v:v) on a rotary shaker at 180 rpm. Minimal medium (20 mL) was used for the biology and 5 mL n-dodecane were used as organic phase for an *in situ* product removal. Closed symbols are the mean values of two independent experiments represented by the open symbols. Cells were induced with 2 g L^{-1} L-rhamnose after a cultivation time of 6.25 h.

In a next set of experiments, α-humulene production was measured using four strains in order to compare their α-humulene production properties: *C. necator* wild type, *C. necator* pKR-hum, *C. necator* pKR-hum ΔMVA and *C. necator* pKR-hum ΔZSSI (Figure 42). No α-humulene was measured in cultures containing the wild type and the strain containing pKR-hum ΔZSSI. This indicates that *C. necator* does not have a native terpene synthase, which produces terpenes (and α-humulene) up to a measurable level. Concentrations of approximately 4 mg L^{-1} α-humulene were measured in the strain containing the pKR-hum ΔMVA plasmid, indicating a basic activity of the native DXP pathway in *C. necator* providing the precursors IPP and DMAPP. A significant increase with maximum α-humulene concentration of approx. 6 mg L^{-1} were measured using pKR-hum containing all relevant enzymes described before in Sonntag et al. (2015) compared to the constructed knock out strains, indicating the relevance of the mevalonate pathway for

terpenoid synthesis is *C. necator*. However, concentrations are still rather low compared to literature, where 60 mg L^{-1} and 1.65 g L^{-1} were achieved in shake-flasks and an optimized methanol limiting fed-batch with *M. extorquens*, respectively (Sonntag et al., 2015). This possibly indicates a non-identified limitation in the metabolic pathway, which needs to be investigated for a further increase of productivity by *C. necator* pKR-hum.

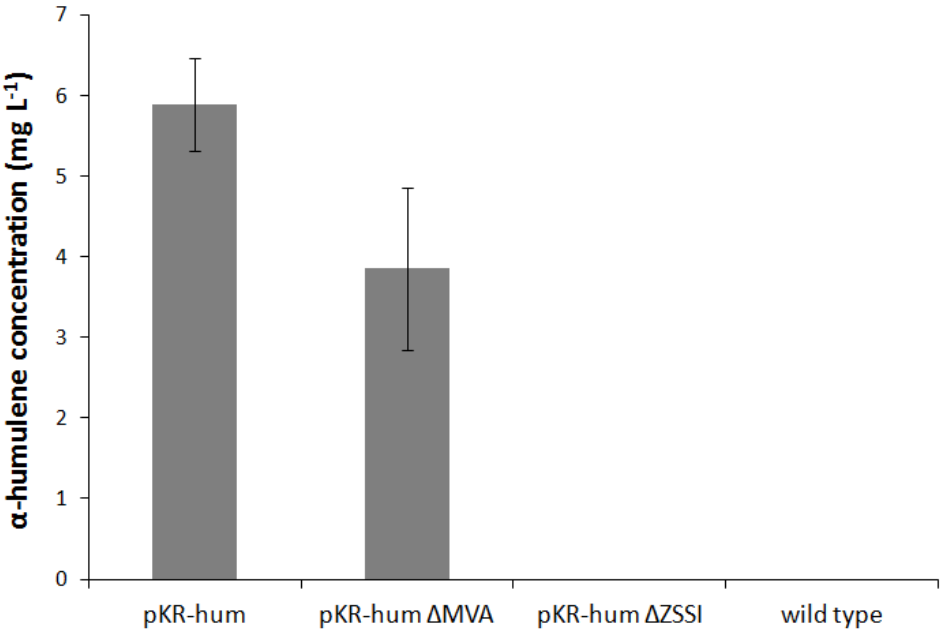

Figure 42: Comparison of autotrophic α-humulene production with *C. necator* pKR-hum, *C. necator* pKR-hum ΔMVA, *C. necator* pKR-hum ΔZSSI and *C. necator* wild type, respectively. The experiment was performed in n=3 and mean cell dry weight concentrations were 2.25 ± 0.16 mg L^{-1}. A significant increase (p=0.04) in α-humulene production using pKR-hum compared to pKR-hum ΔMVA was verified by a one-sided t-test.

5.4.4 Electroautotrophic production of α-humulene in H-cells

As a consequence of the results described before, a MES with *C. necator* pKR-hum producing α-humulene was carried out. Since hydrogen and oxygen are needed as electron donor and acceptor, respectively, a non-separated single-chamber H-cell was chosen as reaction system. A recently developed medium was used to prevent the production of toxic chlorine species using the electrochemical conditions needed for the electroautotrophic growth of *C. necator* (Sydow et al., 2017a). Hydrogen was produced at the stainless steel working electrode (cathode) at a potential of -2 V, while oxygen was produced at the counter electrode (anode), which was a dimensional stable anode with a titanium/indium catalyst (Section 4.2.18). CO_2 was used as sole carbon source and purged into the aqueous phase of the reactor system. Cells were induced 3.5 and 16.5 h after inoculation, respectively, and grew up to a cell dry weight concentration of approximately 0.7 g L^{-1} within 1.8 d (see Figure 43). This is comparable to the autotrophic growth and indicates that no

toxic byproducts such as reactive oxygen species were produced during the electrochemical cultivation of *C. necator* as described by Li et al. (2012).

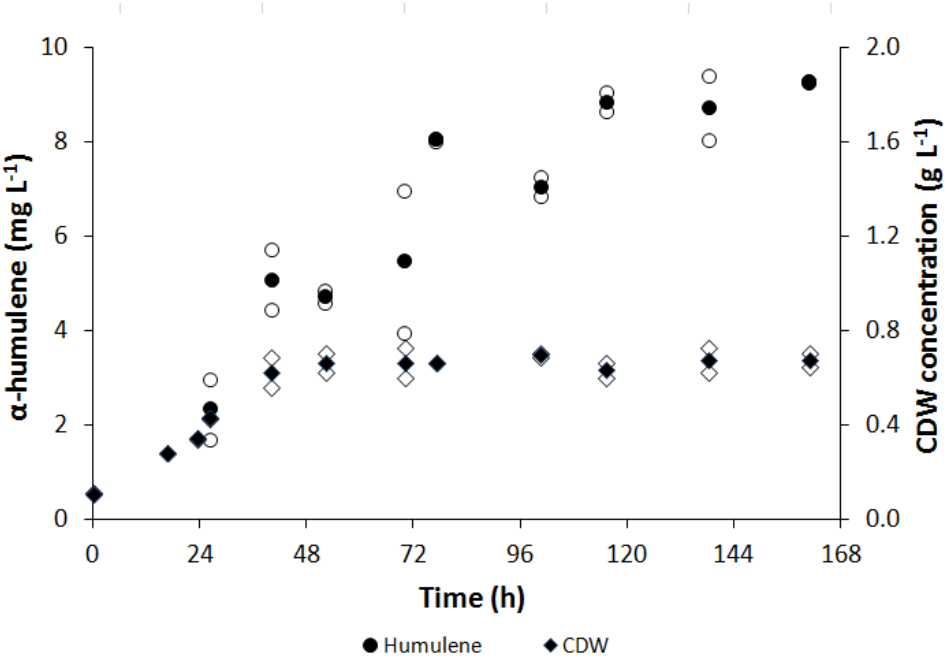

Figure 43: Electroautotrophic production of α-humulene with *C. necator* by microbial electrosynthesis at 30°C and a potential of -2 V in a non-separated, single-chamber H-cell. The system was purged with 10 to 15 mL min^{-1} CO_2 and mixed by a magnetic stirring bar at 150 rpm. Minimal medium (100 mL) was used for growth and 20 mL n-dodecane were used as organic phase for an *in situ* product removal. Cells were induced with 2 g L^{-1} L-rhamnose after a cultivation time of 3.5 h and 16.5 h, respectively. Closed symbols are the mean values of two independent experiments (open symbols).

α-Humulene was measurable after a cultivation time of 1 d and was produced over the whole cultivation time of 7 d up to a concentration of 10 mg L^{-1} related to the cultivation phase. This is a 2 fold increase compared to heterotrophic and autotrophic production conditions. Differences can be explained by the seed train, where an autotrophic preculture was used to inoculate the electroautotrophic system in comparison to autotrophic conditions with a heterotrophic preculture (Section 4.2.18). The microorganism may have adapted better to the autotrophic lifestyle and CO_2 fixation. Furthermore, the continuous electrochemically production of hydrogen and oxygen may have eliminated a limitation in the system. Oxygen availability has been identified as crucial parameter for PHB production from acetoacetyl-CoA and thus could also alter the efficiency of the mevalonate pathway initiated from the same precursor molecule (Garcia-Gonzalez et al., 2015). Therefore, a continuous electrochemical production at the anode seems to be beneficial.

Concentrations of up to 60 mg L^{-1} α-humulene were produced with *M. extorquens* in shaking flask cultures. Similar concentrations were reported in engineered *E. coli* using glucose as a substrate and an *in situ* product removal using a hydrophobic resin (Alemdar et al., 2017). The highest concentrations of up to 1.65 g L^{-1} α-humulene were obtained

in a fed-batch cultivation with a methanol feed in a bioreactor, where cell dry weights of up to 28 g L^{-1} were reached (Sonntag et al., 2015).

According to the time dependent growth and the production processes described by Sonntag et al. (2015) and Alemdar et al. (2017), α-humulene production seems to be a biomass coupled process and the concentration also in the *C. necator* based process may be increased by optimizing the medium or growth conditions for high cell densities. High cell density cultivations for autotrophic and heterotrophic growth of *C. necator* to produce recombinant proteins have been already described and may also increase heterologous production of α-humulene (Repaske and Mayer, 1976; Shang et al., 2007; Srinivasan et al., 2003). Huschner et al. (2015) reported cell densities of up to 112 g L^{-1} in a fed-batch cultivation with organic acids and their salts as substrates. Garcia-Gonzalez et al. (2015) reported an oxygen dependency for autotrophic production of PHB in *C. necator* and glycerol-grown cells performed best. This may be a good starting point for an optimization of α-humulene production under autotrophic and electroautotrophic conditions. Possible limitations should be investigated further, e.g. electrochemical oxygen production could be enhanced by screening for better anode materials or applying higher reductive potentials. Furthermore, an external purging with oxygen may lead to higher cell densities and thus further increasing α-humulene production. Metabolic engineering of the pathway itself investigating possible accumulation of precursors for α-humulene and their elimination or balancing is also promising for an improved production (Jang et al., 2011; Peralta-Yahya et al., 2012; Tang et al., 2007).

Electroautotrophic productions were performed successfully in H-cells and serve as proof of principle for further production of other high value compounds. Production rates may be increased by using more controlled reactor concepts in terms of mixing, pH values and constant electrode distances among others. The developed electrobioreactors in this study could be an ideal reactor concept, however, the production was not performed due to security issues by the produced "Knallgas" amounts in the system, which remains to be an issue that needs to be solved in the future. Furthermore, this electrobiotechnological process is out of the pH measurement range, which was defined in this study to be between -1,000 mV and +600 mV (Section 5.3.3). A solution might be the genetical engineering of electron uptake pathways into *C. necator* to enable productions at potentials less negative than -1,000 mV (Li et al., 2018). Furthermore, *C. necator* is able to grow on formic acid if the concentration is kept low by a fed-batch or continuous process (Grunwald et al., 2015). Formic acid can be produced electrochemically and dosed "on-demand", which may be the solution for the formic acid mediated cell toxicity at high concentrations and to overcome security issues of the "Knallgas" (Hegner et al., 2018; Srikanth et al., 2014; Wang et al., 2014).

6 Conclusion and Outlook

Electrobiotechnology is a wide and interdisciplinary field with many different aspects of a variety of disciplines. In Krieg et al. (2014) the most important questions and a knowledge-based rational process design to push the field of bioelectrochemical systems into applications were defined at the start of this study. An overview of the process is shown in Figure 7 in Section 3. In this work especially the first three process parts were addressed and are summarized here:

i) **catalysis** by engineering the EAM *C. necator* for electrobiotechnological terpenoid production and improving electrode microorganism interaction for *G. sulfurreducens* based MFCs by altering the reactor geometry/inlet setup,

ii) **syntheses in lab reactors** by designing and characterizing an electrobioreactor and comparing the performance to other reactor concepts,

iii) **modeling and simulation** by simulating substrate distribution in MFCs and linking it to the performance and simulating the mixing and flow patterns in the modified electrobioreactor.

In the following sections the key findings and possible future perspectives of the defined goals in Section 3 of this study to push the field of electrobiotechnology forward are outlined.

6.1 Improved microbial fuel cell performance by altering flow properties at the working electrode

For MFCs the reactors and their operating setup need to be optimized. In the field application for waste water treatment no engineering of the electroactive microorganisms is possible due to high costs and official and legal requirements. Experiments for single-chamber flat-plate MFCs and simulations of the substrate distribution in porous electrode materials to identify mass-transport related limitations were combined. Experimental results showed an increased current output by altering the inlet flow setups from a parallel to the anode flow pattern to a perpendicular flow setup. Perpendicular flow through a porous carbon electrode increased the power density by 3.2 fold *vs.* a parallel flow in the used reactor system. Simulations indicated that the increased performance of the MFC can be explained by an optimized substrate distribution in case of a perpendicular

flow through the porous electrode. The velocity through the porous layer enhanced the substrate transport and thus biological availability.

In contrast, the parallel flow system just enables a diffusional flux. The substrate was completely distributed in the porous electrode after 10 h *vs.* 30 h for the perpendicular flow setup *vs.* the parallel inlet setup. Consequently, the substrate availability on the anode was improved for the perpendicular flow, resulting in a higher biofilm coverage. No electrode fouling was observed for the perpendicular flow and pressure drops were comparable to the parallel inlet setup. The simulations reveal that permeability and porosity are important parameters. If the cloth is too permeable the benefits of the perpendicular inflow are reduced, because the substrate is not distributed well and just goes through the cloth as a jet at the inlet. It can be concluded that electrode permeability and porosity should be characterized and investigated while new MFCs are built and electrodes are engineered in the future.

6.2 Design and characterization of a electrobioreactor for bioelectrochemical systems

While MFCs for energy conversion require reactors with cheap materials and easy designs, more sophisticated designs are required for the MES of fine and bulk chemicals. Autoclavable reactors and the integration of electrodes into controlled standard systems used in biotechnology should be preferred as postulated at the start of this work. Two assemblies were designed based on previous studies (Section 5.3): a membrane-less system for a proof of principle electrobioreactor enabling simple "one-pot" reactions (assembly 1) and a more sophisticated design where the counter electrode can be separated from the working electrode by a membrane (assembly 2). Computational fluid dynamics show that the insertion of assemblies to host electrodes does not create dead zones, the mixing is not affected and can be compared to a conventional bioreactor (Section 5.3.2).

The designed electrobioreactors were characterized electrochemically and compared to H-cells, which are commonly used in studies of BESs. The potential losses caused by the electrolyte were comparable between the systems. Potential losses caused by the membrane were reduced in the designed electrobioreactor. This can be explained by a higher membrane surface area, which reduce the membrane resistance compared to the H-cells. One advantage of using bioreactors is that the pH can be controlled over the process. Using the presented electrobioreactor the pH signal was not influenced by the electrochemical measurement in a potential range between -1,000 mV and +600 mV *vs.* Ag/AgCl. Current densities of up to 154 ± 13 µA cm^{-2} were measured in the non-separated electrobioreactor using *S. oneidensis* (assembly 1), while the separated electrobioreactor

(assembly 2) had current densities up to 96 ± 14 µA cm^{-2}. Higher internal resistances are not be blamed for the difference between the separated and non-separated reactor concepts, since the electrochemical characterization showed rather low electrochemical losses due to the membrane. Furthermore, the influence of oxygen was excluded by calculating the theoretical oxygen flux through the used membrane, which accounted only for a loss of 1% of the consumed lactate. However, leaks between the membrane and the silicone seals may still cause an oxygen diffusion from the cathode chamber to the anode chamber in practice. To date, the highest current densities in a electrobioreactor achieved with *S. oneidensis* were 55 µA cm^{-2} and were increased in this study (Rosa et al., 2016). Coulombic efficiencies were highest with 66 ± 12 % in the non-separated electrobioreactor and 27 ± 8 % in the separated electrobioreactor. This is an increase of 2.7 to 6.6 fold compared to values reported in literature (Rosa et al., 2016). Finally, the anaerobic bioelectrochemical production of lysine and organic acids using *C. glutamicum* was performed in the assembly 2 electrobioreactor. Comparable results to another electrobioreactor were achieved providing that the designed electrobioreactor, and also modified stirred tank (electrobio)reactors in general are suitable for bioelectrochemical production of chemicals (Vassilev et al., 2018).

Two different assemblies were developed and characterized in detail and can now be applied in a variety of applications of BES. The decision if a membrane-separated or a membrane-less assembly should be applied must be weighed up carefully against the effectiveness and the costs of a complete system. Finally, it must be mentioned that the investigations in this study showed, that the influence of the membrane as separator on the performance of the BES was less than expected.

6.3 Heterologous α-humulene production in *Cupriavidus necator*

This study shows for the first time the chemolithoautotrohic as well as electroautotrophic *de novo* production of a terpene from CO_2 (Krieg et al., 2018). The described production of α-humulene presents a promising starting point for the production of different high value compounds within the plethora of terpenes and terpenoids with different sizes and structures, which result in different biological functions and thus applications. α-Humulene concentrations of up to 10 mg L^{-1} in the autotrophic cultivation systems were produced by less than 1 g L^{-1} biomass. Furthermore, this study demonstrates that high value compounds can be produced efficiently in BESs. So far, mainly bulk chemicals (organic acids such as acetate or methane) are produced in this research field. This study demonstrates that surplus energy generated by renewable sources and the greenhouse gas CO_2

can be stored and upgraded, which is a promising starting point for future economically feasible processes. The next step for application in MES should be the evaluation of a formic acid based production to overcome security issues, which are raised by the use of "Knallgas". Simultaneously a lower potential to enable the production process should be targeted, because this study showed that pH measurement based on glass electrodes only allow potentials between -1,000 and 600 mV. If potentials lower than -1,000 mV are needed for the production of either hydrogen or formic acid, a further modification of the used electrobioreactor for the use of alternative pH measurement modes needs to be performed. Finally, due to the unique natural flexibility of the production host *C. necator* it is possible to use different carbon and energy sources depending on the availability and the prices (Section 2.3.4).

6.4 Final remarks

The conclusions highlight general challenges in the field of electrobiotechnology. On the one hand electrochemical and biotechnological aspects have to be combined for efficient cultivation systems. On the other hand the biological catalyst needs to be modified in order to produce valuable products or enhance productivity where applicable (in MFCs, which should be used for waste water treatment no genetically modified microorganisms are allowed in nature due to official prohibitions). Furthermore, the properties of EAM and electrobioreactors have to fit:

In this study different electron transfer mechanisms were applied. Direct electron transfer (DET) with *G. sulfurreducens* in the designed MFC and the H-cell, a mixture of direct and mediated electron transfer (MET) using *S. oneidensis* in the designed electrobioreactor, MET for the production of lysine and other organics with *C. glutamicum* in the electrobioreactor and indirect electron transfer (IET) *via* hydrogen and oxygen for the production of α-humulene in the engineered *C. necator* strain were used. Looking at possible applications of the systems, MFCs should be used for an efficient waste water clarification with a subsequent current production with mixed cultures. Mixed cultures are isolated from waste water and are dominated by *G. sulfurreducens* among others. Biofilm based reactors are needed for cell retention and most likely only DET with minor MET is performed, if natural mediators are produced by microorganisms in the mixed culture. For MES it can be concluded that IET seems to be beneficial, because processes become more flexible. However, substrates with security issues such as hydrogen in the presence of oxygen should be avoided if possible. Soluble substrates such as formic acid can be dosed either electrochemically or by simply adding the compounds from other resource streams. The development of the electrochemical part (e.g. electrodes) can be uncoupled from the biological part. Strains can be engineered and characterized without the use of electrochemistry and knowledge gained from different disciplines can be merged

at a later development phase.

Electrobiotechnology is an interdisciplinary field and can be approached from different starting points: there is engineering, electrochemistry and biotechnology. As shown in this study there needs to be progress in all fields, which needs to be merged by electrobiotechnologists for improved, economically reliable microbial electrochemical technologies.

Bibliography

Affoune, A. M., Yamada, A., and Umeda, M. (2005). "Conductivity and surface morphology of Nafion membrane in water and alcohol environments". *Journal of Power Sources*, 148, pp. 9–17.

Ahn, Y. and Logan, B. E. (2012). "A multi-electrode continuous flow microbial fuel cell with separator electrode assembly design". *Applied Microbiology and Biotechnology*, 93(5), pp. 2241–2248.

Ajikumar, P. K., Xiao, W.-H., Tyo, K. E. J., Wang, Y., Simeon, F., Leonard, E., Mucha, O., Phon, T. H., Pfeifer, B., and Stephanopoulos, G. (2010). "Isoprenoid Pathway Optimization for Taxol Precursor Overproduction in Escherichia coli". *Science*, 330(6000), pp. 70–74.

Alemdar, S., König, J. C., Hartwig, S., Frister, T., Scheper, T., and Beutel, S. (2017). "Bioproduction of α-humulene in metabolically engineered Escherichia coli and application in zerumbone synthesis". *Engineering in Life Sciences*, pp. 1–22.

Alonso-Gutierrez, J., Chan, R., Batth, T. S., Adams, P. D., Keasling, J. D., Petzold, C. J., and Lee, T. S. (2013). "Metabolic engineering of Escherichia coli for limonene and perillyl alcohol production". *Metabolic Engineering*, 19, pp. 33–41.

Ausfelder, F., Beilmann, C., Bertau, M., Bräuninger, S., Heinzel, A., Hoer, R., Koch, W., Mahlendorf, F., Metzelthin, A., Peuckert, M., Plass, L., Räuchle, K., Reuter, M., Schaub, G., Schiebahn, S., Schwab, E., Schüth, F., Stolten, D., Teßmer, G., Wagemann, K., and Ziegahn, K. F. (2015). "Energiespeicherung als Element einer sicheren Energieversorgung". *Chemie-Ingenieur-Technik*, 87(1-2), pp. 17–89.

Batlle-Vilanova, P., Puig, S., Gonzalez-Olmos, R., Balaguer, M. D., and Colprim, J. (2016). "Continuous acetate production through microbial electrosynthesis from CO2 with microbial mixed culture". *Journal of Chemical Technology & Biotechnology*, 91(4), pp. 921–927.

Baudler, A., Schmidt, I., Langner, M., Greiner, A., and Schröder, U. (2015). "Does it have to be carbon? Metal anodes in microbial fuel cells and related bioelectrochemical systems". *Energy & Environmental Science*, 8(7), pp. 2048–2055.

Becker, J. and Wittmann, C. (2012). "Bio-based production of chemicals, materials and fuels – Corynebacterium glutamicum as versatile cell factory". *Current Opinion in Biotechnology*, 23(4), pp. 631–640.

Bernotienë, G., Nivinskienë, O., Butkienë, R., and Mockutë, D. (2004). "Chemical composition of essential oils of hops (Humulus lupulus L.) growing wild in Aukštaitija". *Chemija*, 15(2), pp. 31–36.

Bursac, T., Gralnick, J. A., and Gescher, J. (2017). "Acetoin production via unbalanced fermentation in Shewanella oneidensis". *Biotechnology and Bioengineering*, 114(6), pp. 1283–1289.

Caccavo, F., Lonergan, D. J., Lovley, D. R., Davis, M., Stolz, J. F., and McInerney, M. J. (1994). "Geobacter sulfurreducens sp. nov., a hydrogen- and acetate-oxidizing dissimilatory metal-reducing microorganism." *Applied and Environmental Microbiology*, 60(10), pp. 3752–3759.

Calloway, D. H. and Kumar, A. M. (1969). "Protein Quality of the Bacterium Hydrogenomonas eutropha". *Applied Microbiology*, 17(1), pp. 176–178.

Campos-Rodrigues, T. de and Rosenbaum, M. A. (2014). "Microbial Electroreduction: Screening for New Cathodic Biocatalysts". *ChemElectroChem*, 1(11), pp. 1916–1922.

Canstein, H. von, Ogawa, J., Shimizu, S., and Lloyd, J. R. (2008). "Secretion of flavins by Shewanella species and their role in extracellular electron transfer." *Applied and Environmental Microbiology*, 74(3), pp. 615–623.

Chae, K. J., Choi, M., Ajayi, F. F., Park, W., Chang, I. S., and Kim, I. S. (2008). "Mass Transport through a Proton Exchange Membrane (Nafion) in Microbial Fuel Cells". *Energy & Fuels*, 22(1), pp. 169–176.

Chang, M. C. Y. and Keasling, J. D. (2006). "Production of isoprenoid pharmaceuticals by engineered microbes." *Nature Chemical Biology*, 2(12), pp. 674–681.

Chen, S., He, G., Hu, X., Xie, M., Wang, S., Zeng, D., Hou, H., and Schröder, U. (2012a). "A three-dimensionally ordered macroporous carbon derived from a natural resource as anode for microbial bioelectrochemical systems." *ChemSusChem*, 5(6), pp. 1059–1063.

Chen, S., He, G., Liu, Q., Harnisch, F., Zhou, Y., Chen, Y., Hanif, M., Wang, S., Peng, X., Hou, H., and Schröder, U. (2012b). "Layered corrugated electrode macrostructures boost microbial bioelectrocatalysis". *Energy & Environmental Science*, 5(12), p. 9769.

Cheng, S., Liu, H., and Logan, B. E. (2006). "Increased power generation in a continuous flow MFC with advective flow through the porous anode and reduced electrode spacing". *Environmental Science and Technology*, 40(7), pp. 2426–2432.

Cheng, S. and Logan, B. E. (2011). "Increasing power generation for scaling up single-chamber air cathode microbial fuel cells". *Bioresource Technology*, 102(6), pp. 4468–4473.

Choi, O., Kim, T., Woo, H. M., and Um, Y. (2014). "Electricity-driven metabolic shift through direct electron uptake by electroactive heterotroph Clostridium pasteurianum." *Scientific Reports*, 4, p. 6961.

Christodoulou, X. and Velasquez-Orta, S. B. (2016). "Microbial electrosynthesis and anaerobic fermentation: An economic evaluation for acetic acid production from CO2 and CO". *Environmental Science & Technology*, 50(20), pp. 11234–11242.

Chung, D. W., Ebner, M., Ely, D. R., Wood, V., and Edwin García, R. (2013). "Validity of the Bruggeman relation for porous electrodes". *Modelling and Simulation in Materials Science and Engineering*, 21(7), p. 074009.

Clauwaert, P., Aelterman, P., Pham, T. H., De Schamphelaire, L., Carballa, M., Rabaey, K., and Verstraete, W. (2008). "Minimizing losses in bio-electrochemical systems: The road to applications". *Applied Microbiology and Biotechnology*, 79(6), pp. 901–913.

Corey, E. J., Daigneault, S., and Dixon, B. R. (1993). "A biomimetic chemical synthesis of humulene from farnesol". *Tetrahedron Letters*, 34(23), pp. 3675–3678.

Crépin, L., Lombard, E., and Guillouet, S. E. (2016). "Metabolic engineering of Cupriavidus necator for heterotrophic and autotrophic alka(e)ne production". *Metabolic Engineering*, 37, pp. 92–101.

Cusick, R. D., Bryan, B., Parker, D. S., Merrill, M. D., Mehanna, M., Kiely, P. D., Liu, G., and Logan, B. E. (2011). "Performance of a pilot-scale continuous flow microbial electrolysis cell fed winery wastewater". *Applied Microbiology and Biotechnology*, 89(6), pp. 2053–2063.

del Pilar Anzola Rojas, M., Zaiat, M., Gonzalez, E. R., De Wever, H., and Pant, D. (2018). "Effect of the electric supply interruption on a microbial electrosynthesis system converting inorganic carbon into acetate". *Bioresource Technology*, 266, pp. 203–210.

Deutzmann, J. S., Merve, S., and Spormann, A. M. (2015). "Extracellular Enzymes Facilitate Electron Uptake in Biocorrosion and Bioelectrosynthesis". *mBio*, 6(2), pp. 1–8.

Dewan, A., Beyenal, H., and Lewandowski, Z. (2008). "Scaling up Microbial Fuel Cells". *Environmental Science & Technology*, 42(20), pp. 7643–7648.

Dolch, K., Danzer, J., Kabbeck, T., Bierer, B., Erben, J., Förster, A. H., Maisch, J., Nick, P., Kerzenmacher, S., and Gescher, J. (2014). "Characterization of microbial current production as a function of microbe-electrode-interaction". *Bioresource Technology*, 157, pp. 284–292.

Dulon, S., Parot, S., Delia, M.-L., and Bergel, A. (2006). "Electroactive biofilms: new means for electrochemistry". *Journal of Applied Electrochemistry*, 37(1), pp. 173–179.

Dumas, C., Basseguy, R., and Bergel, A. (2008). "Microbial electrocatalysis with Geobacter sulfurreducens biofilm on stainless steel cathodes". *Electrochimica Acta*, 53(5), pp. 2494–2500.

Dusting, J., Sheridan, J., and Hourigan, K. (2006). "A fluid dynamics approach to bioreactor design for cell and tissue culture". *Biotechnology and Bioengineering*, 94(6), pp. 1196–1208.

Emde, R. and Schink, B. (1990). "Enhanced propionate formation by Propionibacterium freudenreichii subsp. freudenreichii in a three-electrode amperometric culture system". *Applied and Environmental Microbiology*, 56(9), pp. 2771–2776.

Escapa, A., San-Martín, M. I., Mateos, R., and Morán, A. (2015). "Scaling-up of membraneless microbial electrolysis cells (MECs) for domestic wastewater treatment: Bottlenecks and limitations". *Bioresource Technology*, 180, pp. 72–78.

Fan, Y., Han, S.-K., and Liu, H. (2012). "Improved performance of CEA microbial fuel cells with increased reactor size". *Energy & Environmental Science*, 5(8), p. 8273.

Faraday, M. (1834). "Experimental Researches in Electricity. Seventh Series". *Philosophical Transactions of the Royal Society of London*, 124(0), pp. 77–122.

Feiner, A.-S. and McEvoy, A. J. (1994). "The Nernst Equation". *Journal of Chemical Education*, 71(6), p. 493.

Feng, Y., He, W., Liu, J., Wang, X., Qu, Y., and Ren, N. (2014). "A horizontal plug flow and stackable pilot microbial fuel cell for municipal wastewater treatment". *Bioresource Technology*, 156, pp. 132–138.

Fernandes, E. S., Passos, G. F., Medeiros, R., Cunha, F. M. da, Ferreira, J., Campos, M. M., Pianowski, L. F., and Calixto, J. B. (2007). "Anti-inflammatory effects of compounds alpha-humulene and (−)-trans-caryophyllene isolated from the essential oil of Cordia verbenacea". *European Journal of Pharmacology*, 569(3), pp. 228–236.

Fischer, M. J. C., Meyer, S., Claudel, P., Bergdoll, M., and Karst, F. (2011). "Metabolic engineering of monoterpene synthesis in yeast." *Biotechnology and Bioengineering*, 108(8), pp. 1883–1892.

Flynn, J. M., Ross, D. E., Hunt, K. A., Bond, D. R., and Gralnick (2010). "Enabling Unbalanced Fermentations by Using Engineered Electrode-Interfaced Bacteria". 1(5), pp. 1–8.

Förster, A. H., Beblawy, S., Golitsch, F., and Gescher, J. (2017). "Electrode-assisted acetoin production in a metabolically engineered Escherichia coli strain". *Biotechnology for Biofuels*, 10(1), p. 65.

Gálvez, A., Greenman, J., and Ieropoulos, I. (2009). "Landfill leachate treatment with microbial fuel cells; scale-up through plurality". *Bioresource Technology*, 100(21), pp. 5085–5091.

Ganigué, R., Puig, S., Batlle-Vilanova, P., Dolors Balaguer, M., and Colprim, J. (2015). "Microbial electrosynthesis of butyrate from carbon dioxide". *Chemical Communications*, 51(7000), pp. 3235–3238.

Garcia-Gonzalez, L., Mozumder, M. S. I., Dubreuil, M., Volcke, E. I., and De Wever, H. (2015). "Sustainable autotrophic production of polyhydroxybutyrate (PHB) from CO 2 using a two-stage cultivation system". *Catalysis Today*, 257, pp. 237–245.

George, K. W., Alonso-Gutierrez, J., Keasling, J. D., and Lee, T. S. (2015). "Isoprenoid Drugs, Biofuels, and Chemicals—Artemisinin, Farnesene, and Beyond". In: *Biotechnology of Isoprenoids*. Ed. by J. Schrader and J. Bohlmann. Cham: Springer International Publishing, pp. 355–389.

Gibbs W., J. (1873). "A Method of Geometrical Representation of the Thermodynamic Properties by Means of Surfaces". *Transactions of Connecticut Academy of Arts and Sciences*, pp. 382–404.

Gibson, D. G., Young, L., Chuang, R.-Y., Venter, J. C., Hutchison, C. A., and Smith, H. O. (2009). "Enzymatic assembly of DNA molecules up to several hundred kilobases". *Nature Methods*, 6(5), pp. 343–345.

Giddings, C. G. S., Nevin, K. P., Woodward, T., Lovley, D. R., and Butler, C. S. (2015). "Simplifying microbial electrosynthesis reactor design". *Frontiers in Microbiology*, 6, p. 468.

Gildemyn, S., Rozendal, R. A., and Rabaey, K. (2017). "A Gibbs Free Energy-Based Assessment of Microbial Electrocatalysis". *Trends in Biotechnology*, 35(5), pp. 393–406.

Gildemyn, S., Verbeeck, K., Slabbinck, R., Andersen, S. J., Prévoteau, A., and Rabaey, K. (2015). "Integrated production, extraction, and concentration of acetic acid from CO2 through microbial electrosynthesis". *Environmental Science and Technology Letters*, 2(11), pp. 325–328.

Grousseau, E., Lu, J., Gorret, N., Guillouet, S. E., and Sinskey, A. J. (2014). "Isopropanol production with engineered Cupriavidus necator as bioproduction platform". *Applied Microbiology and Biotechnology*, 98(9), pp. 4277–4290.

Gruber, S., Hagen, J., Schwab, H., and Koefinger, P. (2014). "Versatile and stable vectors for efficient gene expression in Ralstonia eutropha H16". *Journal of Biotechnology*, 186, pp. 74–82.

Gruber, S., Schwendenwein, D., Magomedova, Z., Thaler, E., Hagen, J., Schwab, H., and Heidinger, P. (2015). "Design of inducible expression vectors for improved protein production in Ralstonia eutropha H16 derived host strains". *Journal of Biotechnology*, 235, pp. 92–99.

Grunwald, S., Mottet, A., Grousseau, E., Plassmeier, J. K., Popović, M. K., Uribelarrea, J.-L., Gorret, N., Guillouet, S. E., and Sinskey, A. (2015). "Kinetic and stoichiometric characterization of organoautotrophic growth of Ralstonia eutropha on formic acid in fed-batch and continuous cultures". *Microbial Biotechnology*, 8(1), pp. 155–163.

Guo, K., Prévoteau, A., Patil, S. A., and Rabaey, K. (2015). "Engineering electrodes for microbial electrocatalysis". *Current Opinion in Biotechnology*, 33, pp. 149–156.

Hanahan, D. (1983). "Studies on transformation of Escherichia coli with plasmids". *Journal of Molecular Biology*, 166(4), pp. 557–580.

Hanson, M. A., Ge, X., Kostov, Y., Brorson, K. A., Moreira, A. R., and Rao, G. (2007). "Comparisons of optical pH and dissolved oxygen sensors with traditional electrochemical probes during mammalian cell culture". *Biotechnology and Bioengineering*, 97(4), pp. 833–841.

Harnisch, F., Rosa, L. F. M., Kracke, F., Virdis, B., and Krömer, J. O. (2015). "Electrifying white biotechnology: Engineering and economic potential of electricity-driven bioproduction". *ChemSusChem*, 8(5), pp. 758–766.

Harnisch, F. and Schröder, U. (2009). "Selectivity versus mobility: Separation of anode and cathode in microbial bioelectrochemical systems". *ChemSusChem*, 2(10), pp. 921–926.

– (2010). "From MFC to MXC: chemical and biological cathodes and their potential for microbial bioelectrochemical systems". *Chemical Society Reviews*, 39(11), p. 4433.

Hau, H. H., Gilbert, A., Coursolle, D., and Gralnick, J. A. (2008). "Mechanism and consequences of anaerobic respiration of cobalt by Shewanella oneidensis strain MR-1". *Applied and Environmental Microbiology*, 74(22), pp. 6880–6886.

Hegner, R., Rosa, L. F., and Harnisch, F. (2018). "Electrochemical CO2 reduction to formate at indium electrodes with high efficiency and selectivity in pH neutral electrolytes". *Applied Catalysis B: Environmental*, 238, pp. 546–556.

Heinzle, E. and Lafferty, R. M. (1980). "A kinetic model for growth and synthesis of poly-β-hydroxybutyric acid (PHB) in Alcaligenes eutrophus H 16". *European Journal of Applied Microbiology and Biotechnology*, 11(1), pp. 8–16.

Heipieper, H. J., Weber, F. J., Sikkema, J., Keweloh, H., and Bont, J. A. de (1994). "Mechanisms of resistance of whole cells to toxic organic solvents". *Trends in Biotechnology*, 12(10), pp. 409–415.

Hintermayer, S., Yu, S., Krömer, J. O., and Weuster-Botz, D. (2016). "Anodic respiration of Pseudomonas putida KT2440 in a stirred-tank bioreactor". *Biochemical Engineering Journal*, 115, pp. 1–13.

Horst, A. E. W., Mangold, K. M., and Holtmann, D. (2015). "Application of gas diffusion electrodes in bioelectrochemical syntheses and energy conversion". *Biotechnology and Bioengineering*, 113(2), pp. 260–267.

Hu, T. and Corey, E. J. (2002). "Short Syntheses of ($\pm$)-δ-Araneosene and Humulene Utilizing a Combination of Four-Component Assembly and Palladium-Mediated Cyclization". *Organic Letters*, 4(14), pp. 2441–2443.

Huang, L., Regan, J. M., and Quan, X. (2011). "Electron transfer mechanisms, new applications, and performance of biocathode microbial fuel cells." *Bioresource technology*, 102(1), pp. 316–23.

Huschner, F., Grousseau, E., Brigham, C. J., Plassmeier, J., Popovic, M., Rha, C., and Sinskey, A. J. (2015). "Development of a feeding strategy for high cell and PHA density fed-batch fermentation of Ralstonia eutropha H16 from organic acids and their salts". *Process Biochemistry*, 50(2), pp. 165–172.

Huysmans, M. and Dassargues, A. (2005). "Review of the use of Péclet numbers to determine the relative importance of advection and diffusion in low permeability environments". *Hydrogeology Journal*, 13(5-6), pp. 895–904.

Jang, Y.-S., Park, J. M., Choi, S., Choi, Y. J., Seung, D. Y., Cho, J. H., and Lee, S. Y. (2011). "Engineering of microorganisms for the production of biofuels and perspectives based on systems metabolic engineering approaches." *Biotechnology Advances*, 30(5), pp. 989–1000.

Janicek, A., Fan, Y., and Liu, H. (2014). "Design of microbial fuel cells for practical application: a review and analysis of scale-up studies". *Biofuels*, 502, pp. 79–92.

Jiang, D., Curtis, M., Troop, E., Scheible, K., McGrath, J., Hu, B., Suib, S., Raymond, D., and Li, B. (2011). "A pilot-scale study on utilizing multi-anode/cathode microbial fuel cells (MAC MFCs) to enhance the power production in wastewater treatment". *International Journal of Hydrogen Energy*, 36(1), pp. 876–884.

Kadier, A., Simayi, Y., Abdeshahian, P., Azman, N. F., Chandrasekhar, K., and Kalil, M. S. (2014). "A comprehensive review of microbial electrolysis cells (MEC) reactor designs and configurations for sustainable hydrogen gas production". *Alexandria Engineering Journal*, 55(1), pp. 427–443.

Kahar, P., Tsuge, T., Taguchi, K., and Doi, Y. (2004). "High yield production of polyhydroxyalkanoates from soybean oil by Ralstonia eutropha and its recombinant strain". *Polymer Degradation and Stability*, 83(1), pp. 79–86.

Khang, S. J. and Levenspiel, O. (1976). "New scale-up and design method for stirrer agitated batch mixing vessels". *Chemical Engineering Science*, 31(7), pp. 569–577.

Kim, B., Cho, B. R., and Hahn, J. S. (2014). "Metabolic engineering of Saccharomyces cerevisiae for the production of 2-phenylethanol via Ehrlich pathway". *Biotechnology and Bioengineering*, 111(1), pp. 115–124.

Kim, H. M., Heinzle, E., and Wittmann, C. (2006). "Deregulation of aspartokinase by single nucleotide exchange leads to global flux rearrangement in the central metabolism of Corynebacterium glutamicum". *Journal of Microbiology and Biotechnology*, 16(8), pp. 1174–1179.

Kim, J. R., Boghani, H. C., Amini, N., Aguey-Zinsou, K. F., Michie, I., Dinsdale, R. M., Guwy, A. J., Guo, Z. X., and Premier, G. C. (2012). "Porous anodes with helical flow pathways in bioelectrochemical systems: The effects of fluid dynamics and operating regimes". *Journal of Power Sources*, 213, pp. 382–390.

Kim, T. S. and Kim, B. H. (1988). "Electron flow shift in Clostridium acetobutylicum fermentation by electrochemically introduced reducing equivalent". *Biotechnology Letters*, 10(2), pp. 123–128.

Kipf, E., Koch, J., Geiger, B., Erben, J., Richter, K., Gescher, J., Zengerle, R., and Kerzenmacher, S. (2013). "Systematic screening of carbon-based anode materials for microbial fuel cells with Shewanella oneidensis MR-1". *Bioresource Technology*, 146, pp. 386–392.

Kircher, M. (2012). "The transition to a bio-economy: national perspectives". *Biofuels, Bioproducts and Biorefining*, 6(3), pp. 240–245.

Kita, A., Iwasaki, Y., Sakai, S., Okuto, S., Takaoka, K., Suzuki, T., Yano, S., Sawayama, S., Tajima, T., Kato, J., Nishio, N., Murakami, K., and Nakashimada, Y. (2013). "Development of genetic transformation and heterologous expression system in carboxydotrophic thermophilic acetogen Moorella thermoacetica." *Journal of Bioscience and Bioengineering*, 115(4), pp. 347–352.

Koch, C. and Harnisch, F. (2016). "Is there a Specific Ecological Niche for Electroactive Microorganisms?" *ChemElectroChem*, 3(9), pp. 1282–1295.

Krieg, T., Hüttmann, S., Mangold, K.-M., Schrader, J., and Holtmann, D. (2011). "Gas diffusion electrode as novel reaction system for an electro-enzymatic process with chloroperoxidase". *Green Chemistry*, 13(10), pp. 2686–2689.

Krieg, T., Sydow, A., Faust, S., Huth, I., and Holtmann, D. (2018). "CO2 to Terpenes: Autotrophic and Electroautotrophic α-Humulene Production with Cupriavidus necator". *Angewandte Chemie*, 130(7), pp. 1897–1900.

Krieg, T., Sydow, A., Schröder, U., Schrader, J., and Holtmann, D. (2014). "Reactor concepts for bioelectrochemical syntheses and energy conversion". *Trends in Biotechnology*, 32(12), pp. 645–655.

Krömer, J. O., Sorgenfrei, O., Klopprogge, K., Heinzle, E., and Wittmann, C. (2004). "In-depth profiling of lysine-producing Corynebacterium glutamicum by combined analysis of the transcriptome, metabolome, and fluxome." *Journal of Bacteriology*, 186(6), pp. 1769–1784.

Kusterer, A., Krause, C., Kaufmann, K., Arnold, M., and Weuster-Botz, D. (2008). "Fully automated single-use stirred-tank bioreactors for parallel microbial cultivations". *Bioprocess and Biosystems Engineering*, 31(3), pp. 207–215.

Kuzmin, D., Mierka, O., and Ture, S. (2006). "On the implementation of the k $-$ ϵ turbulence model in incompressible flow solvers based on a finite element discretization". *International Journal of Computing Science and Mathematics*, 1(2-4), pp. 193–206.

Kuzuyama, T. (2002). "Mevalonate and Nonmevalonate Pathways for the Biosynthesis of Isoprene Units". *Bioscience, Biotechnology, and Biochemistry*, 66(8), pp. 1619–1627.

Lai, B., Yu, S., Bernhardt, P. V., Rabaey, K., Virdis, B., and Krömer, J. O. (2016). "Anoxic metabolism and biochemical production in Pseudomonas putida F1 driven by a bioelectrochemical system". *Biotechnology for Biofuels*, 9(1), p. 39.

Leang, C., Ueki, T., Nevin, K. P., and Lovley, D. R. (2013). "A genetic system for Clostridium ljungdahlii: a chassis for autotrophic production of biocommodities and a model homoacetogen." *Applied and Environmental Microbiology*, 79(4), pp. 1102–1109.

Leong, J. X., Daud, W. R. W., Ghasemi, M., Liew, K. B., and Ismail, M. (2013). "Ion exchange membranes as separators in microbial fuel cells for bioenergy conversion: A comprehensive review". *Renewable and Sustainable Energy Reviews*, 28, pp. 575–587.

Li, F., Wang, L., Liu, C., Wu, D., and Song, H. (2018). "Engineering exoelectrogens by synthetic biology strategies". *Current Opinion in Electrochemistry*.

Li, H., Opgenorth, P. H., Wernick, D. G., Rogers, S., Wu, T.-Y., Higashide, W., Malati, P., Huo, Y.-X., Cho, K. M., and Liao, J. C. (2012). "Integrated Electromicrobial Conversion of CO2 to Higher Alcohols". *Science*, 335(6076), pp. 1596–1596.

Liu, C., Colon, B. C., Ziesack, M., Silver, P. a., and Nocera, D. G. (2016). "Water splitting-biosynthetic system with CO2 reduction efficiencies exceeding photosynthesis". *Science*, 352(6290), pp. 1210–1213.

Liu, H. and Logan, B. E. (2004). "Electricity generation using an air-cathode single chamber microbial fuel cell in the presence and absence of a proton exchange membrane." *Environmental Science & Technology*, 38(14), pp. 4040–4046.

Logan, B., Cheng, S., Watson, V., and Estadt, G. (2007). "Graphite fiber brush anodes for increased power production in air-cathode microbial fuel cells." *Environmental Science & Technology*, 41(9), pp. 3341–3346.

Lohner, S. T., Deutzmann, J. S., Logan, B. E., Leigh, J., and Spormann, A. M. (2014). "Hydrogenase-independent uptake and metabolism of electrons by the archaeon Methanococcus maripaludis". *The ISME Journal*, 8(8), pp. 1673–1681.

Lovley, D. R. (2011). "Powering microbes with electricity: direct electron transfer from electrodes to microbes." *Environmental Microbiology Reports*, 3(1), pp. 27–35.

Lovley, D. R. and Nevin, K. P. (2013). "Electrobiocommodities: Powering microbial production of fuels and commodity chemicals from carbon dioxide with electricity". *Current Opinion in Biotechnology*, 24(3), pp. 385–390.

Luo, S., Sun, H., Ping, Q., Jin, R., and He, Z. (2016). "A Review of Modeling Bioelectrochemical Systems: Engineering and Statistical Aspects". *Energies*, 9(2), p. 111.

Lütz, S., Steckhan, E., and Liese, A. (2004). "First asymmetric electroenzymatic oxidation catalyzed by a peroxidase". *Electrochemistry Communications*, 6(6), pp. 583–587.

Marc, J., Grousseau, E., Lombard, E., Sinskey, A. J., Gorret, N., and Guillouet, S. E. (2017). "Over expression of GroESL in Cupriavidus necator for heterotrophic and autotrophic isopropanol production". *Metabolic Engineering*, 42(Supplement C), pp. 74–84.

Marshall, C. W., Ross, D. E., Fichot, E. B., Norman, R. S., and May, H. D. (2012). "Electrosynthesis of Commodity Chemicals by an Autotrophic Microbial Community". *Applied and Environmental Microbiology*, 78(23), pp. 8412–8420.

Marsili, E., Baron, D. B., Shikhare, I. D., Coursolle, D., Gralnick, J. A., and Bond, D. R. (2008). "Shewanella secretes flavins that mediate extracellular electron transfer." *Proceedings of the National Academy of Sciences of the United States of America*, 105(10), pp. 3968–3973.

Mayer, F., Stöckl, M., Krieg, T., Mangold, K.-M., and Holtmann, D. (2018). "Adsorption of Shewanella oneidensis MR-1 to the electrode material Activated Carbon Fabric". *Journal of Chemical Technology & Biotechnology*, (April).

McMurry, J. E., Matz, J. R., and Kees, K. L. (1987). "Synthesis of macrocyclic terpenoids by intramolecular carbonyl coupling: flexibilene and humulene". *Tetrahedron*, 43(23), pp. 5489–5498.

Mi, J., Becher, D., Lubuta, P., Dany, S., Tusch, K., Schewe, H., Buchhaupt, M., and Schrader, J. (2014). "De novo production of the monoterpenoid geranic acid by metabolically engineered Pseudomonas putida". *Microbial Cell Factories*, 13(1), p. 170.

Mirata, M. A., Heerd, D., and Schrader, J. (2009). "Integrated bioprocess for the oxidation of limonene to perillic acid with Pseudomonas putida DSM 12264". *Process Biochemistry*, 44(7), pp. 764–771.

Miyaura, N., Suginome, H., and Suzuki, A. (1984). "New stereo- and regiospecific synthesis of humulene by means of the palladium-catalyzed cyclization of haloalkenylboranes". *Tetrahedron Letters*, 25(7), pp. 761–764.

Mohan, S. V., Modestra, J. A., Amulya, K., Butti, S. K., and Velvizhi, G. (2016). "A Circular Bioeconomy with Biobased Products from CO2 Sequestration". *Trends in Biotechnology*, 34(6), pp. 506–519.

Moscoviz, R., Toledo-Alarcón, J., Trably, E., and Bernet, N. (2016). "Electro-Fermentation: How To Drive Fermentation Using Electrochemical Systems". *Trends in Biotechnology*, 34(11), pp. 856–865.

Müller, J., MacEachran, D., Burd, H., Sathitsuksanoh, N., Bi, C., Yeh, Y. C., Lee, T. S., Hillson, N. J., Chhabra, S. R., Singer, S. W., and Beller, H. R. (2013). "Engineering of Ralstonia eutropha H16 for autotrophic and heterotrophic production of methyl ketones". *Applied and Environmental Microbiology*, 79(14), pp. 4433–4439.

Nevin, K. P., Richter, H., Covalla, S. F., Johnson, J. P., Woodard, T. L., Orloff, a. L., Jia, H., Zhang, M., and Lovley, D. R. (2008). "Power output and columbic efficiencies from biofilms of Geobacter sulfurreducens comparable to mixed community microbial fuel cells." *Environmental Microbiology*, 10(10), pp. 2505–2514.

Nevin, K. P., Hensley, S. a., Franks, A. E., Summers, Z. M., Ou, J., Woodard, T. L., Snoeyenbos-West, O. L., and Lovley, D. R. (2011). "Electrosynthesis of organic compounds from carbon dioxide is catalyzed by a diversity of acetogenic microorganisms." *Applied and Environmental Microbiology*, 77(9), pp. 2882–2886.

Nevin, K. P., Woodard, T. L., and Franks, A. E. (2010). "Microbial Electrosynthesis : Feeding Microbial Electrosynthesis : Feeding Microbes Electricity To Convert Carbon Dioxide and Water to Multicarbon Extracellular Organic". *mBio*, 1(2), e00103–10.

Nield, D. A. (1983). "The boundary correction for the Rayleigh-Darcy problem: Limitations of the Brinkman equation". *Journal of Fluid Mechanics*, 128, pp. 37–46.

Nielsen, M. E., Reimers, C. E., and Stecher, H. a. (2007). "Enhanced power from chambered benthic microbial fuel cells." *Environmental Science & Technology*, 41(22), pp. 7895–7900.

Nybo, S. E., Khan, N. E., Woolston, B. M., and Curtis, W. R. (2015). "Metabolic engineering in chemolithoautotrophic hosts for the production of fuels and chemicals". *Metabolic Engineering*, 30, pp. 105–120.

Passos, G. F., Fernandes, E. S., Cunha, F. M. da, Ferreira, J., Pianowski, L. F., Campos, M. M., and Calixto, J. B. (2007). "Anti-inflammatory and anti-allergic properties of the essential oil and active compounds from Cordia verbenacea". *Journal of Ethnopharmacology*, 110(2), pp. 323–333.

Patil, S. a., Hägerhäll, C., and Gorton, L. (2012). "Electron transfer mechanisms between microorganisms and electrodes in bioelectrochemical systems". *Bioanalytical Reviews*, 4(2-4), pp. 159–192.

Peralta-Yahya, P. P. and Keasling, J. D. (2010). "Advanced biofuel production in microbes". *Biotechnology Journal*, 5(2), pp. 147–162.

Peralta-Yahya, P. P., Zhang, F., Cardayre, S. B. del, and Keasling, J. D. (2012). "Microbial engineering for the production of advanced biofuels". *Nature*, 488(7411), pp. 320–328.

Picioreanu, C., Loosdrecht, M. C. M. van, Curtis, T. P., and Scott, K. (2010). "Model based evaluation of the effect of pH and electrode geometry on microbial fuel cell performance". *Bioelectrochemistry*, 78(1), pp. 8–24.

Pohlmann, A., Fricke, W. F., Reinecke, F., Kusian, B., Liesegang, H., Cramm, R., Eitinger, T., Ewering, C., Pötter, M., Schwartz, E., Strittmatter, A., Voss, I., Gottschalk, G., Steinbüchel, A., Friedrich, B., and Bowien, B. (2006). "Genome sequence of the bioplastic-producing

"Knallgas" bacterium Ralstonia eutropha H16." *Nature Biotechnology*, 24(10), pp. 1257–1262.

Potter, M. C. (1911). "Electrical Effects Accompanying the Decomposition of Organic Compounds". *Proceedings of the Royal Society of London. Series B, Containing Papers of a Biological Character*, 84(571), pp. 260–276.

Potter, M. C., Wiggert, D. C., and Ramadan, B. H. (2012). *Mechanics of fluids*. Fourth, p. 105.

Rabaey, K. and Rozendal, R. A. (2010). "Microbial electrosynthesis - revisiting the electrical route for microbial production." *Nature Reviews Microbiology*, 8(10), p. 706.

Raberg, M., Voigt, B., Hecker, M., and Steinbüchel, A. (2014). "A closer look on the polyhydroxybutyrate-(PHB-) negative phenotype of Ralstonia eutropha PHB-4". *PLoS ONE*, 9(5), pp. 1–11.

Rader, G. K. and Logan, B. E. (2010). "Multi-electrode continuous flow microbial electrolysis cell for biogas production from acetate". *International Journal of Hydrogen Energy*, 35(17), pp. 8848–8854.

Repaske, R. and Mayer, R. (1976). "Dense autotrophic cultures of Alcaligenes eutrophus". *Applied and Environmental Microbiology*, 32(4), p. 592.

Ro, D.-K., Paradise, E. M., Ouellet, M., Fisher, K. J., Newman, K. L., Ndungu, J. M., Ho, K. a., Eachus, R. a., Ham, T. S., Kirby, J., Chang, M. C. Y., Withers, S. T., Shiba, Y., Sarpong, R., and Keasling, J. D. (2006). "Production of the antimalarial drug precursor artemisinic acid in engineered yeast." *Nature*, 440(7086), p. 940.

Rosa, L. F. M., Hunger, S., Gimkiewicz, C., Zehnsdorf, A., and Harnisch, F. (2016). "Paving the way for Bioelectrotechnology: Integrating Electrochemistry into Bioreactors". *Engineering in Life Sciences*, 53(9), pp. 1689–1699.

Rosenbaum, M. a. and Henrich, A. W. (2014). "Engineering microbial electrocatalysis for chemical and fuel production". *Current Opinion in Biotechnology*, 29, pp. 93–98.

Rosenbaum, M., Aulenta, F., Villano, M., and Angenent, L. T. (2011). "Cathodes as electron donors for microbial metabolism: which extracellular electron transfer mechanisms are involved?" *Bioresource Technology*, 102(1), pp. 324–333.

Rosenbaum, M., Cotta, M. a., and Angenent, L. T. (2010). "Aerated Shewanella oneidensis in continuously fed bioelectrochemical systems for power and hydrogen production." *Biotechnology and Bioengineering*, 105(5), pp. 880–888.

Ross, D. E., Flynn, J. M., Baron, D. B., Gralnick, J. a., and Bond, D. R. (2011). "Towards electrosynthesis in shewanella: energetics of reversing the mtr pathway for reductive metabolism." *PloS one*, 6(2), e16649.

Roy, S., Schievano, A., and Pant, D. (2016). "Electro-stimulated Microbial Factory for value added product synthesis". *Bioresource Technology*, 213, pp. 129–139.

Rozendal, R. A., Hamelers, H. V., Euverink, G. J., Metz, S. J., and Buisman, C. J. (2006). "Principle and perspectives of hydrogen production through biocatalyzed electrolysis". *International Journal of Hydrogen Energy*, 31(12), pp. 1632–1640.

Ruzicka, L. (1953). "The isoprene rule and the biogenesis of terpenic compounds". *Experientia*, 9(10), pp. 357–367.

Sajana, T., Ghangrekar, M., and Mitra, a. (2014). "Effect of operating parameters on the performance of sediment microbial fuel cell treating aquaculture water". *Aquacultural Engineering*, 61, pp. 17–26.

Sawyer, D. T., Sobkowiak, A., Roberts, J. L., and Sawyer, D. T. (1995). *Electrochemistry for chemists*. Wiley, p. 505.

Scarlat, N., Dallemand, J. F., Monforti-Ferrario, F., and Nita, V. (2015). "The role of biomass and bioenergy in a future bioeconomy: Policies and facts". *Environmental Development*, 15, pp. 3–34.

Schewe, H., Mirata, M. A., and Schrader, J. (2015). "Bioprocess Engineering for Microbial Synthesis and Conversion of Isoprenoids". In: *Biotechnology of Isoprenoids*. Ed. by J. Schrader and J. Bohlmann. Springer International Publishing, pp. 251–286.

Schievano, A., Pepé Sciarria, T., Vanbroekoven, K., De Wever, H., Puig, S., Andersen, S. J., Rabaey, K., and Pant, D. (2016). "Electro-fermentation – Merging electrochemistry with fermentation in industrial applications". *Trends in Biotechnology*, 34(11), pp. 866–878.

Schlegel, H. G. (1965). "Growth of 'knallgas' bacteria (Hydrogenomonas) using direct electrolysis of the culture medium". *Nature*, 205(4968), pp. 308–309.

Schlegel, H. G., Gottschalk, G., and Von Bartha, R. (1961). "Formation and utilization of poly-β-hydroxybutyric acid by Knallgas bacteria (Hydrogenomonas)". *Nature*, 191(4787), pp. 463–465.

Schlegel, H. G. and Lafferty, R. (1964). "Submerskultur von Hydrogenomonas mit elektrolytischer Knallgaserzeugung im Kulturgefäss". *Zentrabl. Bakteriol. Parasitenk. Infektionskr. Hyg. Abt. II*, 118, pp. 483–490.

Schlegel, H. G. and Lafferty, R. M. (1971). "Novel energy and carbon sources A. The production of biomass from hydrogen and carbon dioxide". In: *Advances in Biochemical Engineering, Volume 1*. Berlin/Heidelberg: Springer-Verlag, pp. 143–168.

Schmitz, S., Nies, S., Wierckx, N., Blank, L. M., and Rosenbaum, M. A. (2015). "Engineering mediator-based electroactivity in the obligate aerobic bacterium Pseudomonas putida KT2440". *Frontiers in Microbiology*, 6, p. 284.

Schröder, U., Harnisch, F., and Angenent, L. T. (2015). "Microbial electrochemistry and technology: terminology and classification". *Energy & Environmental Science*, 8(2), pp. 513–519.

Schrott, G. D., Bonanni, P. S., Robuschi, L., Esteve-Nuñez, A., and Busalmen, J. P. (2011). "Electrochemical insight into the mechanism of electron transport in biofilms of Geobacter sulfurreducens". *Electrochimica Acta*, 56(28), pp. 10791–10795.

Shang, L., Fan, D. D., Kim, M. I., Choi, J.-d.-r., and Chang, H. N. (2007). "Modeling of poly(3-hydroxybutyrate) production by high cell density fed-batch culture of Ralstonia eutropha". *Biotechnology and Bioprocess Engineering*, 12(4), pp. 417–423.

Sharma, C., Malhotra, D., and Rathore, A. S. (2011). "Review of Computational fluid dynamics applications in biotechnology processes". *Biotechnology Progress*, 27(6), pp. 1497–1510.

Sleutels, T. H. J. A., Hamelers, H. V. M., and Buisman, C. J. N. (2011). "Effect of mass and charge transport speed and direction in porous anodes on microbial electrolysis cell performance". *Bioresource Technology*, 102(1), pp. 399–403.

Sleutels, T. H. J. A., Lodder, R., Hamelers, H. V. M., and Buisman, C. J. N. (2009). "Improved performance of porous bio-anodes in microbial electrolysis cells by enhancing mass and charge transport". *International Journal of Hydrogen Energy*, 34(24), pp. 9655–9661.

Sonntag, F., Kroner, C., Lubuta, P., Peyraud, R., Horst, A., Buchhaupt, M., and Schrader, J. (2015). "Engineering Methylobacterium extorquens for de novo synthesis of the sesquiterpenoid α-humulene from methanol". *Metabolic Engineering*, 32, pp. 82–94.

Soussan, L., Riess, J., Erable, B., Delia, M.-L., and Bergel, A. (2013). "Electrochemical reduction of CO2 catalysed by Geobacter sulfurreducens grown on polarized stainless steel cathodes". *Electrochemistry Communications*, 28, pp. 27–30.

Srikanth, S., Maesen, M., Dominguez-Benetton, X., Vanbroekhoven, K., and Pant, D. (2014). "Enzymatic Electrosynthesis of Formate through CO2 Sequestration/Reduction in a Bioelectrochemical System (BES)". *Bioresource Technology*, 165, pp. 350–354.

Srinivasan, S., Barnard, G. C., and Gerngross, T. U. (2003). "Production of recombinant proteins using multiple-copy gene integration in high-cell-density fermentations ofRalstonia eutropha". *Biotechnology and Bioengineering*, 84(1), pp. 114–120.

Steinbüchel, A. and Schlegel, H.-G. (1991). "Physiology and molecular genetics of poly (β-hydroxyalkanoic acid) synthesis in Alcaligenes eutrophus". *Molecular Microbiology*, 5(3), pp. 535–542.

Sydow, A., Krieg, T., Mayer, F., Schrader, J., and Holtmann, D. (2014). "Electroactive bacteria - molecular mechanisms and genetic tools". *Applied Microbiology and Biotechnology*, 98(20), pp. 8481–8495.

Sydow, A., Krieg, T., Ulber, R., and Holtmann, D. (2017a). "Growth medium and electrolyte - how to combine the different requirements on the reaction solution in bioelectrochemical systems using Cupriavidus necator". *Engineering in Life Sciences*, 17(7), pp. 781–791.

Sydow, A., Pannek, A., Krieg, T., Huth, I., Guillouet, S. E., and Holtmann, D. (2017b). "Expanding the genetic tool box for Cupriavidus necator by a stabilized L-rhamnose inducible plasmid system". *Journal of Biotechnology*, 263(Supplement C), pp. 1–10.

Takahashi, T., Kitamura, K., and Tsuji, J. (1983). "Syntheses of new humulene derivatives; (2E,6E,9E)- and (2Z,6E,9E)-cycloundecatrienones, by intramolecular alkylation of protected cyanohydrin. A route to humulene". *Tetrahedron Letters*, 24(43), pp. 4695–4698.

Tang, Y. J., Hwang, J. S., Wemmer, D. E., and Keasling, J. D. (2007). "Shewanella oneidensis MR-1 fluxome under various oxygen conditions." *Applied and Environmental Microbiology*, 73(3), pp. 718–729.

Thauer, R. K., Jungermann, K., and Decker, K. (1977). "Energy conservation in chemotrophic anaerobic bacteria." *Bacteriological Reviews*, 41(1), p. 100.

Tjaden, B., Cooper, S. J., Brett, D. J., Kramer, D., and Shearing, P. R. (2016). "On the origin and application of the Bruggeman correlation for analysing transport phenomena in electrochemical systems". *Current Opinion in Chemical Engineering*, 12, pp. 44–51.

Torella, J. P., Gagliardi, C. J., Chen, J. S., Bediako, D. K., Colon, B., Way, J. C., Silver, P. a., and Nocera, D. G. (2015). "Efficient solar-to-fuels production from a hybrid microbial-water-splitting catalyst system". *Proceedings of the National Academy of Sciences*, 112(8), pp. 2337–2342.

Trombetta, D., Castelli, F., Sarpietro, M. G., Venuti, V., Cristani, M., Daniele, C., Saija, A., Mazzanti, G., and Bisignano, G. (2005). "Mechanisms of antibacterial action of three monoterpenes." *Antimicrobial Agents and Chemotherapy*, 49(6), pp. 2474–2478.

Udupa, K., Subramanian, G., and Udupa, H. (1971). "The electrolytic reduction of carbon dioxide to formic acid". *Electrochimica Acta*, 16(9), pp. 1593–1598.

Utesch, T. and Zeng, A.-P. (2018). "A novel All-in-One electrolysis electrode and bioreactor enable better study of electrochemical effects and electricity-aided bioprocesses". *Engineering in Life Sciences*, 18(8), pp. 600–610.

Vargas, M., Malvankar, N. S., Tremblay, P.-l., Leang, C., Smith, J. A., and Patel, P. (2013). "Aromatic Amino Acids Required for Pili Conductivity and Long- Range Extracellular Electron Transport in Geobacter sulfurreducens". *mBio*, 4(2), e00105–13.

Vassilev, I., Gießelmann, G., Schwechheimer, S. K., Wittmann, C., Virdis, B., and Krömer, J. O. (2018). "Anodic Electro-Fermentation: Anaerobic production of L-Lysine by recombinant Corynebacterium glutamicum". *Biotechnology and Bioengineering*, 115(6), pp. 1499–1508.

Venkateswaran, K., Moser, D. P., Dollhopf, M. E., Lies, D. P., Saffarini, D. A., MacGregor, B. J., Ringelberg, D. B., White, D. C., Nishijima, M., Sano, H., Burghardt, J., Stackebrandt, E., and Nealson, K. H. (1999). "Polyphasic taxonomy of the genus Shewanella and description of Shewanella oneidensis sp. now". *International Journal of Systematic Bacteriology*, 49, pp. 705–724.

Verstraete, W., Rabaey, K., Logan, B. E., Hamelers, B., Rozendal, R., Schröder, U., Keller, J., Freguia, S., and Aelterman, P. (2006). "Microbial fuel cells: methodology and technology." *Environmental Science & Technology*, 40(17), pp. 5181–5192.

Vilà-Rovira, A., Puig, S., Balaguer, M. D., Colprim, J., Bergel, A., Oostveldt, P. van, Verbeken, K., Rabaey, K., and Verstraete, W. (2015). "Anode hydrodynamics in bioelectrochemical systems". *RSC Advances*, 5(96), pp. 78994–79000.

Wang, Q., Dong, H., and Yu, H. (2014). "Development of rolling tin gas diffusion electrode for carbon dioxide electrochemical reduction to produce formate in aqueous electrolyte". *Journal of Power Sources*, 271, pp. 278–284.

Wolf, A. V. (1966). *Aqueous Solutions and Body Fluids*. New York: Harper and Row.

Yu, F., Okamto, S., Nakasone, K., Adachi, K., Matsuda, S., Harada, H., Misawa, N., and Utsumi, R. (2008). "Molecular cloning and functional characterization of α-humulene synthase, a possible key enzyme of zerumbone biosynthesis in shampoo ginger (Zingiber zerumbet Smith)". *Planta*, 227(6), pp. 1291–1299.

Zhang, F., Liu, J., Ivanov, I., Hatzell, M. C., Yang, W., Ahn, Y., and Logan, B. E. (2014). "Reference and counter electrode positions affect electrochemical characterization of bioanodes in different bioelectrochemical systems." *Biotechnology and Bioengineering*, 110(10), pp. 1931–1939.

Zhang, F., Rodriguez, S., and Keasling, J. D. (2011a). "Metabolic engineering of microbial pathways for advanced biofuels production." *Current Opinion in Biotechnology*, 22(6), pp. 775–783.

Zhang, T., Nie, H., Bain, T. S., Lu, H., Cui, M., Snoeyenbos-West, O. L., Franks, A. E., Nevin, K. P., Russell, T. P., and Lovley, D. R. (2013). "Improved cathode materials for microbial electrosynthesis". *Energy & Environmental Science*, 6(1), p. 217.

Zhang, X., Cheng, S., Liang, P., and Huang, X. (2011b). "Scalable air cathode microbial fuel cells using glass fiber separators, plastic mesh supporters, and graphite fiber brush anodes". *Bioresource Technology*, 102(1), pp. 372–375.

Zhang, Y. and Angelidaki, I. (2014). "Microbial electrolysis cells turning to be versatile technology: Recent advances and future challenges". *Water Research*, 56, pp. 11–25.

Zhao, L., Li, J., Battaglia, F., and He, Z. (2016). "Investigation of multiphysics in tubular microbial fuel cells by coupled computational fluid dynamics with multi-order Butler–Volmer reactions". *Chemical Engineering Journal*, 296, pp. 377–385.

Zhao, L., Chang, W.-c., Xiao, Y., Liu, H.-w., and Liu, P. (2013). "Methylerythritol Phosphate Pathway of Isoprenoid Biosynthesis". *Annual Review of Biochemistry*, 82(1), pp. 497–530.

Zhou, M. (2013). "The Next Breakthrough in Microbial Fuel Cells and Microbial Electrolysis Cells for Bioenergy and Bioproducts". *Journal of Microbial & Biochemical Technology*, 01(S12), pp. 10–13.

Zhuang, L., Yuan, Y., Wang, Y., and Zhou, S. (2012). "Long-term evaluation of a 10-liter serpentine-type microbial fuel cell stack treating brewery wastewater". *Bioresource Technology*, 123, pp. 406–412.

Appendix

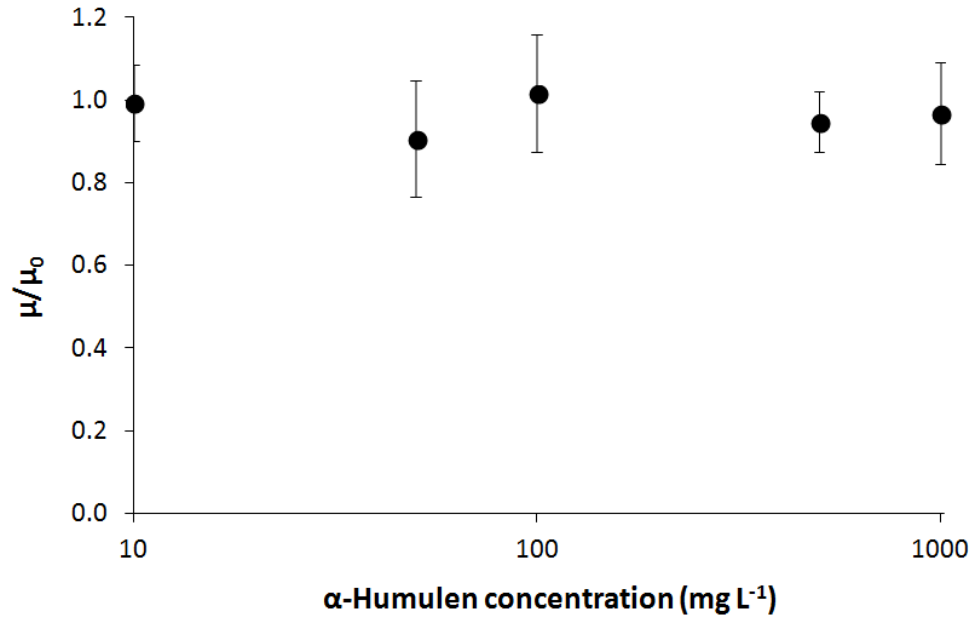

Figure 44: Toxicity test of α-humulene solved in a 20% n-dodecane phase.